Shedding Light on Photosystem I

From Charge-transport to Bio-photovoltaics

university of groningen / faculty of mathematics and natural sciences / zernike institute for advanced materials

This project was carried out in the Organic-Materials Chemistry research group which is part of Chemistry of (Bio)Molecular Materials and Devices basiseenheid at the Stratingh Institute for Chemistry and the Zernike Institute for Advanced Materials at the University of Groningen, The Netherlands. The work here presented was financially supported by the Zernike National Research Center. The European Research Council for ERC Strating Grant 335473 (MOLECSYNCON) is also acknowledged.

Printed by: GVO drukkers & vormgevers B.V.

Front & Back: Representation of a life journey. Photographs of microfluidic channels filled with eutectic gallium indium (black), food coloring (blue) and photosystem I (green). Microfluidic art designed by O.E.Castañeda Ocampo. Cover design by O.E.C.O. and G.V.O.

ISBN: 978-90-367-9555-5 (Printed version)
ISBN: 978-90-367-9554-8 (Electronic version)

An electronic version of this dissertation is available at
`http://www.rug.nl/research/portal/`

university of groningen / faculty of mathematics and natural sciences

university of groningen

Shedding Light on Photosystem I

From Charge-transport to Bio-photovoltaics

PhD thesis

to obtain the degree of PhD at the
University of Groningen
on the authority of the
Rector Magnificus Prof. E. Sterken
and in accordance with
the decision by the College of Deans.

This thesis will be defended in public on

Friday 17 February 2017 at 09.00 hours

by

Olga Elena Castañeda Ocampo

born on 18 April 1985
in Medellín, Colombia

Supervisor

Prof. R.C. Chiechi
Prof. A. Herrmann

Assessment Committee

Prof. M.D. Dickey
Prof. C.H. van der Wal
Prof. E.M.J. Verpoorte

You have brains in your head. You have feet in your shoes.
You can steer yourself any direction you choose.
You're on your own. And you know what you know.
And you are the one who'll decide where to go.

DR. SEUSS

Contents

1

Introduction

Anybody who has been seriously engaged in scientific work
of any kind realizes that over the entrance to the gates
of the temple of science are written the words: "Ye must have faith."

MAX PLANCK

1

Abstract

Independent of how long it will take before we run out of fossil-based fuel, scientists around the world need to come up with new and "green" ideas to rid our planet from toxic reaction byproducts. Renewable sources, such as solar energy, provide a clean and promising solution for our energetic problems.

Clearly fossil-fuel based energy will continue to dominate the market for still some decades but we believe that the effects of depletion will eventually overwhelm such developments and give way to alternative sources. This chapter introduces all of the key elements discussed throughout this thesis, from our motivation to an insight into our proposed devices. By presenting the work done in this thesis, it is our hope to take a step forward in the right direction, that of a cleaner, healthier world.

1.1. *Motivation*

The industrial revolution brought an ever-growing energy demand. Our dependence on fossil-based energy sources plus an escalating world population has brought us to a peak fossil fuel production. According to the Key World Energy Statistics of 2016 from the International Energy Agency [1], oil consumption in 2014 accounted for 39.9% of the total energy used worldwide while biofuels accounted for an encouraging 14% but renewable sources such as solar, wind, and geothermal power represented only 3.3% of the total energy consumption of 9,425 MTOE (million tons of oil equivalent). One of the biggest problems related to the increase in fossil-based fuel consumption is CO_2 emissions. Carbon dioxide is one of the most abundant green-house gases. That means it is present in the atmosphere and absorbs and emits thermal radiation. This heat entrapment enhances the so-called "greenhouse effect". According to Oak Ridge National Laboratory, global carbon emissions from fossil fuels have significantly increased over the last decades [2]. Since 1970, CO_2 emissions had increased by about 90% (until 2011). Emissions from fossil fuel combustion and industrial processes constituted about 78% of the total greenhouse gas emissions. Given the imperative to reduce CO_2 emissions, we need to look to alternative, cleaner energy sources and promote their use. Renewable sources such as solar, wind, and geothermal seem to provide an ecological approach to the impending problem. However, at the moment, they only represent 1.4% of the world total primary energy supply. Besides, it would be beneficial if we were able to find uses for the emitted CO_2. An ideal solution would be to have a type of device that could act as photosynthetic organisms do. In other words, take polluting CO_2 and in return, produce clean oxygen and energy. This would not only contribute towards producing green energy, but also towards providing a "green task" for carbon dioxide.

During photosynthesis, plants and other organisms absorb sunlight and convert it into chemical energy. Although this process is not the same for all photosynthetic species, it starts with the intake of photons by protein reaction centers located in chloroplasts –in the case of plants– or in the plasma membrane –in the case of bacteria. These light-dependent reactions create nicotinamide adenine dinucleotide phosphate (NADPH) and adenosine triphosphate (ATP), the "molecular units of currency" of intracellular energy transfer [3] or "energy store". During the last stage of photosynthesis, the light-independent reactions use ATP and NADPH (in the Calvin or reverse Krebs cycles depending on the organism) to capture and reduce carbon dioxide in order to produce carbohydrates. Here, the energy absorbed as photons winds up in the bonds of the glucose and other sugars produced, as seen in the general photosynthetic reaction:

$6H_2O + 6CO_2 \longrightarrow C_6H_{12}O_6 + 6O_2$
In cyanobacteria, just like in plants, ATP and NADPH are used for CO_2 fixation and for other cell processes.

Solar radiation plays then a key role in such processes and thus, a solar-powered device capable of simulating this process would provide a promising, multifaceted solution. Taking advantage of solar energy makes sense since sunlight is the most abundant and sustainable source of energy available (and it is free). The sun provides the earth with solar energy at the rate of approximately 120 PW (1 PW = 1 x 10^{15} W, 1 W = 1 J/s), which is about eight thousand times our current annual global energy consumption rate [4]. This means that the energetic needs of the total population for one year, could be met by the energy provided by the sun in just one hour. The problem we have is that we are still not able to harvest, convert and store this power. It is now up to us to try to understand better the innate processes we observe in nature and try to come up with better solutions.

1.2. *Bio-Photovoltaics and Photosystem*

Bio-photovoltaics is a technology geared towards the generation of electrical power from organisms or biological complexes by harvesting light energy. These devices are sometimes called "living solar cells" and are defined by the type of active material, and the mode of electron transfer. The main types are: PV based on light harvesting materials, isolated photosystems, sub-cellular fractions or whole organisms [5–9].

One of the motivations behind this research is that by using living organisms or biological complexes as the light harvesting material, the devices would be cost-effective and eventually serve as alternative to artificial photovoltaics. Another motivation is that these systems need no additional supply of reducing equivalents to the system. Additionally, because they use CO_2 in the photosynthetic reactions, the devices could actually have a negative carbon footprint.

It was our goal to work towards an ideal solar-powered device capable of simulating photosynthesis. When considering what the "active ingredient" would be in these devices, the obvious choice was to use the complex that accomplishes this reaction in nature, that is, photosystem I (PSI). Photosystem I is an integral membrane protein complex located in the thylakoid membrane of cyanobacteria and plants. The complex is oriented within this membrane in such a way that the light active enzymes face the lumen while the enzymes that break down carbon face the stroma (Fig. 1.1). Photosystem I houses the reaction center where the

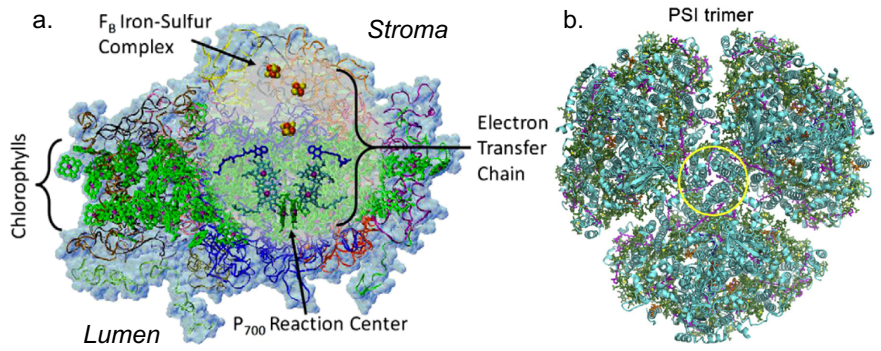

Figure 1.1. a. Schematic representation of the structure of Photosystem I. Electron transfer takes place through the electron transport chain (ETC). The iron-sulfur cluster, denoted F_B is located on the opposite side of the protein complex [12]. **b.** Resolution model of cyanobacterial trimeric PSI as viewed from the stromal side ([13]). Each monomer consists of 12 proteins (shown in a backbone representation in cyan) and 96 light sensitive Chlorophyll *a* (Chl*a*) molecules (green). Other pigments are phylloquinones (blue), carotenoids (magenta) and lipids (orange).

conversion of solar energy to electron hole pairs takes place and is, in fact, a promising choice because of its photovoltage of 1 V under illumination and its internal quantum efficiency close to unity [10, 11]. These features make PSI a unique and interesting protein complex to study.

The trimeric photosynthetic complexes studied here are isolated from the thermophilic unicellular cyanobacterium *Thermosynechococcus elongatus BP-1* also known as the "blue and green algae". This organism is fairly ubiquitous, especially in lakes and ponds during warm seasons (see Fig. 1.2). The shape of a cyanobacterial PSI trimer is ellipsoidal, with an approximate diameter of 22 nm and thickness of 8 nm. It contains 96 light sensitive Chlorophyll *a* (Chl*a*) molecules that are densely packed in the protein scaffold [13] to harvest light. Light is harvested and converted into excited electrons by chlorophylls at P700. This transfer occurs from the primary electron donor complex to the primary electron acceptor A_0, to the ferredoxine (F_D) docking region through the built-in electron transport chain and Fe_4S_4 clusters. In nature, the electron is transferred here through a series of redox reactions, eventually reaching NADP+ and H+ to produce NADPH, an energy carrier. This way the transduction cycled is completed.

The entire PSI complex, as well as the reaction center (RC) from plants and cyanobacteria have been extensively characterized and the electrical properties have been observed by a variety of experimental techniques [13–25]. We studied

Figure 1.2. Photos taken in the Groningen canals during the summer months. Lakes and ponds covered by "blue and green algae", an ubiquitous source of Photosystem I. (Photos provided by author (left) and T. L. Krijger (right)).

the entire PSI complex, not isolated RC, because it contains the electron transport chain, the light-harvesting array of chlorophylls and the protein scaffold that holds them in place.

1.3. *Integrating Photosystem into Electrical Devices*

In nature, electrons are shuttled through PSI via a series of Marcus-type electron-transfer processes requiring close contact and proper alignment of molecular orbitals. Photovoltaic devices, however, require the direct extraction of electrons/holes from the photo-active component(s) which requires materials than are energy-matched to the levels of PSI (specifically, P700) in the ground and excited states. Solid-state devices also require that the PSI complexes be oriented correctly with respect to the electron- and hole-collecting electrodes. Previous attempts were made to orient and immobilize PSI or its reaction center. Greenbaum *et al.* reported being able to orient PSI on Au surfaces by PSI-Pt-Au bonding [21]. They theorized that PSI complexes carried positively-charged domain(s) and interacted electrostatically with negatively charged surfaces and through Pt affinities and the interactions between the substrate and the complex, they induced a torque moment to orient the PSI. Later on, the same group found a simpler technique to achieve orientation by making use of a short molecule. The researchers performed STM (scanning tunneling microscopy) measurements on the monolayers and assigned different rectification by the supposed orientation provided by the short molecules [20]. The assumption of which orientation the

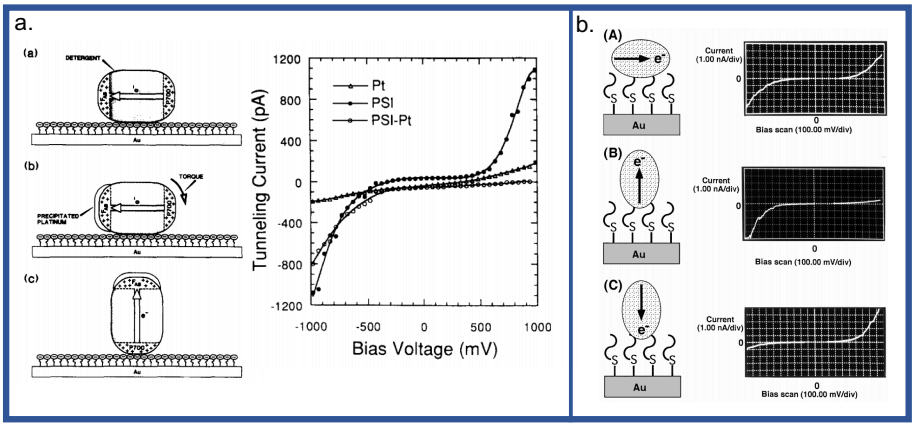

Figure 1.3. **a.** Schematic representation of PSI electrostatic immobilization on a mercaptoacetate-modified gold surface by means of platinization. Greenbaum *et al.* [21] assume that Pt deposits preferentially near the F_{AB} complexes, electrostatic shielding by the metal reduces the force between PSI polar end and the surface. This single-sided reduction creates an imbalance of forces, causing a rotational torque to occur orienting the complex. Next to it the *I-V* curves gotten by the assumed orientation. **b.** Possible orientations of the PSI RC on a functionalized gold surface and the attributed *I-V* curves [20].

PSI had was based on the assumption that tunneling in the reaction centers would proceed preferentially via the electron transport chain, that is, electron transport would have to happen from P700 to the Fe-complexes but would be hindered in the opposite direction. They defined the orientation by comparing the *I-V* traces to their previous results (see Fig. 1.3). Others subsequently observed this behavior in single reaction centers [22] and in SAMs [23]. In 2011, Greenbaum *et al.* made a high electron mobility transistor out of reaction centers [26].

Photosystem I has already been incorporated into actual devices: solar and fuel cells. In 2005, Terasaki *et al.* prepared a novel bio-nanohybrid electrode made from PSI-Au nanoparticles to enhance photocurrent [27]. In 2009, Ciesielski *et al.* developed biohybrid photoelectrochemical cells with dense multilayers of Photosystem I complexes. In 2011 a group from MIT achieved record biophotovoltaic performances: open circuit photovoltage of 0.5 V, fill factor of 71%, electrical power density of 81 mW/cm^2 and photocurrent density of 362 mA/cm^2 [28] (see geometry in Fig. 1.4). In the time following, an organic, biohybrid photoelectrode was fabricated by depositing a multilayer of PSI on a carbon-based electrode. This had the advantage that reduced graphene oxide (RGO) is cheaper than gold and the photocurrent densities are comparable to a PSI-modified gold electrode and

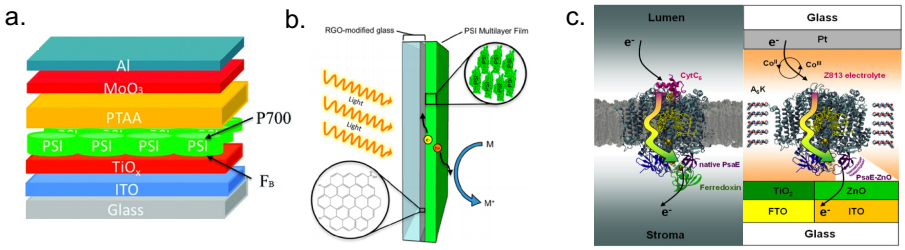

Figure 1.4. a. Structure of solid-state biophotovoltaic cells [31]. **b.** Organic, biohybrid electrode system. Light reaches the PSI multilayer film by passing through the RGO electrode. An electrochemical mediator (M) is used to provide electrons to the PSI film where they are excited and passed on to the RGO electrode [29]. **c.** Schematic of PSI in cellular membrane and in the two types of biophotovoltaic cells [28].

nearly 10 times the photocurrent densities of a PSI-graphene electrode [29]. This group later optimized their devices by using polyaniline/TiO_2. The new geometries yielded an average photocurrent density of 72 mA cm^2, with an approximate open-circuit voltage of 300 mV, and an external quantum efficiency of 0.01% [30]. Lastly, in 2014 Gordiichuk *et al.* [31] constructed an oriented, functional solid-state device for solar energy conversion. The devices were characterized by a large open-circuit voltage and a typical photocurrent action spectrum. Since then, new solid-state devices containing oriented PSI have been made and measured. Chapters 2 and 3 of this thesis provide details of our research on this area.

1.4. *EGaIn in Molecular Electronics*

Contacting biological complexes has always been one of the top challenges when designing bio-devices. In most cases, complexes are too fragile and top electrodes cannot be evaporated or otherwise, chemically deposited onto them. Metals might penetrate the monolayer propitiating shorts, might destroy the monolayer, chemicals might react with the molecules or might denature them as well. Many other techniques have been developed over the years, such as indirect evaporation [32], film transfer (such as the lift-of-float-on method) [33, 34], spin coating, *etc.* with the hanging mercury drop (HMD) being one of the most widely used [35]. Ron *et al.* [36] used HMDs as a non-damaging method for forming top-contacts to measure the electron transfer (ET) through three protein (complexes) on doped-Si substrates: azurin (Az), bacteriorhodopsin (bR), and bovine serum albumin (BSA) establishing that proteins can function as building blocks for bottom-up tunneling junctions. Although non-damaging, Hg is better suited for

Si substrates than metals, with which it tends to form amalgams (Au and Ag are the most common metals used in bottom-up tunneling junctions). These studies on complete proteins were preceded by discussed models of mechanisms of electron transport through peptides and proteins, for example, by Giese *et al.* [37, 38]. Shinawari *et al.* [39] reviewed biomolecular charge transport, with a particular focus on DNA and protein molecules.

In this thesis, we illustrate the first use of the liquid metal eutectic, Ga-In (EGaIn) to measure monolayers of macroscopic biological complexes (it had already been used to contact multiple small-molecule self-assembled monolayers (SAMs)). EGaIn consists of 75% Ga, 25% In by weight and has a melting point of 15.5 °C [40]. This liquid metal can function similarly to Hg in the HMD method, but unlike Hg, it exhibits a non-Newtonian rheology [42], and does not seek to spontaneously minimize its surface energy forming a sphere [41]. Because of the oxide skin that is immediately formed when exposed to oxygen, EGaIn has many interesting rheological properties that allow it to be shaped into stable forms, including small, soft tips to safely contact biological complexes (see Fig. 1.5) [41, 43, 44].

Figure 1.5. "Tips" or top electrodes are created by lowering an EGaIn drop at the tip of a syringe onto a sacrificial substrate. Two conical shapes are formed as the syringe is pulled up. The tip is formed upon breaking.

1.5. *Thesis Outline*

Chapter 2 provides a more detailed information about PSI, EGaIn and the importance of our findings. We expand on our solid-state devices and how the orientation of PSI plays a role in electron transfer and therefore the overall performance of the devices. Since it was the first time that EGaIn was used for the measurement of biological complexes, we also establish the EGaIn tip technique by comparing our results to those of the long-used technique, contact probe atomic force microscopy (CP-AFM). We elucidate the mechanism of transport in tunneling junctions and explain the role of the internal dipole moment. By studying the *J*-*V* curves, we can distinguish a clear rectification ratio (*R*) between devices with most of the complexes facing "up" or "down", that is with the elec-

trons travelling towards the top electrode, or the substrate, respectively. The maximum achieved orientation of PSI is of 70% of the complexes facing "down" thanks to the electrostatical interactions and a short molecule used as linker. In **Chapter 3**, however, we increase such percentage to 98% by making use of an old technique but a new protocol. By making use of the technique phage-display (PD) we engineer short binding-peptides that attach themselves with precision to certain areas of the complexes affording near-perfect control over how PSI orients on ITO (indium tin oxide). In this chapter we characterize the general orientation of the monolayer by making use of the EGaIn tip technique and by comparing the behavior of the single-complexes to that of a monolayer. Similarly as done in Chapter 2 we use R as key parameter of comparison, except we use the difference (Δ) in $\log|R|$ at 1 V to compare the values of a monolayer with only modified peptides vs. monolayers of the peptides with PSI complexes.

In **Chapter 4** I make a slight change of topic by introducing co-fabricated PDMS microchannels and their mechanical properties. This chapter serves as an introduction and as background for the following one (where we introduce our soft, PSI devices). It presents the reader with a step-by-step description of the fabrication starting from the design and photolithographic steps to make rigid Si/SiO_2 masters and then moving on to the actual fabrication of the microchannels. We further explain the filling of the channels with EGaIn and the challenges met in the way until finally tying it together by testing their resilience while testing their electrical properties. This chapter includes as well a special observation about the rheological characteristics of EGaIn when measuring macromolecules. **Chapter 5** is the implementation of the previous one. The idea consists in finding the optimal way to contact and use PSI and its high internal efficiency to make this "ideal" bio-photovoltaic device mentioned at the beginning of this introduction. In this chapter we take the microchannels described and tested in Chapter 4 and investigate different possible materials and configurations. The microfluidic channels in these devices are defined by an array of closely-spaced posts through which chemical reactions can take place when the contents from one channel come in contact with the other. Through these posts, it is also possible to send electrons/holes back and forth from one electrode to the other. We demonstrate a proof-of-concept device which follows the concept of a dye-sensitized solar cell.

References

[1] *Key World Energy Statistics*, Tech. Rep. (International Energy Agency, Paris, France, 2016).

[2] T. Boden, R. Andres, and G. Marland, *Global, Regional, and National Fossil-Fuel CO2 Emissions,* (2015).

[3] J. R. Knowles, *Enzyme-Catalyzed Phosphoryl Transfer Reactions,* Annual Review of Biochemistry **49**, 877 (1980).

[4] R. E. Blankenship, D. M. Tiede, J. Barber, G. W. Brudvig, G. Fleming, M. Ghirardi, M. R. Gunner, W. Junge, D. M. Kramer, A. Melis, T. A. Moore, C. C. Moser, D. G. Nocera, A. J. Nozik, D. R. Ort, W. W. Parson, R. C. Prince, and R. T. Sayre, *Comparing Photosynthetic and Photovoltaic Efficiencies and Recognizing the Potential for Improvement,* Science **332**, 805 (2011).

[5] O. Yehezkeli, R. Tel-Vered, J. Wasserman, A. Trifonov, D. Michaeli, R. Nechushtai, and I. Willner, *Integrated photosystem II-based photo-bioelectrochemical cells,* Nature Communications **3**, 742 (2012).

[6] M. Kato, T. Cardona, A. W. Rutherford, and E. Reisner, *Photoelectrochemical Water Oxidation with Photosystem II Integrated in a Mesoporous Indium–Tin Oxide Electrode,* Journal of the American Chemical Society **134**, 8332 (2012).

[7] R. Carpentier, S. Lemieux, M. Mimeault, M. Purcell, and D. Goetze, *A photoelectrochemical cell using immobilized photosynthetic membranes,* Bioelectrochemistry and Bioenergetics **22**, 391 (1989).

[8] A. J. McCormick, P. Bombelli, A. M. Scott, A. J. Philips, A. G. Smith, A. C. Fisher, and C. J. Howe, *Photosynthetic biofilms in pure culture harness solar energy in a mediatorless bio-photovoltaic cell (BPV) system,* Energy & Environmental Science **4**, 4699 (2011).

[9] M. Torimura, A. Miki, A. Wadano, K. Kano, and T. Ikeda, *Electrochemical investigation of cyanobacteria Synechococcus sp. PCC7942-catalyzed photoreduction of exogenous quinones and photoelectrochemical oxidation of water,* Journal of Electroanalytical Chemistry **496**, 21 (2001).

[10] R. Croce and H. van Amerongen, *Light-harvesting in photosystem I,* Photosynthesis Research **116**, 153 (2013).

[11] A. Nakamura, T. Suzawa, Y. Kato, and T. Watanabe, *Species Dependence of the Redox Potential of the Primary Electron Donor P700 in Photosystem I of Oxygenic Photosynthetic Organisms Revealed by Spectroelectrochemistry,* Plant and Cell Physiology **52**, 815 (2011).

[12] P. N. Ciesielski, F. M. Hijazi, A. M. Scott, C. J. Faulkner, L. Beard, K. Emmett, S. J. Rosenthal, D. Cliffel, and G. Kane Jennings, *Photosystem I – Based biohybrid photoelectrochemical cells,* Bioresource Technology **101**, 3047 (2010).

[13] P. Jordan, P. Fromme, H. T. Witt, O. Klukas, W. Saenger, and N. Krauss, *Three-dimensional structure of cyanobacterial photosystem I at 2.5 A resolution,* Nature **411**, 909 (2001).

[14] K. Brettel, *Electron transfer in photosystem I,* Biochimica et Biophysica Acta (BBA) - Bioenergetics **1507**, 100 (2001).

[15] J. H. Golbeck, *Structure and Function of Photosystem I,* Annual Review of Plant Physiology and Plant Molecular Biology **43**, 293 (1992).

[16] R. Das, P. J. Kiley, M. Segal, J. Norville, A. A. Yu, L. Wang, S. A. Trammell, L. E. Reddick, R. Kumar, F. Stellacci, N. Lebedev, J. Schnur, B. D. Bruce, S. Zhang, and M. Baldo, *Integration of Photosynthetic Protein Molecular Complexes in Solid-State Electronic Devices,* Nano Letters **4**, 1079 (2004).

[17] D. Gerster, J. Reichert, H. Bi, J. V. Barth, S. M. Kaniber, A. W. Holleitner, I. Visoly-Fisher,

S. Sergani, and I. Carmeli, *Photocurrent of a single photosynthetic protein,* Nat Nano **7**, 673 (2012).

[18] I. Carmeli, L. Frolov, C. Carmeli, and S. Richter, *Photovoltaic Activity of Photosystem I-Based Self-Assembled Monolayer,* J. Am. Chem. Soc. **129**, 12352 (2007).

[19] J. Lee, I. Lee, P. Laible, T. Owens, and E. Greenbaum, *Chemical platinization and its effect on excitation transfer dynamics and P700 photooxidation kinetics in isolated photosystem I,* Biophysical Journal **69**, 652 (1995).

[20] I. Lee, J. Lee, and E. Greenbaum, *Biomolecular Electronics: Vectorial Arrays of Photosynthetic Reaction Centers,* Physical Review Letters **79**, 3294 (1997).

[21] I. L. James W. Lee, *Platinization: A novel technique to anchor photosystem I reaction centres onto a metal surface at biological temperature and pH,* Biosensors and Bioelectronics **11**, 375 (1996).

[22] A. Stamouli, J. W. M. Frenken, T. H. Oosterkamp, R. J. Cogdell, and T. J. Aartsma, *The electron conduction of photosynthetic protein complexes embedded in a membrane,* FEBS Letters **560**, 109 (2004).

[23] T. Mikayama, K. Iida, Y. Suemori, T. Dewa, T. Miyashita, M. Nango, A. T. Gardiner, and R. J. Cogdell, *The Electronic Behavior of a Photosynthetic Reaction Center Monitored by Conductive Atomic Force Microscopy,* Journal of Nanoscience and Nanotechnology **9**, 97 (2009).

[24] L. Frolov, Y. Rosenwaks, C. Carmeli, and I. Carmeli, *Fabrication of a Photoelectronic Device by Direct Chemical Binding of the Photosynthetic Reaction Center Protein to Metal Surfaces,* Advanced Materials **17**, 2434 (2005).

[25] B. Reiss, D. Hanson, and M. Firestone, *Evaluation of the Photosynthetic Reaction Center Protein for Potential Use as a Bioelectronic Circuit Element,* Biotechnology Progress **23**, 985 (2007).

[26] S. A. Eliza, I. Lee, F. S. Tulip, S. Mostafa, E. Greenbaum, M. N. Ericson, and S. K. Islam, *Isolated Photosystem I Reaction Centers on a Functionalized Gated High Electron Mobility Transistor,* IEEE Transactions on NanoBioscience **10**, 201 (2011).

[27] N. Terasaki, N. Yamamoto, T. Hiraga, I. Sato, Y. Inoue, and S. Yamada, *Fabrication of novel photosystem I–gold nanoparticle hybrids and their photocurrent enhancement,* Thin Solid Films **499**, 153 (2006).

[28] A. Mershin, K. Matsumoto, L. Kaiser, D. Yu, M. Vaughn, M. K. Nazeeruddin, B. D. Bruce, M. Graetzel, and S. Zhang, *Self-assembled photosystem-I biophotovoltaics on nanostructured TiO2 and ZnO,* Scientific Reports **2** (2012), 10.1038/srep00234.

[29] E. Darby, G. LeBlanc, E. A. Gizzie, K. M. Winter, G. K. Jennings, and D. E. Cliffel, *Photoactive Films of Photosystem I on Transparent Reduced Graphene Oxide Electrodes,* Langmuir **30**, 8990 (2014).

[30] E. A. Gizzie, J. Scott Niezgoda, M. T. Robinson, A. G. Harris, G. Kane Jennings, S. J. Rosenthal, and D. E. Cliffel, *Photosystem I-polyaniline/TiO $_2$ solid-state solar cells: simple devices for biohybrid solar energy conversion,* Energy Environ. Sci. **8**, 3572 (2015).

[31] P. I. Gordiichuk, G.-J. A. H. Wetzelaer, D. Rimmerman, A. Gruszka, J. W. de Vries, M. Saller, D. A. Gautier, S. Catarci, D. Pesce, S. Richter, P. W. M. Blom, and A. Herrmann, *Solid-State Biophotovoltaic Cells Containing Photosystem I,* Adv. Mater. **26**, 4863 (2014).

[32] H. Haick, J. Ghabboun, and D. Cahen, *Pd versus Au as evaporated metal contacts to molecules,* Applied Physics Letters **86**, 042113 (2005).

[33] F. Milani, C. Grave, V. Ferri, P. Samorì, and M. A. Rampi, *Ultrathin -Conjugated Polymer Films for Simple Fabrication of Large-Area Molecular Junctions,* ChemPhysChem **8**, 515 (2007).

[34] H. B. Akkerman, P. W. M. Blom, D. M. de Leeuw, and B. de Boer, *Towards molecular electronics with large-area molecular junctions,* Nature **441**, 69 (2006).

[35] W. D. Ellis, *Anodic stripping voltammetry,* Journal of Chemical Education **50**, A131 (1973).

[36] I. Ron, L. Sepunaru, S. Itzhakov, T. Belenkova, N. Friedman, I. Pecht, M. Sheves, and D. Cahen, *Proteins as Electronic Materials: Electron Transport through Solid-State Protein Monolayer Junctions,* Journal of the American Chemical Society **132**, 4131 (2010).

[37] B. Giese, M. Graber, and M. Cordes, *Electron transfer in peptides and proteins,* Current Opinion in Chemical Biology **12**, 755 (2008).

[38] B. Giese, S. Eckhardt, and M. Lauz, *Electron Transfer in Peptides and Proteins,* in *Encyclopedia of Radicals in Chemistry, Biology and Materials*, edited by C. Chatgilialoglu and A. Studer (John Wiley & Sons, Ltd, Chichester, UK, 2012).

[39] M. Waleed Shinwari, M. Jamal Deen, E. B. Starikov, and G. Cuniberti, *Electrical Conductance in Biological Molecules,* Advanced Functional Materials **20**, 1865 (2010).

[40] R. Chiechi, E. Weiss, M. Dickey, and G. Whitesides, *Eutectic Gallium–Indium (EGaIn): A Moldable Liquid Metal for Electrical Characterization of Self-Assembled Monolayers,* Angewandte Chemie International Edition **47**, 142 (2008).

[41] M. D. Dickey, R. C. Chiechi, R. J. Larsen, E. A. Weiss, D. A. Weitz, and G. M. Whitesides, *Eutectic Gallium-Indium (EGaIn): A Liquid Metal Alloy for the Formation of Stable Structures in Microchannels at Room Temperature,* Adv. Funct. Mater. **18**, 1097 (2008).

[42] L. Cademartiri, M. M. Thuo, C. A. Nijhuis, W. F. Reus, S. Tricard, J. R. Barber, R. N. S. Sodhi, P. Brodersen, C. Kim, R. C. Chiechi, and G. M. Whitesides, *Electrical Resistance of* Ag^{ts}*–*$S(CH_2)_{n1}CH_3$*//*Ga_2O_3*/EGaIn Tunneling Junctions,* The Journal of Physical Chemistry C **116**, 10848 (2012).

[43] C. A. Nijhuis, W. F. Reus, J. R. Barber, M. D. Dickey, and G. M. Whitesides, *Charge Transport and Rectification in Arrays of SAM-Based Tunneling Junctions,* Nano Letters **10**, 3611 (2010).

[44] J.-H. So and M. D. Dickey, *Inherently aligned microfluidic electrodes composed of liquid metal,* Lab on a Chip **11**, 905 (2011).

1

-

2

The Mechanism of Tunneling Junctions Comprising Photosystem I

What is a scientist after all?
It is a curious man looking through a keyhole,
the keyhole of nature, trying to know what is going on.

JACQUES YVES COUSTEAU

Parts of this chapter have been published in J. Am. Chem. Soc., 2015, 137 (26), pp 8419-8427.
P. Gordiichuk carried out all single molecule experiments. S. Catarci and D. A. Gautier isolated and prepared PSI solutions.

2

Abstract

This chapter describes the measurement of the asymmetry of current transport of self-assembled monolayers (SAMs) of the photosystem I (PSI) protein complex, on two different "director SAMs" supported by ultra-flat Au substrates. The director SAMs induce the preferential orientation of PSI, which manifests as asymmetry in tunneling charge-transport. We measured the oriented SAMs of PSI using eutectic Ga-In (EGaIn), a large-area technique, and conducting probe atomic force microscopy (CP-AFM), a single-complex technique, and determined that the transport properties are comparable. By varying the temperatures at which the measurements were performed (from 298 to 198 K), we found that there is no measurable dependence of the current on temperature from ± 0.1 *to* ± 1.0 *V bias, and thus, we suggest tunneling as the mechanism for transport; there are no thermally activated processes. Therefore, it is likely that relaxation in the electron transport chain is not responsible for the asymmetry in the conductance of SAMs of PSI complexes in these junctions, which we ascribe instead to the presence of a large, net dipole moment present in PSI.*

2.1. *Introduction*

There are two basic strategies for constructing devices in which the flow of electrons is mitigated by single molecules: top-down and bottom up. Top-down methods rely on nanofabrication or mechanical control to form the nanometer-scale junctions between "top" and "bottom" electrodes necessary to contact molecules end-to-end. Bottom-up methods typically rely on the self-assembly of molecules onto a bottom electrode in which the junction is defined by the molecules themselves when a top electrode (top-contact) is applied; these are devices that, in part, fabricate themselves [1]. Nature provides a plethora of intricate molecular complexes that form by and are prone to self-assembly, however, these complexes are subject to different constraints than their simpler, synthetic counterparts such as the well-studied alkanethiols [2]. Conventional techniques for forming top-contacts for devices or for measuring electrical properties over large areas of self-assembled monolayers (SAMs) of organic molecules have been thus far limited to the direct deposition of metals [3] by electron-beam or thermal evaporation or the addition of an electrically conductive polymer layer between the SAM and a metallic top contact [4, 5]; however, in these techniques, the high temperatures, vacuum processing and the need for acidic or organic solvents to spin coat the polymers are not ideal for biomacromolecules. Other, "soft", non-damaging methods for forming top-contacts, such as the use of hanging Hg drops [6] (HMDs), are better suited to this task [7, 8]. A recent progress report by Amdursky *et al.* [9] compares current densities for different techniques, including conducting-probe atomic force microscopy (CP-AFM), scanning tunneling microscopy (STM) and macroscopic, for junctions comprising proteins and small molecules.

The liquid metal eutectic, Ga-In (which we abbreviate "EGaIn"; 75% Ga, 25% In by weight, m.p.=15.5 °C), can function similarly to Hg in the HMD method, but does not amalgamate [10]. It also exhibits non-Newtonian rheology, driven by a self-limiting oxide [12], and does not spontaneously reorganize to minimize its surface energy [11]. Thus, it can be formed into stable, non-spherical tips to form 100 μm^2 contacts and is stable in microfluidic channels, which facilitates variable-temperature measurements [11, 13, 14].

Photosystem I (PSI) is a complex that houses one of the two reaction centers used in the photosynthetic reactions in cyanobacteria, algae and plants where the conversion of solar energy to electron hole pairs takes place. Isolated PSI complexes from thermophilic unicellular cyanobacterium *Thermosynechococcus elongatus BP-1* have evolutionally formed a trimer structure for improved light absorption efficiency and stability at harsh conditions. The monomer of PSI has a polar stroma and lumen and an apolar backbone. Its size is approx. 13 x 8 x 9 nm

and contains 96 light sensitive Chlorophyll *a* (Chl*a*) molecules that are densely packed in the protein scaffold [15] to harvest light. In the complex, harvested photons are converted into excited electrons by chlorophylls at P700 (via a special pair of Chl*a* molecules). This transfer occurs from the primary electron donor complex to the primary electron acceptor A_0, to the ferredoxine (F_D) docking region through the built-in electron transport chain A_1 (phylloquinone), F_X, F_A and F_B (Fe_4S_4 clusters) (Fig. 2.1a). The complex has a photovoltage of 1 V under illumination with an internal quantum efficiency close to unity [16, 17]. These features make PSI a unique and interesting protein complex to study.

We investigated the *J-V* characteristics of SAMs of PSI in the dark on template-stripped Au [18] measured by forming top-contacts from tips of EGaIn. EGaIn has been used to measure current density *(J)* versus applied voltage *(V)* through SAMs of a variety of molecules to form rectifiers [13, 19–21], to observe quantum interference effects [22], to relate dipole moments to vacuum-level shifts [23], and it is sensitive enough to resolve the odd-even effect in SAMs of alkanethiolates [24, 25]. Unlike SAMs of small molecules, however, there are no data from EGaIn tunneling junctions of PSI or any other protein complexes against which to compare. Thus, we characterized SAMs of PSI trimers by interrogating the complexes in the dark, one at a time, by conducting-probe atomic force microscopy (CP-AFM) and compared those data to the ensemble averages produced by EGaIn contacts in order to relate our findings to previous studies. We use the asymmetry of the conductance data (*i.e.*, rectification) to elucidate the orientation of PSI because it is self-referencing and, therefore, is less sensitive than the magnitude of *J* to other structural features of the SAM, but very sensitive to the specific geometry of the SAM/EGaIn interface [26] (*e.g.*, orientation). Asymmetry observed in current transport is particularly useful for elucidating the transport properties of protein complexes, which are vastly more complex in structure, size, self-assembly and electrical properties than small molecules, because it eliminates the uncertainty of area calculations that arises from topology, packing density, *etc* [20]. And while virtually all tunneling junctions with EGaIn top contacts show some asymmetry (because the junction itself is asymmetric), the rectifying behavior of the SAM is readily distinguishable [27]. We are not suggesting that SAMs of PSI make particularly good rectifiers of current—the magnitude of the asymmetry of the current is quite small—only that small changes in asymmetry can provide information about the orientation of PSI complexes.

Photosystem I can be anchored in a "down" orientation in which the natural flow of photo-generated electrons is to the electrode surface (F_B down), an "up" orientation where electrons would flow in the opposite direction (P700 adja-

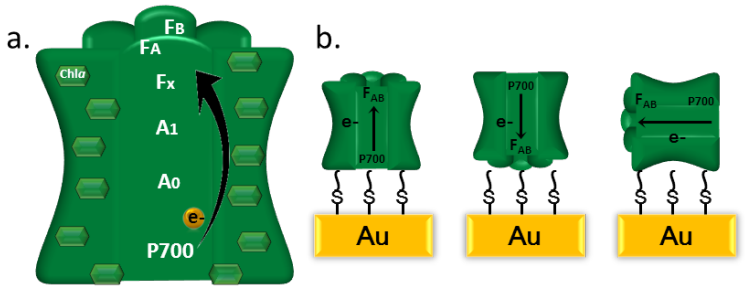

Figure 2.1. a. Schematic representation of electron transfer chain in Photosystem I (ET Chain). **b.** Possible orientations of PSI on Au surfaced induced by chemical modification. Photosystem I can be anchored in an "up" orientation where the flow is in the opposite direction (P700 adjacent to substrate), a "down" orientation in which the natural direction of the flow of electrons is towards the electrode surface (F_B down), or with its electron transport vector parallel to the substrate.

cent to substrate), or with its electron transport vector parallel to the substrate (Fig. 2.1b). This level of control over the orientation of the electron transport chain provides an opportunity to determine its role in the tunneling transport through PSI through the self-assembly process rather than by modifying the complexes themselves. Different methods have been used to control the orientation of PSI and RCI on surfaces, ranging from surface modification with different functional groups that interact electrostatically with different parts of the protein complex, to direct covalent attachment via mutation [28] and SAMs with different functional head groups [29, 30]. With EGaIn, we can address the monolayers of PSI complexes electrically and from these electrical measurements we can probe the average orientation of the complexes in the monolayer to compare against AFM images and CP-AFM *I-V* data.

According to previous reports on single complexes of RCI (*i.e.*, not SAMs or ensembles and not PSI), asymmetric charge transport is completely dependent on the orientation on the surface of the electrode. Greenbaum and co-workers [31, 32] were the first to observe this behavior. They platinized one end of the photosynthetic complex and "welded" it to a Au surface using SAMs of small molecules as "director" monolayers [29]. They used scanning tunneling spectroscopy (STS) to examine the electronic properties of each RCI, which elicited orientation-dependent asymmetry. Others subsequently observed this behavior in RCI as single complexes [33] and in SAMs [30]. This phenomenon is easily conflated with light-driven processes [34], which involves *hopping* transport (to move through the transport chain as the electron changes in energy) and therefore

should not play a role in *tunneling* measurements. Yet, the absolute orientation of RCI and, by extension, PSI is assigned from STS data based on the assumption that the direction of asymmetry (rectification) follows the electron transport chain [31, 32]. By measuring tunneling junctions comprising PSI in the dark, we found that this assignment of the orientation does not, in fact, map onto PSI—it is backwards—and that tunneling transport, therefore, likely dominates any hopping contribution from the electron transport chain.

2.2. *Fabrication - Short Linkers*

We thermally deposited a 120 nm-thick layer of gold (Au 111) onto a technical-grade 3" silicon wafer supporting a native oxide layer (Si/SiO_2). We fabricated the substrates by template stripping (TS) [18], where a drop of ultraviolet (UV)-curable optical adhesive (OA) was used to adhere a 1 x 1 cm piece of glass to a pre-prepared gold coated wafer. The glass was then mechanically cleaved exposing an ultra-flat Au surface with a root-mean-squared roughness of 0.3 nm (as measured using tapping-mode AFM).

We exposed the Au^{TS} substrates to a solution of 1mM 2-mercaptoethanol (2ME) or sodium 3-mercapto-1-propanesulfonate (MPS) (Scheme 2.1) to direct the PSI complexes to adopt a down or up orientation (F_B iron-sulfur cluster adjacent or away from substrate) [29, 30, 35]. The time of immersion was limited to 2 h to avoid the formation of multilayers or aggregates. After this step, were rinsed the substrates with MQ water (MPS) or ethanol (2ME), dried them with nitrogen and incubated them in a previously prepared PSI solution. The PSI solution consisted of 1:1 in buffer A (20 mM HEPES (pH 7.5); 10 mM $MgCl_2$; 10 mM $CaCl_2$; 500 mM Mannitol with 0.05% DDM (n-Dodecyl-β-D-maltoside)) for 2 h. They were then rinsed with MQ water and dried with nitrogen. We immobilized PSI on the substrates by drop casting from aqueous buffer and incubating them (*i.e.*, leaving them in contact) for 2 h. We investigated each SAM topographically by AFM and electrically using CP-AFM and EGaIn. The CP-AFM data are averages of *I-V* curves from 100 complexes for each director SAM. Thus, they sample the distribution of orientations similarly to the large-area EGaIn measurements and can be compared directly.

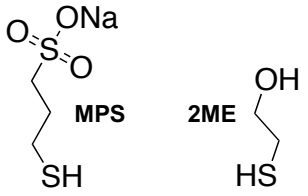

Scheme 2.1. Chemical structures of the director molecules: 2-mercaptoethanol (2ME) and sodium 3-mercapto-1-propanesulfonate (MPS). They direct the PSI complexes to adopt a down or up orientation (F_B iron-sulfur cluster adjacent or away from substrate), respectively.

2.3. *Results*

These director SAMs differ in length by 1.7 Å, which may affect the magnitude of the tunneling current, but we do not rely on this magnitude as a measure in this work and small changes in the thickness of the director SAM are unlikely to influence asymmetry. The PSI in cyanobacteria has an asymmetric distribution of surface charges in the stroma and lumen (see Appendix for details). Two thirds of all the charged surface residues are concentrated at the "top" of the complex; the stromal, F_{AB} electron acceptor side (Fig. 2.1a). This difference is likely what determines the preferred orientation during self-assembly on modified surfaces. We define the asymmetry of current transport (rectification ratio), R, as the ratio of J or I at positive to negative bias; $R = |J(-)/J(+)|$ for EGaIn and $R = |I(-)/I(+)|$ for CP-AFM, both with respect to the wiring convention for CP-AFM (see Appendix). Measured AFM height profile images show better PSI coverage for 2ME than for MPS, with protein heights close to 6 nm on Au^{TS} (this value is less than the 9 nm thickness derived from the crystal structure data because these SAMs are measured under ambient, anhydrous conditions). We imaged individual PSI trimers within SAMs of PSI formed on both director SAMs by AFM to determine the density (per μm^2) and measured their electrical properties by CP-AFM to determine the orientation of the complexes, assigning low values of R to PSI that is oriented up and high values to down. Values of unity were assigned to PSI that is oriented parallel to the substrate (sideways). The results are summarized in Table 2.1 and the average values of R for EGaIn and CP-AFM are given in Table 2.2. Individual I-V traces were averaged over 100 PSI complexes at different locations within the SAMs.

For EGaIn measurements, the SAMs of PSI on both director SAMs were contacted by lowering a syringe (connected to an electrometer) supporting a tip of EGaIn. Recent reports on EGaIn junctions comprising alkanethiolates employ

Director SAM	Up (%)	Down (%)	Sideways (%)	Coverage (PSI trimer/μm^2)
MPS	57	18	25	723
2ME	11	69	20	853

Table 2.1. Percentage of average orientation of PSI depending on the different director SAMs. The results were obtained by measuring the asymmetry of the *I-V* curves by CP-AFM. The average coverage on an area of 1μm^2 was calculated from AFM height images. The table summarizes the statistical distributions of the *I-V* curves of over 100 points for both director SAMs.

	R (±1 V)	
Method	MPS	2ME
EGaIn	2.0	5.0
CP-AFM	0.8	1.8
EGaIn (Deactivated PSI)	0.9	1.0

Table 2.2. Rectification ratio (R) of devices by method of measurement. R is defined as the ratio of J or I at positive to negative bias; $R = |J(-)/J(+)|$ for EGaIn and $R = |I(-)/I(+)|$ for CP-AFM, both with respect to the wiring convention for CP-AFM.

a slightly different method in which the tips are first flattened against a Si wafer and then pressed into the SAM [36], however, light contact with as-prepared tips yielded stable and reproducible results on SAMs of PSI. We observed four different behaviors: (i) shorts, characterized by linear *J-V* curves with currents in the μA regime; (ii) no contact, characterized by noisy currents in the pA regime; (iii) poor contact, which begins with noisy, no-contact *J-V* curves, but is followed by shorts after further lowering of the EGaIn tip; and (iv) good contact, characterized by S-shaped *J-V* curves of reproducible, low-noise currents. The yield of working devices (good contacts) was higher than 70%. These data are summarized in Table 2.3 and show higher rectification ratio when 2ME is used as opposed to MPS, which we ascribe to the different distributions of orientations of PSI induced by the director SAMs. We analyzed the data identically to the CP-AFM data by averaging log *J*.

Charge-transport Occurs Through Intact PSI Complexes

As control experiments, we measured the electrical properties of denatured PSI. We boiled PSI for 20 min at 99 °C, which is sufficient to denature it completely

Method	SAM	J (A/cm^2)	Yield (%) Good Contact	Short/No Contact	Poor Contact
EGaIn PSI	2ME	1.69 E-04	74	9	17
EGaIn PSI	MPS	1.48 E-03	72	14	14
Deact. PSI	2ME	1.87 E-04	100	0	0
Deact. PSI	MPS	1.57 E-04	100	0	0
No PSI	2ME	2.04	-	-	-
No PSI	MPS	0.020	-	-	-

Table 2.3. Characterization of junctions by director SAM, method, complex, current density (J) and percent yield of working junctions. Junctions with good contacts produced S-shaped J-V curves of reproducible, low-noise currents. Shorts produced linear J-V curves with currents in the μA regime. No contact were characterized by noisy currents in the pA regime; and poor contact, began with noisy J-V curves followed by shorts.

and then prepared SAMs of deactivated PSI by following the same procedures used to prepare SAMs of active PSI. We observed no rectifying behavior in EGaIn junctions comprising boiled PSI, nor did we observe shorts (Table 2.3). The lack of shorts implies that denatured PSI still covers the substrate, as SAMs of 2ME and MPS are fragile and give mostly shorts. Thus, the origin of the asymmetry is dependent on the presence of intact PSI structures (*i.e.*, the overall asymmetry of the junction depends on the presence of intact complexes of PSI). We varied the density (surface coverage) of the SAMs of PSI by preparing PSI trimer solutions of different concentrations (dilutions from 1:1 to 1:130) while keeping the incubation time fixed. From AFM images, we determined the surface coverage by comparing the PSI-covered surface to the total surface area; $\chi_{PSI} = [N \cdot A_{PSI}/A_{total}] \cdot 100\%$, where N is the number density of PSI, A_{PSI} is the area occupied by PSI complexes (25 nm, determined from TEM), A_{total} is the total area investigated. Fig. 2.2 shows the correlation between χ_{PSI} and the magnitude of J in EGaIn junctions. The exponential relationship between J and surface coverage is further evidence that the charges are flowing through the PSI complexes. Below 23% coverage the junctions become unstable, irreproducible, and yield mostly shorts (as do bare director SAMs). Presumably this percentage is the cutoff value below which EGaIn is able to penetrate between the PSI complexes and contact the director SAM (see Chapter 4). This behavior is not unlike defect-mediated transport in which the electrical properties of highly conductive defects (space between PSI complexes) become dominant at a critical density [37]. The saturation of J at 23% implies that transport occurs exclusively through PSI and that there is no (or constant) leakage

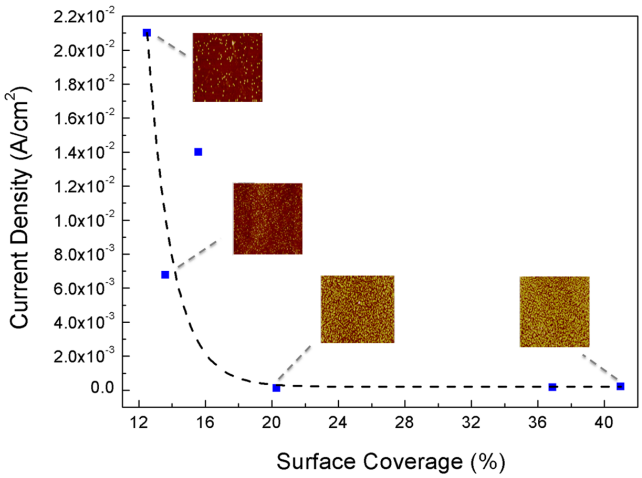

Figure 2.2. Asymptotic fit of J at 1 V vs. percentage of surface coverage for PSI on 2ME as director SAM. The blue squares are the experimental points. The threshold limit of coverage is 23% as determined by imaging surfaces at different PSI:buffer concentrations and characterizing their behavior with an EGaIn tips. Inset images show PSI complexes on Au^{TS} at different concentrations which correspond to the percent coverages shown. The devices were imaged on an AFM at 2.5 µm.

current, which allows the direct comparison of the data from EGaIn and CP-AFM junctions.

To evaluate the influence of contact with tips of EGaIn, we marked areas of the SAMs of PSI and imaged them by AFM before and after forming EGaIn junctions and acquiring *J-V* data (see Appendix). We observed no qualitative damage to the monolayers and, by counting the number of complexes in each junction before and after forming EGaIn junctions, determined that no complexes were removed from the monolayer. From these experiments, we conclude that the SAMs of PSI are not damaged and that the individual complexes do not move and are not removed during measurement. Thus, EGaIn is a demonstrably non-damaging method for investigating charge-transport through SAMs of PSI and is capable of forming reversible junctions, which may be useful for characterizing SAMs of PSI (or other protein complexes) as an intermediate step in the fabrication of devices to, for example, verify the orientation of the complexes.

PSI Rectifies Current

The rectifying behavior of RCI (not PSI) was previously observed by STM [29] and CP-AFM [30] on individual protein complexes. In our studies with EGaIn, PSI assembled on director SAMs exhibited an asymmetric conductance between

bias voltages with $R = 5.0$ with 2ME and 2.0 with MPS (Table 2.2). The direction of rectification does not invert when the orientation of the complexes is reversed because there is some built-in asymmetry in these junctions; the bottom electrode supports a covalently bound director SAM that supports the PSI complexes, while the top-contact is physisorbed either via contact with an AFM tip or by supporting an EGaIn electrode. Thus, one orientation works with the built-in asymmetry and the other against it, but not sufficiently to overcome it completely. We ascribe the asymmetry in both cases to the ratio of the orientation of the complexes (Table 2.1). An important distinction between single-complex studies (*e.g.*, CP-AFM and STM) and large-area studies (*e.g.*, EGaIn and HMD) is that the latter sample the average orientation. Coupled with the ability to measure many locations across many different substrates, large-area measurements are useful for characterizing the self-assembly of PSI (or any protein with direction-dependent rectification). Additionally, the non-damaging nature of EGaIn makes it a useful tool for investigating SAMs of PSI during the fabrication of a thin-film device, for example, a photovoltaic device, the properties of which are dominated by the average orientation of PSI [38–40]. Single-complex measurements provide details that are difficult or impossible to extract from large-area measurements, thus the combination of the two gives a complete picture, capturing the details of transport through individual complexes and the supramolecular structure of the SAM. Although it is clear that the relative orientation of RCI and PSI is influenced by the chemistry at the surface of the bottom electrode (Au^{TS} in our case), the absolute orientation of either has not been determined unambiguously. It was observed that RCI preferentially platinizes at one side, which was assumed to occur at the more polar (electron accepting) side of the complex [31].

Despite the lack of direct evidence, this one study has become the reference point for the absolute orientation of RCI and, by extension, PSI. Our data were acquired on SAMs of PSI, which has a different electrostatic profile than RCI and therefore does not necessarily orient identically to RCI. We propose two possible mechanisms for rectification. The first is that charges (electrons or holes) take advantage of the electron transport chain or directly traverse it; both mechanisms involve thermally activated hopping processes. These mechanisms (it is not clear specifically which) are used to infer the absolute orientation of RCI and predict higher values of R when PSI is oriented up. The second mechanism assumes that tunneling charges do not hop through electron transport pathway and the rectification is instead driven by the large dipole moment of the whole PSI structure between the luminal and the stromal surface (*i.e.*, perpendicular to the substrate when PSI is in the up or down orientation). Van Haeringen *et*

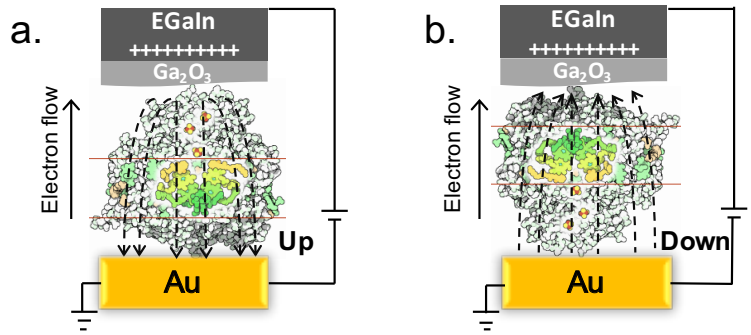

Figure 2.3. The direction of the electrical field (dashed lines) that arises from the PSI dipole moment within PSI-EGaIn devices, which are shown with EGaIn biased positively (with respect to the normal wiring of EGaIn). The direction of this field goes from negative to positive in the complex. **a.** When PSI is oriented "up", the electric field from the applied bias opposes the internal electric field of the PSI complexes. **b.** When PSI is oriented "down", the direction of the internal electric field is the same as the applied bias. Thus, this mechanism predicts that PSI in the down orientation will give higher values of *R*.

al. used linear dichroism to elucidate the dipole moment within the structure of trimeric PSI [41]. The direction of the dipole is parallel to the C3-symmetry axis of the protein trimer complex, with positive side of the dipole moment on the luminal side and negative on the stromal side. The dipole effect within PSI trimers was also observed on solid-state bulk heterojunction (BHJ) solar cells with a work function shift [38]. There, a monolayer of PSI trimers was self-assembled at a metal-oxide electrode rather than Au. The electric field of this dipole moment can either enhance or oppose the total field created by biasing the electrodes as is shown in Fig. 2.3. This mechanism would show higher values of *R* when PSI is oriented down. Although we have no way to observe the absolute up/down orientations of PSI directly, we can assign the absolute orientation by determining which mechanism (the electron transport chain or the internal electric field) is more likely. First, however, we must establish that CP-AFM and EGaIn are in agreement in order to relate our observations to previous reports (which exist for CP-AFM, but not for EGaIn).

EGaIn and CP-AFM Data are Directly Comparable

Although the influence of the native oxide layer on EGaIn has been thoroughly studied on aliphatic SAMs and has been shown to have a negligible influence on transport properties [12], it is necessary to confirm that the same holds true for protein complexes. Due to the size of complexes of PSI, we are able to isolate individual complexes for CP-AFM measurements, meaning that the calculation

of per-complex resistivity is unambiguous. For EGaIn junctions, we know the density of PSI complexes and the measured contact area, A_{geo}, but not the actual contact area, A_{eff}, which is considerably smaller due to the topology of the EGaIn tip [36]. Thus, we can calculate the number of complexes in A_{geo}, compute the resistance and determine the correction factor to relate A_{geo} and A_{eff}. If the oxide is benign in this study, this correction should be comparable to the values reported for aliphatic SAMs. For a given EGaIn junction, we considered every oriented PSI complex as a resistor in parallel. We calculated the resistance of individual complexes (R_i) from average values of I from CP-AFM measurements at 1 V (range of 10^9 to 10^{10} Ohms depending on the orientation). The resistance, R_{obs}, is the total resistance of the circuit and, at $V = 1V$, is the reciprocal of the current calculated for an area with n number of complexes, allowing the calculation of n from Eq. 1 where I_{EGaIn} is the measured current of an EGaIn/Ga_2O_3//PSI junction.

$$\frac{V}{R_{obs}} = I_{EGaIn} = \sum_{1}^{n} \frac{1}{R_i} \tag{2.1}$$

The values of n given by Eq. 1 are 4.5 and 2.2 x 10^2 for 2ME and MPS, respectively. Using these values of n, we calculated A_{eff} from the densities of PSI complexes shown in Table 1. From the measured value of A_{geo}, Eq. 2 gives the overestimation of the area, α.

$$\frac{A_{geo}}{A_{eff}} = \alpha \tag{2.2}$$

From this calculation we find $\alpha \sim 10^3$, which is consistent with the values of 10^4 that have been observed for aliphatic SAMs [36, 42]. Thus, using the per-complex conductivity determined by CP-AFM and the magnitude of the current obtained from large-area measurements with EGaIn, we arrive at a value of α that is within a factor of 10 of previously reported values. This result shows that the contact resistance associated with the physisorbed electrode-PSI interface is comparable for EGaIn/Ga_2O_3 and a Pt-Ir CP-AFM tip and, therefore, that the influence of the oxide layer on charge-transport is negligible (*i.e.*, it does not contribute to R_{obs} more than a CP-AFM tip); CP-AFM and EGaIn data are comparable. This results is unsurprising in the context of existing studies on SAMs of alkanethiolates [27], but it is necessary to establish the benign nature of the oxide specifically in junctions incorporating proteins.

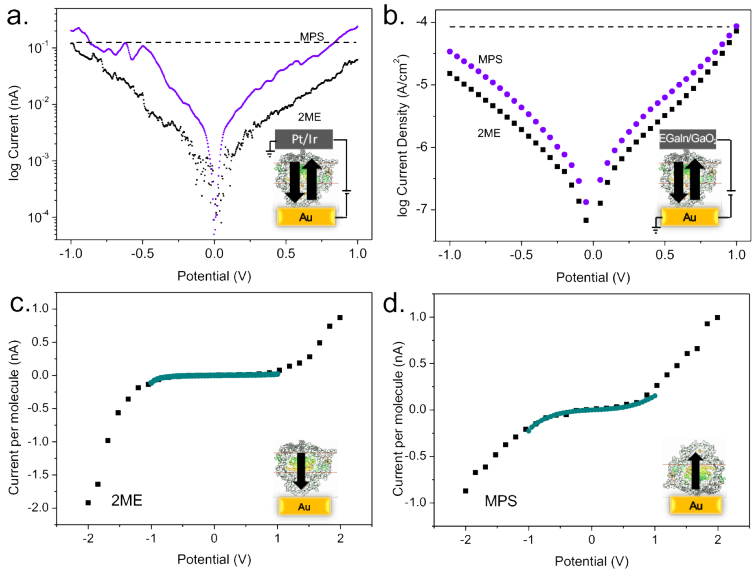

Figure 2.4. Semi-log plots of current and current density versus voltage for junctions measured using **a.** CP-AFM and **b.** EGaIn for SAMs of PSI on MPS (purple) and 2ME (black). The black arrows indicate the orientation of the PSI complexes on the surface. The horizontal, dashed lines guide the eye. Per-complex *J*-*V* curves for SAMs of PSI on **c.** 2ME and **d.** MPS, measured by CP-AFM (black) and EGaIn (green) plotted with respect to the standard wiring of CP-AFM.

Using our computed value of α, we plotted the per-complex current-densities from CP-AFM and EGaIn (Fig. 2.4 c and d). The values of R from EGaIn are in agreement with the values of R from CP-AFM data, but Fig. 2.4c and d also show a qualitative agreement between the line shapes. For comparison reasons, we added the averaged *I*-*V*, *J*-*V* curves with respect to the original wiring for CP-AFM and EGaIn, respectively (Fig. 2.4 a and b).

While EGaIn junctions cannot be scanned past ±1 V without precipitating shorts (from electrostatic pressure), CP-AFM junctions can be scanned further because the height of the tip is fixed by the instrument rather than the SAM of PSI. Thus, while the CP-AFM and EGaIn data are in remarkably close agreement at ±1 V, we cannot know for certain that they would not diverge at higher potentials.

The Mechanism of Charge-transport is Tunneling

Cahen and co-workers have shown, using HMDs, that the electrical properties of junctions comprising metalloproteins are affected by the removal of the metal centers [43]. These studies show that tunneling electrons can take advantage

of the accessible states of the metal centers. In studies of RCI (not PSI) where rectification is observed, the mechanism is almost always ascribed to the electron transport chain [29–33], however, no evidence is offered to support or refute that hypothesis. Previous studies have shown that, when the electron transport chain is deliberately engaged, the rate of electron transfer in RCI is higher from P700 to F_{AB} (forward) than in the reverse direction [31, 44], which could explain the diode-like behavior seen in the *J*-*V* curves [32]. The two most straightforward experiments for establishing the mechanism are removing the electron transport chain variable-temperature studies. The former is not possible without substantially influencing the structure of RCI/PSI and the latter is not possible with the techniques that have been used to study RCI thus far. Fortunately, the (remarkable) robustness of SAMs of PSI *in vacuo* [38] extends to sufficiently low temperatures to enable variable-temperature studies using microfluidic channels filled with EGaIn in a crossbar configuration [11].

One of the most robust rectifying tunneling junctions comprises ferrocene-terminated SAMs on Ag with EGaIn top-contacts [13, 19, 20]. The mechanism of rectification in these SAMs is the (partial) pinning of the HOMO of the ferrocene to EGaIn, which pushes it either into or out of resonance with a Ag^{TS} electrode depending on the sign of the applied potential on EGaIn; when it moves into resonance (negative potential), charges tunneling onto the HOMO and then hops onto the EGaIn, shortening the effective tunneling distance. This mechanism was proven by Arrhenius plots (ln |*J*| vs. 1/T), which clearly show the "freezing out" of the hopping component, leading to the loss of rectification at temperatures below the activation energy of the hopping process [13]. If the mechanism of rectification in PSI involves thermally-activated hopping processes in the electron transport chain, it should freeze out as well. Thermally-activated transport processes have also been observed in CP-AFM studies of long conjugated molecules [45, 46] and proteins such as azurin [47, 48], ferritin [49], and cytochrome [50] at elevated temperatures. We did not collect transport data above room temperature, but at low temperature we observed comparable results. Thus, there may be temperature-dependent transport pathways at elevated temperatures, but they do not contribute to the asymmetric transport at room temperature.

If the mechanism of rectification in our PSI junctions involves the electron transport pathway then it must also involve a hopping process, as the electrons change energy inside the complexes; moving with the electron transport chain (downhill) then leads to higher values of *J* than against it (uphill) at a particular value of |*V*|. If, however, the mechanism of rectification is the interaction of the applied field with the built-in field of the collective dipole moments of the PSI

complexes, the process is entirely tunneling; the rectification arises from the different probabilities of tunneling from left to right and right to left. The former mechanism, therefore, will show a loss of rectification at low temperatures as the hopping processes are frozen out, while the latter will be completely independent of temperature.

We fabricated microfluidic devices following literature procedures and acquired *J*-*V* traces at different temperatures. An Arrhenius plot of ln |*J*| at ±0.50 V for PSI on both director SAMs is shown in Fig. 2.5 (the raw data are shown in the Appendix.) The magnitude of *R*, shown by the difference in the magnitude of *J* at positive and negative bias, is invariant with temperature. The values of ln |*J*| are also nearly invariant, showing only a slight perturbation only near room temperature. These data are unambiguous evidence that the mechanism of charge transport through SAMs of PSI on MPS and 2ME is independent of temperature and, therefore, that the mechanism of rectification does not involve hopping and/or the electron transport chain. From this conclusion, we can ascribe an absolute orientation of PSI; it is oriented "down" (P700 adjacent to the EGaIn substrate) on 2ME and "up" on MPS. Thus, the direction of rectification is exactly opposite to the natural flow of electrons through the electron transport chain, which predicts higher currents at positive bias (with respect to EGaIn) when P700 is adjacent to the EGaIn electrode. An energy level diagram based on Nakamura's *et al.* observation [17] is shown in Fig. 2.6. It not only predicts that asymmetry will be more pronounced in the "up" orientation, but that $R < 1$. Note that this diagram is drawn with respect to the normal wiring of EGaIn and is, therefore, backwards from the wiring convention of CP-AFM. The distances between co-factors were estimated with the software PyMOL from a crystal structure of PSI taken from the Protein Data Bank (1JB0).

A common test for tunneling transport is to compare the decay coefficient, β, against literature values. This value is obtained from Simmons' approximation, $J = J_0 e^{-\beta d}$, where d is distance between the electrodes and β is obtained by varying d. This study is not possible with PSI because d is fixed by the complex at 6 nm. Ron et al. estimated β by comparing I in the presence and absence of a protein, arriving at values of 0.18, 0.12, and 0.27 $Å^{-1}$ for three different proteins on Si surfaces modified with octadecyltrimethoxysilane [43]. Using the same analysis, we arrive at a value of 0.16 for PSI on 2ME and 0.08 $Å^{-1}$ for PSI on MPS with Δd = 60 Å, values of J taken from Table 2.3.

To gain more experimental insight into the mechanism of rectification, we measured the transport properties of bovine and human serum albumin (BSA and HSA), which have been studied extensively [47, 50, 50–52].

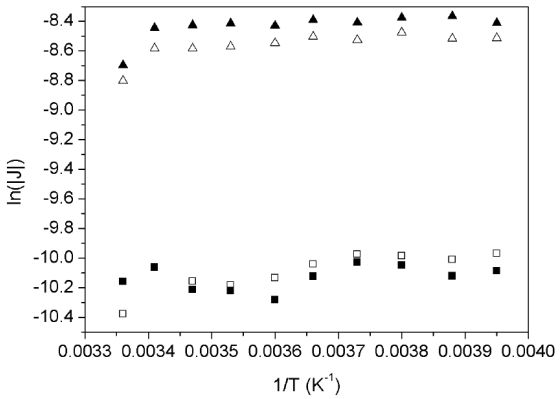

Figure 2.5. ln $|J|$ at ±0.50 V as a function of inverse temperature for PSI on director SAMs of MPS (triangles) and 2ME (squares). The solid symbols represent the positive bias (+0.50 V) and hollow represent the negative bias (-0.50 V). The linearity indicates that the mechanism of charge transport is dominated by tunneling as no temperature dependence was observed.

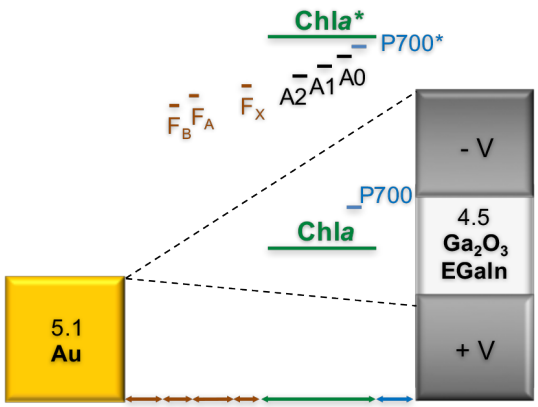

Figure 2.6. Energy level diagram across Au^{TS}-PSI($P700/F_B$)//(Ga_2O_3)/EGaIn junctions (drawn with respect to the wiring of EGaIn junctions). The barrier width is defined by the thickness of a oriented PSI complex in the "down" orientation with respect to the natural direction of electron flow. The sizes of the constituents (denoted by the bottom arrows) are 1.5 nm, 0.6 nm, 1.3 nm, 0.5 nm, 4.1 nm and 1.0 nm (left to right). The green lines are the frontier orbital energies of the chlorophyll molecules, which are distributed evenly through the thickness of the PSI complex. The black lines represent the energies of the electron transport chain and their relative spatial positions.

We observed $R \sim 5.5$ and 3.0 on 2ME and MPS, respectively (see Appendix). This observation can only be reconciled using the mechanism of rectification proposed in this paper, given that SAMs of BSA and HSA show preferential ordering [53] and that they contain only alpha helices, which contribute to a collective dipole moment. It also explains the observation by Ron *et al.* that BSA rectifies on Br-terminated Si surfaces using HMD electrodes [43].

2.4. *Conclusions*

We have established a clear relationship between the average orientation of PSI (not RCI) in SAMs and the asymmetry (rectification) of current in metal/protein/metal junctions on template-stripped Au surfaces modified with director SAM. Asymmetry is a useful observable for capturing the complexities of assemblies of large, biological molecules, particularly in combination with single-complex measurements, which are insensitive to collective properties, but which provide details that are missed by large-area methods. The average orientation is affected by the identity of the director SAM used to control the surface chemistry of the substrate. Through variable-temperature measurements we have established that the dominant mechanism of charge-transport through SAMs of PSI on Au is likely tunneling and that, at the very least, it does not involve thermally activated transport. This observation refutes the hypothesis that rectification is due to the natural direction of the flow of electrons through the transport chain, which involve thermally-activated processes, and instead is likely the result of the internal electric field that arises from the collective action of dipoles (and multipoles) in the peptide backbone. It opposes the natural direction of electron flow through the electron transport pathway and therefore predicts that 2ME preferentially orients PSI "down" and MPS "up" with respect to the direction of the flow of electrons through the transport chain in vivo; *i.e.*, with P700 adjacent to the EGaIn substrate. This assignment of the orientations of PSI is in agreement with solid-state, thin-film devices comprising PSI (not RCI) that is oriented by modifying the surface of the bottom electrode [38, 40].

2.A. *Appendix*

All reagents and solvents were purchased from commercial sources and used without further purification unless otherwise indicated.

2.A.1. Data Acquisition - EGaIn Tips

For room-temperature measurements, a junction is first formed by slowly bringing the EGaIn tip into contact with the protein monolayer with the use of a manual micro-controller. The source-meter is set at a 1 V fixed bias and once the current is stable, an *I-V* sweep is performed from -1 V to 1 +V; 5-10 traces are recorded. The camera is fixed on the EGaIn tip and the diameter of the junction is measured on-screen. Exceeding the current threshold value of 105 μA produces Ohmic *I-V* curves and means that the junction has shorted and data is not recorded. Noisy, hysteretic currents lower than 5 nA indicate "no-contact" behavior. To have representative data points, this procedure is repeated until the data from at least five working junctions per substrate is recorded across several substrates. The aggregate datasets comprise data acquired on different days, across different devices, and from different batches of PSI. Although the actual contact area is smaller than what we can optically see [36], this discrepancy is systematic and therefore not corrected for except when otherwise noted.

2.A.2. Data Processing and Analysis

The software used for the gathering and analysis of the data comprise homemade LabView scripts for acquiring raw data and Python scripts that employ SciPy for data analysis. The raw *J-V* traces are manually filtered to prune the no-contact traces and shorts by line-shape and magnitude, which interfere with calculations of the asymmetry ratio; *e.g.*, if a junction shorts mid-trace, the apparent value of R will be on the order of 10^5. The values of J are aligned to their corresponding values of V and the average of $\log|J|$ is computed. This methodology (including the exclusion of short- and open-circuit graces) is in accordance with standard practices for CP- AFM. Histograms of unfiltered values of $\log|J|$ at ±1 V are shown in Fig. 2.7, demonstrating that the asymmetry of the *J-V* curves is statistically significant and distinct for 2ME and MPS director SAMs. We analyzed the statistical significance of R in accordance with previous studies on ferrocene-terminated SAMs [13, 19, 20] by comparing the histograms of $\log R$ for PSI junctions on 2ME and MPS director SAMs using tips of EGaIn at room temperature that are shown in Fig. 2.8. Although there is a greater spread in the values for 2ME than MPS, there is a statistical difference. The peak values (Gaussian means) are also in agreement with the values taken from the averaged data for EGaIn tips, EGaIn crossbars (at variable temperatures) and CP-AFM Table 2.3.

To contextualize our results, we converted the EGaIn-derived data to units of A/nm^2 and compared the value with those of Amdursky *et al.* [50]. We obtained a value of $\pm 10^{-18}$ A/nm^2, which is in good agreement with other macroscopic

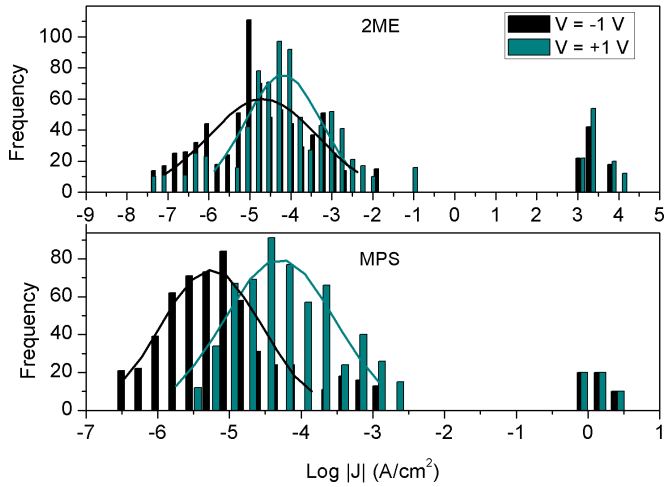

Figure 2.7. Histograms of log |*J*| for PSI junctions on both director SAMs measured using EGaIn tips. The black and green histograms are the counts for log |*J*| at -1 V and +1 V respectively. Top PSI oriented with 2ME, bottom with MPS.

measurement techniques (Fig. 2.9).

2.A.3. Optimization of Monolayer Formation

Previous studies have shown that PSI tends to aggregate when the orienting layer has gone through immersion/incubation times over 2 h [30]. Thus, we conducted control experiments by incubating Au substrates in solutions of 2ME and MPS from 1 h to 4 h and overnight to study the effect on PSI coverage and the variation in *J*. The results are shown in Fig. 2.10 and demonstrate that aggregation is not a problem even when the director SAM is formed at immersion times exceeding 3 h; the difference in *J* is within error. From this study, we chose an optimal incubation time for 2ME and MPS of 2 h with 2 h immersion time for PSI. Fig. 2.11 shows the difference in *J* at optimal times for both orienting layers.

2.A.4. Variable Temperature Experiments

Soft Device Fabrication for Variable Temperature Studies

We vacuum deposited Ag and Au through a stencil mask of three parallel electrodes onto a 3" Si/SiO_2 wafer. The resulting 200 nm thick electrodes were 300 µm wide, 9000 µm long and had round pads (d=1500 µm) at their ends to facilitate addressing the electrodes with probes. The Si/SiO_2 wafer with the metal lines was functionalized with 1H, 1H, 2H, 2H-perfluorooctyl-trichlorosilane by gas

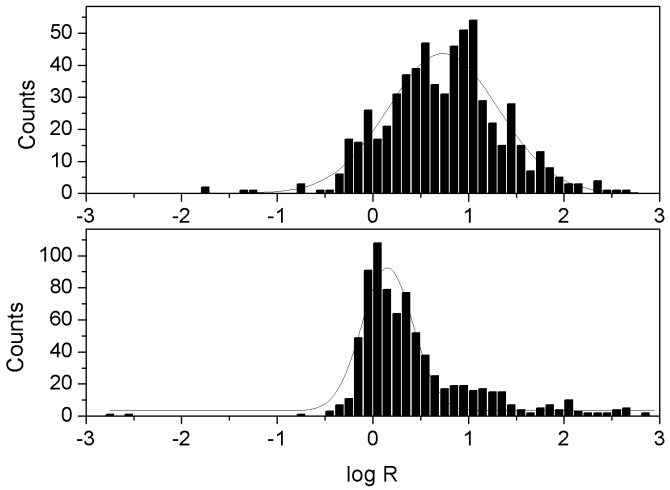

Figure 2.8. Histograms of log *R* for PSI junctions on both director SAMs measured using EGaIn tips; 2ME (top) and MPS (bottom).

deposition to minimize its interaction with the optical adhesive. The electrodes were then template-stripped onto clean 2 x 1.5 cm glass substrates to reduce the number of defects in the layer. We immersed each substrate in a solution of 2ME or MPS overnight, then washed them with ethanol and DI water. We then placed the electrodes on a solution of PSI for 2 h. The devices were then carefully rinsed with DI water and dried with nitrogen. We positioned PDMS microchannels (50 µm deep, 300 µm wide, 10000 µm long, inlet/outlet, d=1000 µm) perpendicularly to the electrodes to form a crossbar structure of EGaIn/PSI/Metal. The structures bonded with the substrate without any further steps. We filled a microchannel by gently injecting a drop of EGaIn through the inlet with the help of a metallic precision syringe and applying reduced pressure to the outlet of the channel. A schematic of the devices can be seen in Fig. 2.12.

Measurements

The temperature dependent measurements were performed on a custom-built cryogenic probe station in vacuum (pressures varied between 6 x 10^{-7} and 3 x 10^{-6} mbar). The devices were slowly cooled down and their J-V characteristics were measured from 298 to 198 K. We biased the Ga_2O_3//EGaIn top electrodes and grounded the MetalTS bottom electrode. Using the area defined by the stencil mask and PDMS channels, we measured J as a function of V at intervals of 5 K, allowing the devices to stabilize before performing each scan. We fabricated 3-6

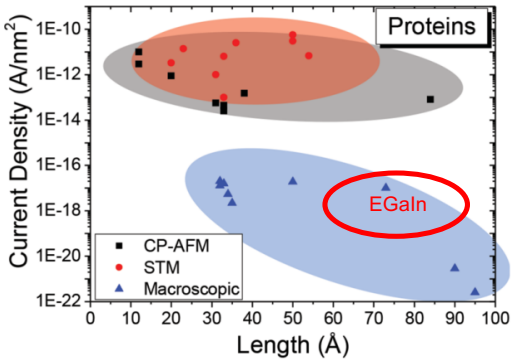

Figure 2.9. Summary of previous experiments for proteins for both nanometer-scale and macroscopic according to the review by Amdursky *et al.* [9]. Current densities of the EGaIn-PSI junctions are in the same order of magnitude as other macroscopic techniques (red circle).

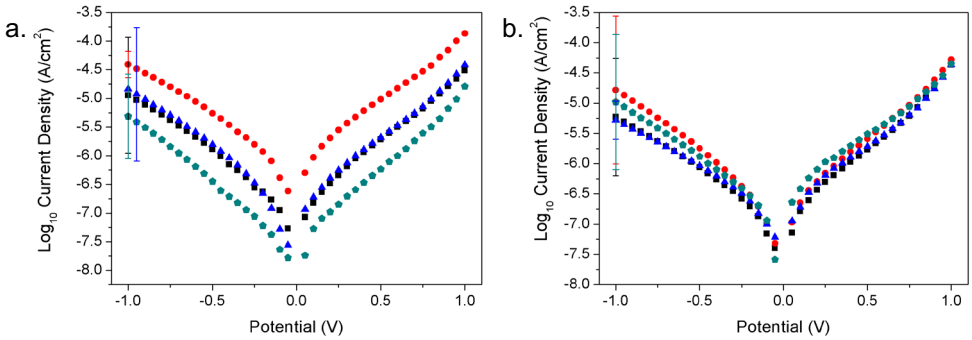

Figure 2.10. Log_{10} current density (J) vs. bias voltage (V) of **a.** PSI on 2ME-modified Au surface and **b.** PSI on MPS-modified Au surface. Graphs show the results from optimization experiments to determine the effect of SAM immersion time on current density (J). Devices were immersed on solution containing the orienting SAM for 1 h (black squares), 2 h (red circles), 3 h (blue triangles) and overnight (green polygons) and 2 h PSI.

devices for each type of orienting SAM (2ME, MPS) and measured 1 of each at a time. The average of working junctions of PSI on Au was ~50%. Every scan of a junction was recorded individually and the aggregate dataset treated identically to the room temperature data as described above. We biased from -1 V to +1 V at steps of 0.02 V with a delay of 0.1 to 0.2 s). The raw data and complete Arrhenius plots are show in Fig. 2.13 - Fig. 2.15.

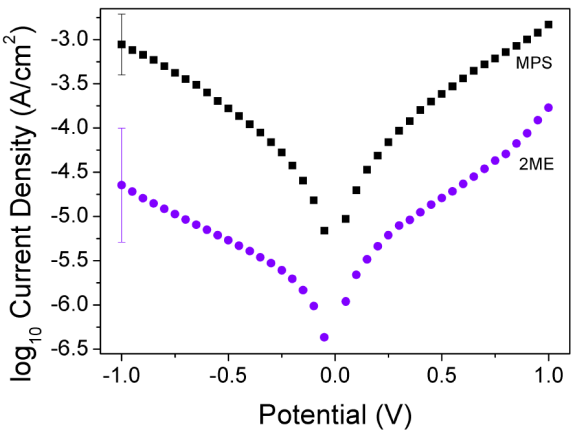

Figure 2.11. Log_{10} current density (J) vs. bias voltage (V) of PSI on Au surface modified with orienting SAMs of MPS (black squares) and 2ME (purple circles) obtained by taking the geometric average of J for each value of V.

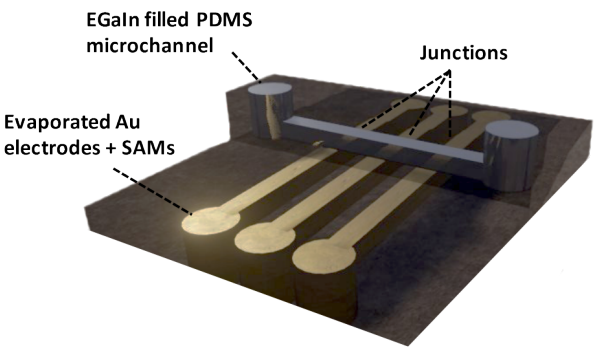

Figure 2.12. Schematic of microfluidic devices used for variable temperature studies. A junction consists of Au^{TS}/orienting SAM/PSI/EGaIn. Orienting SAM and PSI monolayers are grown on Au just like on solid-state devices. EGaIn is injected into the microfluidic channel.

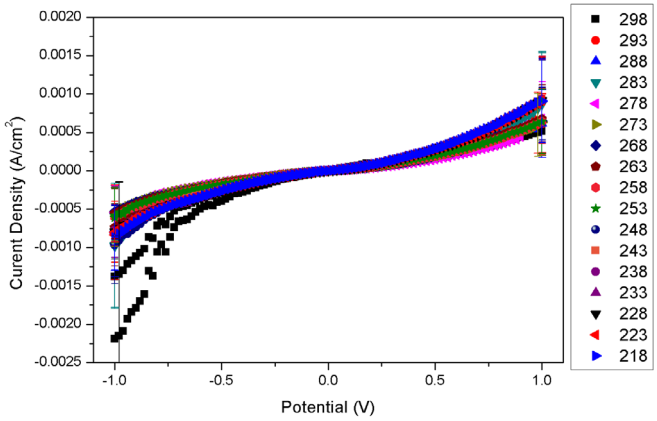

Figure 2.13. Current density (J) vs. bias voltage (V) of PSI on microfluidic device of Au surface modified with orienting SAMs of 2ME. These curves represent the average of the measured devices at 17 different temperatures in vacuum. The error bars indicate the standard deviation. Hysteresis is observed at high temperatures but diminishes with the number of scans.

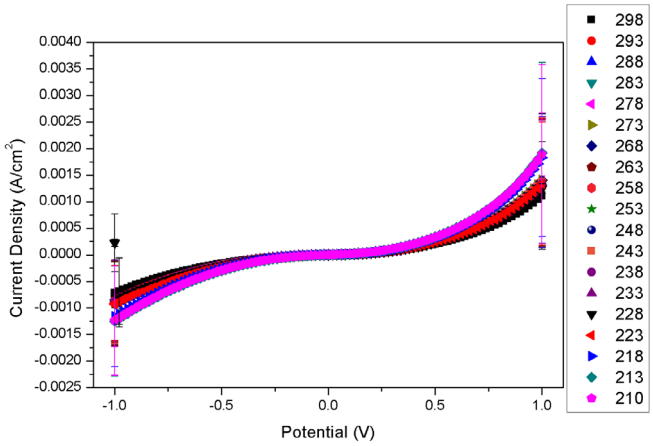

Figure 2.14. Current density (J) vs. bias voltage (V) of PSI on Microfluidic device of Au surface modified with orienting SAMs of MPS. These curves represent the average of the measured devices at 17 different temperatures in vacuum. The error bars indicate the standard deviation. Hysteresis is observed at high temperatures but diminishes with the number of scans.

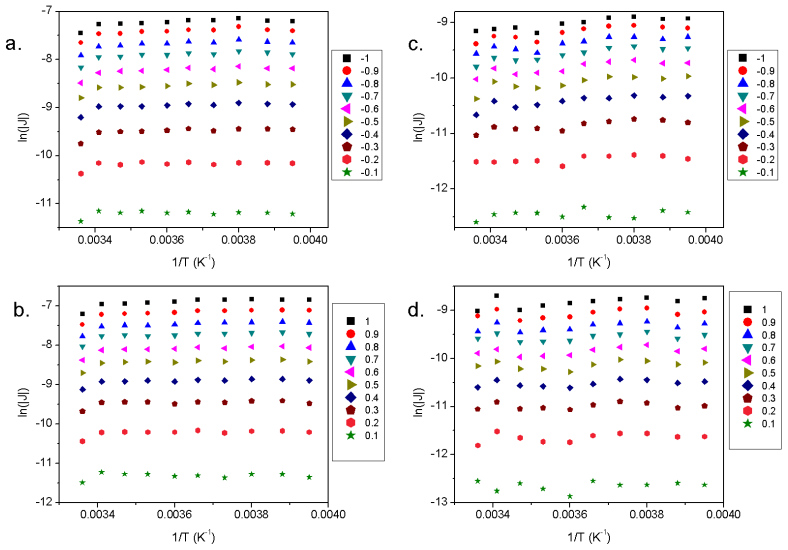

Figure 2.15. Arrhenius plot of junctions for the ln |*J*| as a function of the inverse of the temperature in the range from ±0.1 V to ±1.0 V. Figures **a.** and **b.** represent the data from junctions with MPS as orienting SAMs whereas **c.** and **d.** represent the data when using 2ME. The linearity indicates that the mechanism of charge transport is dominated by tunneling in both biases and for both orientations as the dependence on temperature was negligible.

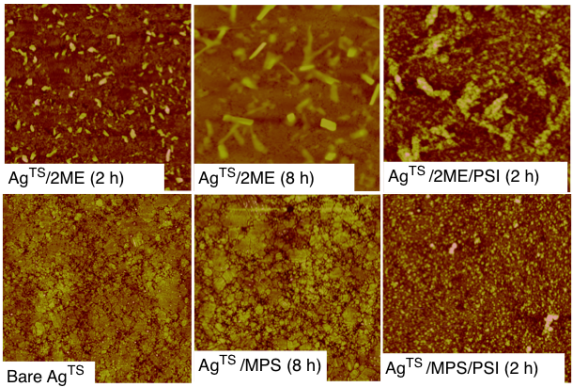

Figure 2.16. Tapping-mode AFM images of Ag^{TS} substrates. All images are 5 x 5 µm. From left to right, top row; After incubating with 2ME for 2 h (left); After incubating with 2ME for 8 h (center); After incubating with 2ME for 8 h and then PSI for 2 h (right). Bottom row; Bare Ag^{TS} as-prepared (left); After incubating with MPS for 8 h (center); After incubating with MPS for 8 h and then PSI for 2 h (right). These images clearly show the formation of undesirable clusters when Ag^{TS} is exposed to 2ME. These clusters negatively impact the self-assembly of PSI and do not form with MPS.

We initially fabricated soft devices for variable-temperature measurements using template-stripped silver (Ag^{TS}), but observed no asymmetry of PSI on 2ME at any temperature. We investigated the substrates by AFM and found that 2ME forms clusters on Ag^{TS}, presumably due to hydrogen bonding or rearrangement of the metal surface that is allowed by the specifics of the packing of 2ME on Ag, but not on Au. After 8 h of incubation with 2ME the Ag^{TS} films appeared opalescent, suggesting that the clusters involve the rearrangement of Ag or AgO and are distributed randomly across the entire substrate. These clusters in turn cause PSI to form clusters instead of the uniform distribution of complexes that we observe for 2ME and MPS on Au^{TS} as is shown in Fig. 2.16. The loss of asymmetry implies that this clustering behavior also leads to the randomization of the orientation of PSI; other than deliberate controls (*e.g.*, boiling PSI) the only junctions that did not show any kind of asymmetry were those comprising PSI on Ag^{TS} with a 2ME director SAM. However, we cannot say for certain that the structure of the director SAM is the only factor. The work function of Ag is closer to EGaIn than Au, thus the overall asymmetry of the junction and, therefore, its magnitude, will be influenced by this difference. Still, it is interesting to note that ordered SAMs of 2ME do not appear to form on Ag and SAMs of PSI formed on these badly-formed director SAMs do not show any asymmetry.

2.A.5. Control Experiments

AFM Imaging

Membrane proteins under natural conditions are surrounded by the bilayer of the membrane and are stabilized by a hydrophobic, lipid microenvironment. When such complexes are immobilized on a surface, they can undergo partial denaturation. In general, it is difficult mimic natural conditions for AFM measurements. To solve this problem, membrane proteins can be crystallized in films with close packing where they have better stability and are less sensitive towards AFM tip induced deformations [43]. This method is used as a general approach to confirm protein structures and their intrinsic parameters. More accurate studies of protein sizes can be done by optimized AFM measurement techniques [53], but are out of scope in our studies. The relatively large size of the PSI complexes enables the extraction of meaningful information from straightforward AFM measurements (unlike SAMS of small-molecules, which cannot be resolved by AFM). Degradation and damage to the monolayer (down to the resolution of a single missing complex) is readily apparent by AFM. We formed junctions with EGaIn tips on SAMs of PSI and cycled them repeatedly, marking the perimeter around the area of the SAMs underneath the tip and then imaged these areas by AFM. These images are shown

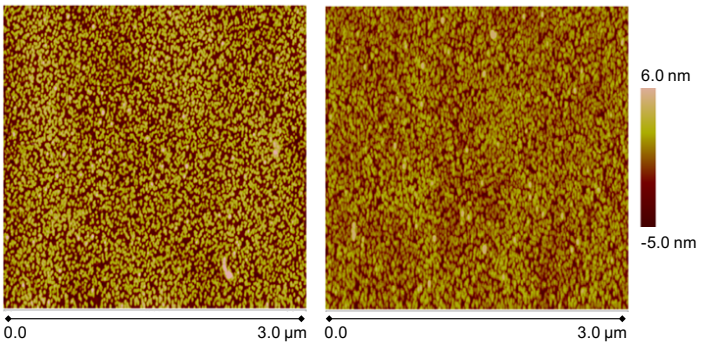

Figure 2.17. AFM height maps of PSI monolayer after electrical measurements. 2ME (left), MPS (right).

in Fig. 2.17, in which there is no detectible damage to the SAMs of PSI or any sign of residual EGaIn or Ga_2O_3.

Wiring

To account for the difference in wiring conventions between CP-AFM, in which the tip is grounded and the substrate is biased and EGaIn, in which the tip is biased and the substrate grounded, we reversed the wiring on our EGaIn setup and recorded *J-V* curves. Curves from the normal and reverse wiring are shown in Fig. 2.18; they mirror each other. Thus, in experiments in which we compare CP-AFM and EGaIn, we reverse the *J-V* curves. We chose this approach over performing the measurements with the wiring reversed to avoid the additional complexity of using a non-standard wiring when making comparisons to the literature, in which the wiring is standard.

Deactivating PSI

We deactivated PSI by performing a series of boiling experiments. Three PSI solutions were subjected to different heat treatments. Each Eppendorf tube (with 70 µl of PSI solution) was placed on a Thermomixer. The temperature was first ramped to 99 °C and then kept constant. Solution 1 was exposed for 10 min at this temperature, and solution 2 and 3 to 20 and 30 min, respectively. We formed a monolayer of these solutions on substrates with SAMs of 2ME and MPS grown and treated identically as with active PSI. We then studied the electrical characterization with EGaIn. We found that PSI was already deactivated by 20 min (we could tell this by the lack of asymmetry from both curves with both orienting SAMs). The resulting curves for devices made from Solution 2 can be seen in Fig. 2.19.

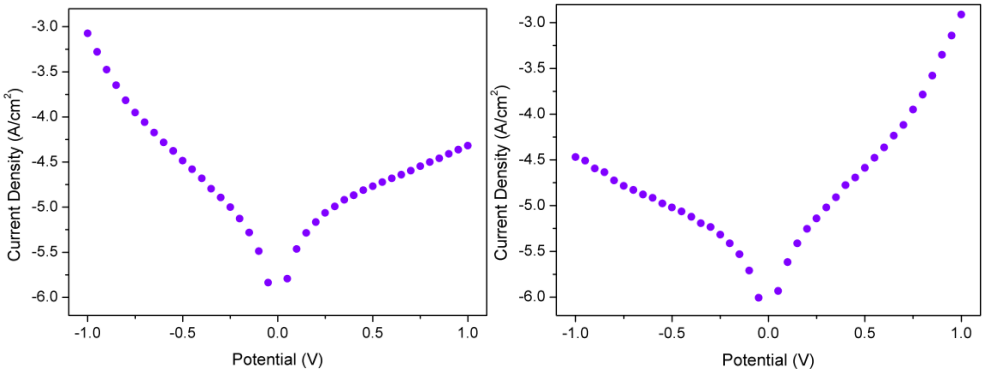

Figure 2.18. Log_{10} current density (J) vs. bias voltage (V) of PSI on Au surface modified with orienting SAMs of 2ME. Left: average of several scans where the top contact (EGaIn) is grounded and the substrate (Au) is biased. Right: opposite set up which is the normal wiring in all of our experiments.

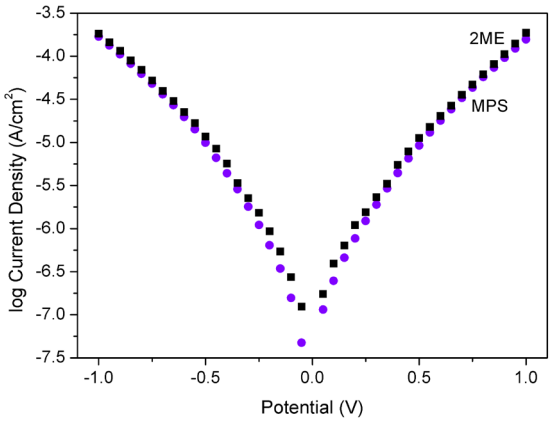

Figure 2.19. Log_{10} current density (J) vs. bias voltage (V) of deactivated PSI on treated Au surfaces with orienting SAMs of 2ME (black squares) and MPS (purple circles). The photosystem used in these devices was deactivated by boiling a PSI solution at 99 °C for 20 min.

2.A.6. Other Biological Complexes

A common control experiment when working with proteins and protein complexes is to substitute serum albumin for the protein/complex being investigated. Both BSA and HSA are simple proteins comprising only alpha helices that are extraordinarily well characterized. This control, however, is not so straightforward with tunneling junctions because, as was reported (in the Supporting Information) by Cahen and co-workers, it strongly rectifies when measured via HMD [43]. We measured BSA on 2ME and MPS by following the same procedure we used to investigate PSI with tips of EGaIn. These data are shown in Fig. 2.20. Not only do BSA and HSA rectify current, the magnitude of J shows the same difference with the two linkers that is observed in the (averaged) J-V data for PSI. The latter observation supports the hypothesis that the rate of tunneling across the director SAM/substrate interface is sufficiently different to appear in the J-V data of PSI on 2ME and MPS. The former observation only makes sense according to the mechanism of asymmetric charge transport that we proposed for PSI (*i.e.*, the collective influence of dipole moments). While it is not as readily observed as it is for PSI, albumins adopt a preferred orientation in SAMs [53]. They also exhibit a large, collective dipole moment that is apparently capable of inducing asymmetry.

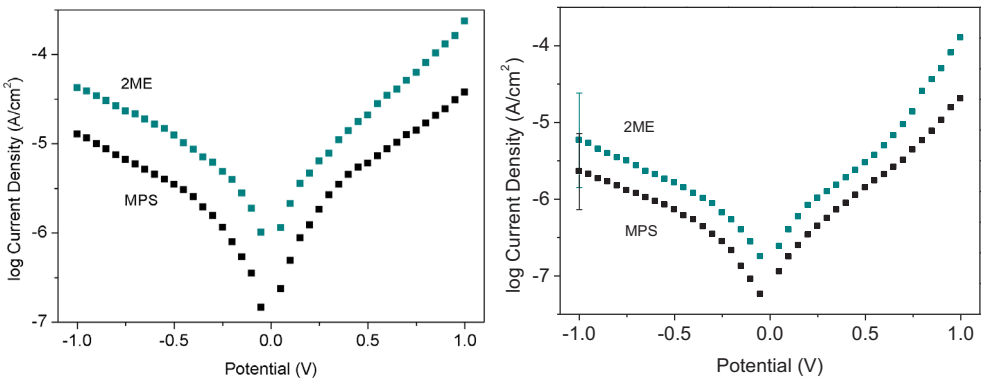

Figure 2.20. Log_{10} current density (J) vs. bias voltage (V) of a monolayer of BSA (left) and HSA (right) on SAMs of 2ME and MPS. The orientation of BSA and HSA on a Au substrate is not known, however, rectification is observed when monolayers of different molecules are used between the metal and the complex. The values of J shift equally between 2ME and MPS, thus the values of R are independent of the directing SAMs.

2.A.7. Conductance Plots

Temperature-independent current and asymmetry is a strong evidence for tunneling-dominated transport, but it is still informative to look at other qualitative measures of tunneling. Fig. 2.21 shows conductance heat map plots; voltage is shown on the x-axis, log|*dJ/dV*| is shown on the y-axis, and the colors correspond to the heights of the histograms at each x-y coordinate (increasing from blue to yellow). A qualitative test for tunneling is the shape of these plots, which should be approximately bowl-shaped, indicating that the junctions become less resistive as a function of increasing bias, as the electrodes come into resonance with states in the gap. By contrast, hopping transport shows distinct regions (*i.e.* low-bias and space-charge) and ohmic transport is a line with zero slope.

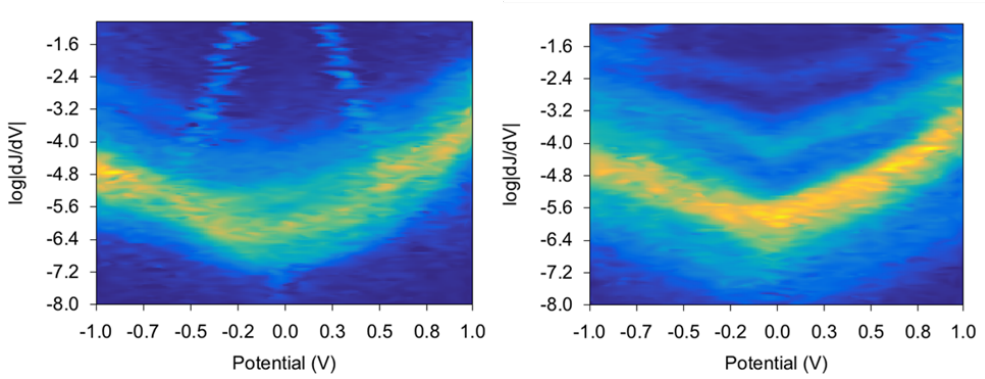

Figure 2.21. Conductance plots for 2ME (left) and MPS (right) showing the bowl-shaped curve that is expected for tunneling transport. The colors correspond to the heights of the histograms at each X/Y coordinate, going from blue to yellow. The difference in *R* is difficult to discern because the data are plotted on a semi-log scale.

2.A.8. Complex Viability and Charge Distribution

Oxygen Consumption Measurement

The electron transport rates of purified PSI complexes were monitored by measuring the light- induced oxygen consumption based on the Mehler reaction [54]. Measurements were obtained with an OXELP oxygen electrode (World Precision Instruments GmbH, Germany) at ambient temperature. After PSI was diluted with reaction buffer [30 mM HEPES (pH 7.5); 3 mM $MgCl_2$; 50 mM KCl; 330 mM mannitol; 0.03% DDM] to a final Chl a concentration of 4 µg/ml, methyl viologen [final concentration: 6 mM], 2,6-Dichlorophenolindophenol [160 µM] and sodium ascorbate [2 mM] were added to the reaction. In order to ensure that the observed oxygen consumption is due to PSI activity, the PSII specific inhibitor

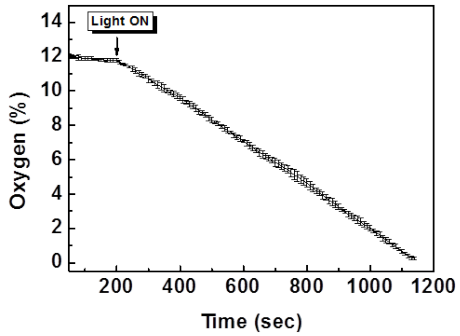

Figure 2.22. Oxygen consumption of PSI in Mehler reaction [54]. Under illumination, the PSI complexes cause a decrease in the oxygen concentration in the buffer.

3-(3,4-dichloro-phenyl)-1,1- dimethyl-urea [10 µM] was present at all times. At first, the solution was stirred in the dark until a stable oxygen concentration was measured (usually 5 min). The assay was started by illumination with actinic light and, subsequently, the oxygen consumption was monitored. Calibration of the setup was realized by measuring total currents of oxygen –versus nitrogen– saturated assay buffer. The results are shown in Fig. 2.22.

Charge Distribution Calculation

The charge distribution on the surface of PSI was calculated with the software PyMOL by employing the structure from the Protein Data Bank. The charge distribution in the PSI protein complex is depicted in Fig. 2.23.

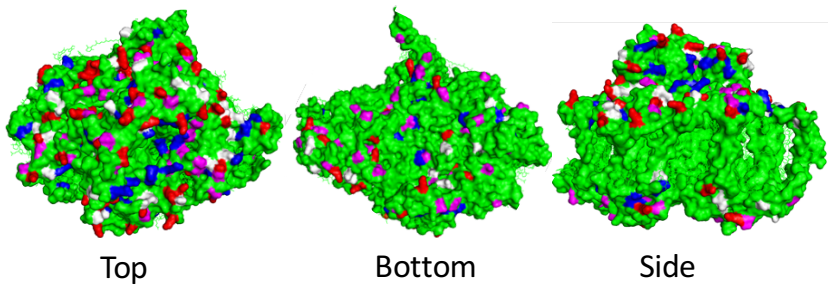

Figure 2.23. PSI monomer structure with marked charges amino acids: in red – lysine, in blue – arginine, in pink – aspartic acid and in white – glutamic acid. Even visually it is possible to see that the distribution of charges in the protein complex is not even.

References

[1] Y. Zhang, Z. Zhao, D. Fracasso, and R. C. Chiechi, *Bottom-Up Molecular Tunneling Junctions Formed by Self-Assembly,* Isr. J. Chem. **54**, 513 (2014).

[2] J. C. Love, L. A. Estroff, J. K. Kriebel, R. G. Nuzzo, and G. M. Whitesides, *Self-Assembled Monolayers of Thiolates on Metals as a Form of Nanotechnology,* Chemical Reviews **105**, 1103 (2005).

[3] H. Haick, J. Ghabboun, and D. Cahen, *Pd versus Au as evaporated metal contacts to molecules,* Applied Physics Letters **86**, 042113 (2005).

[4] F. Milani, C. Grave, V. Ferri, P. Samorì, and M. A. Rampi, *Ultrathin -Conjugated Polymer Films for Simple Fabrication of Large-Area Molecular Junctions,* ChemPhysChem **8**, 515 (2007).

[5] H. B. Akkerman, P. W. M. Blom, D. M. de Leeuw, and B. de Boer, *Towards molecular electronics with large-area molecular junctions,* Nature **441**, 69 (2006).

[6] W. D. Ellis, *Anodic stripping voltammetry,* Journal of Chemical Education **50**, A131 (1973).

[7] M. A. Rampi and G. M. Whitesides, *A versatile experimental approach for understanding electron transport through organic materials,* Chemical Physics **281**, 373 (2002).

[8] F. C. Simeone and M. A. Rampi, *Test-beds for Molecular Electronics: Metal–Molecules–Metal Junctions Based on Hg Electrodes,* CHIMIA International Journal for Chemistry **64**, 362 (2010).

[9] N. Amdursky, D. Marchak, L. Sepunaru, I. Pecht, M. Sheves, and D. Cahen, *Electronic Transport via Proteins,* Advanced Materials **26**, 7142 (2014).

[10] R. Chiechi, E. Weiss, M. Dickey, and G. Whitesides, *Eutectic Gallium–Indium (EGaIn): A Moldable Liquid Metal for Electrical Characterization of Self-Assembled Monolayers,* Angewandte Chemie International Edition **47**, 142 (2008).

[11] M. D. Dickey, R. C. Chiechi, R. J. Larsen, E. A. Weiss, D. A. Weitz, and G. M. Whitesides, *Eutectic Gallium-Indium (EGaIn): A Liquid Metal Alloy for the Formation of Stable Structures in Microchannels at Room Temperature,* Adv. Funct. Mater. **18**, 1097 (2008).

[12] L. Cademartiri, M. M. Thuo, C. A. Nijhuis, W. F. Reus, S. Tricard, J. R. Barber, R. N. S. Sodhi, P. Brodersen, C. Kim, R. C. Chiechi, and G. M. Whitesides, *Electrical Resistance of* Ag^{ts} *–*$S(CH_2)_{n1}CH_3$ *//*Ga_2O_3 */EGaIn Tunneling Junctions,* The Journal of Physical Chemistry C **116**, 10848 (2012).

[13] C. A. Nijhuis, W. F. Reus, J. R. Barber, M. D. Dickey, and G. M. Whitesides, *Charge Transport and Rectification in Arrays of SAM-Based Tunneling Junctions,* Nano Letters **10**, 3611 (2010).

[14] J.-H. So and M. D. Dickey, *Inherently aligned microfluidic electrodes composed of liquid metal,* Lab on a Chip **11**, 905 (2011).

[15] P. Jordan, P. Fromme, H. T. Witt, O. Klukas, W. Saenger, and N. Krauss, *Three-dimensional structure of cyanobacterial photosystem I at 2.5 A resolution,* Nature **411**, 909 (2001).

[16] R. Croce and H. van Amerongen, *Light-harvesting in photosystem I,* Photosynthesis Research **116**, 153 (2013).

[17] A. Nakamura, T. Suzawa, Y. Kato, and T. Watanabe, *Species Dependence of the Redox Potential of the Primary Electron Donor P700 in Photosystem I of Oxygenic Photosynthetic Organisms Revealed by Spectroelectrochemistry,* Plant and Cell Physiology **52**, 815 (2011).

[18] M. Hegner, P. Wagner, and G. Semenza, *Ultralarge atomically flat template-stripped Au surfaces for scanning probe microscopy,*

Surface Science **291**, 39 (1993).

[19] C. A. Nijhuis, W. F. Reus, and G. M. Whitesides, *Mechanism of Rectification in Tunneling Junctions Based on Molecules with Asymmetric Potential Drops,* Journal of the American Chemical Society **132**, 18386 (2010).

[20] C. A. Nijhuis, W. F. Reus, and G. M. Whitesides, *Molecular Rectification in MetalSAM-Metal OxideMetal Junctions,* Journal of the American Chemical Society **131**, 17814 (2009).

[21] C. A. Nijhuis, W. F. Reus, A. C. Siegel, and G. M. Whitesides, *A Molecular Half-Wave Rectifier,* Journal of the American Chemical Society **133**, 15397 (2011).

[22] D. Fracasso, H. Valkenier, J. C. Hummelen, G. C. Solomon, and R. C. Chiechi, *Evidence for Quantum Interference in SAMs of Arylethynylene Thiolates in Tunneling Junctions with Eutectic Ga–In (EGaIn) Top-Contacts,* J. Am. Chem. Soc. **133**, 9556 (2011).

[23] D. Fracasso, M. I. Muglali, M. Rohwerder, A. Terfort, and R. C. Chiechi, *Influence of an Atom in EGaIn/Ga2o3 Tunneling Junctions Comprising Self-Assembled Monolayers,* J. Phys. Chem. C **117**, 11367 (2013).

[24] M. M. Thuo, W. F. Reus, C. A. Nijhuis, J. R. Barber, C. Kim, M. D. Schulz, and G. M. Whitesides, *Odd-even effects in charge transport across self-assembled monolayers,* J. Am. Chem. Soc. **133**, 2962 (2011).

[25] H. J. Yoon, C. M. Bowers, M. Baghbanzadeh, and G. M. Whitesides, *The Rate of Charge Tunneling Is Insensitive to Polar Terminal Groups in Self-Assembled Monolayers in Ag ^{ts} S(CH$_2$)$_n$ M(CH$_2$)$_m$ T//Ga$_2$O$_3$ /EGaIn Junctions,* Journal of the American Chemical Society **136**, 16 (2014).

[26] L. Jiang, L. Yuan, L. Cao, and C. A. Nijhuis, *Controlling Leakage Currents: The Role of the Binding Group and Purity of the Precursors for Self-Assembled Monolayers in the Performance of Molecular Diodes,* Journal of the American Chemical Society **136**, 1982 (2014).

[27] W. F. Reus, M. M. Thuo, N. D. Shapiro, C. A. Nijhuis, and G. M. Whitesides, *The SAM, Not the Electrodes, Dominates Charge Transport in Metal-Monolayer//Ga$_2$O$_3$ /Gallium–Indium Eutectic Junctions,* ACS Nano **6**, 4806 (2012).

[28] I. Carmeli, L. Frolov, C. Carmeli, and S. Richter, *Photovoltaic Activity of Photosystem I-Based Self-Assembled Monolayer,* J. Am. Chem. Soc. **129**, 12352 (2007).

[29] I. Lee, J. Lee, and E. Greenbaum, *Biomolecular Electronics: Vectorial Arrays of Photosynthetic Reaction Centers,* Physical Review Letters **79**, 3294 (1997).

[30] T. Mikayama, K. Iida, Y. Suemori, T. Dewa, T. Miyashita, M. Nango, A. T. Gardiner, and R. J. Cogdell, *The Electronic Behavior of a Photosynthetic Reaction Center Monitored by Conductive Atomic Force Microscopy,* Journal of Nanoscience and Nanotechnology **9**, 97 (2009).

[31] J. Lee, I. Lee, P. Laible, T. Owens, and E. Greenbaum, *Chemical platinization and its effect on excitation transfer dynamics and P700 photooxidation kinetics in isolated photosystem I,* Biophysical Journal **69**, 652 (1995).

[32] I. L. James W. Lee, *Platinization: A novel technique to anchor photosystem I reaction centres onto a metal surface at biological temperature and pH,* Biosensors and Bioelectronics **11**, 375 (1996).

[33] A. Stamouli, J. W. M. Frenken, T. H. Oosterkamp, R. J. Cogdell, and T. J. Aartsma, *The electron conduction of photosynthetic protein complexes embedded in a membrane,* FEBS Letters **560**, 109 (2004).

[34] D. Gerster, J. Reichert, H. Bi, J. V. Barth, S. M. Kaniber, A. W. Holleitner, I. Visoly-Fisher, S. Sergani, and I. Carmeli, *Photocurrent of a single photosynthetic protein,* Nat Nano **7**, 673 (2012).

[35] Y. Yamanoi, N. Terasaki, M. Miyachi, Y. Inoue, and H. Nishihara, *Enhanced photocurrent production by photosystem I with modified viologen derivatives,* Thin Solid Films **520**, 5123 (2012).

[36] F. C. Simeone, H. J. Yoon, M. M. Thuo, J. R. Barber, B. Smith, and G. M. Whitesides, *Defining the Value of Injection Current and Effective Electrical Contact Area for EGaIn-Based Molecular Tunneling Junctions,* Journal of the American Chemical Society **135**, 18131 (2013).

[37] E. A. Weiss, R. C. Chiechi, G. K. Kaufman, J. K. Kriebel, Z. Li, M. Duati, M. A. Rampi, and G. M. Whitesides, *Influence of Defects on the Electrical Characteristics of Mercury-Drop Junctions: Self-Assembled Monolayers of n-Alkanethiolates on Rough and Smooth Silver,* J. Am. Chem. Soc. **129**, 4336 (2007).

[38] P. I. Gordiichuk, G.-J. A. H. Wetzelaer, D. Rimmerman, A. Gruszka, J. W. de Vries, M. Saller, D. A. Gautier, S. Catarci, D. Pesce, S. Richter, P. W. M. Blom, and A. Herrmann, *Solid-State Biophotovoltaic Cells Containing Photosystem I,* Adv. Mater. **26**, 4863 (2014).

[39] E. Darby, G. LeBlanc, E. A. Gizzie, K. M. Winter, G. K. Jennings, and D. E. Cliffel, *Photoactive Films of Photosystem I on Transparent Reduced Graphene Oxide Electrodes,* Langmuir **30**, 8990 (2014).

[40] D. Yu, M. Wang, G. Zhu, B. Ge, S. Liu, and F. Huang, *Enhanced photocurrent production by bio-dyes of photosynthetic macromolecules on designed TiO2 film,* Scientific Reports **5**, 9375 (2015).

[41] B. van Haeringen, J. Dekker, M. Bloemendal, M. Rögner, R. van Grondelle, and H. van Amerongen, *Simultaneous measurement of electric birefringence and dichroism. A study on photosystem 1 particles,* Biophysical Journal **67**, 411 (1994).

[42] C. S. S. Sangeeth, A. Wan, and C. A. Nijhuis, *Equivalent Circuits of a Self-Assembled Monolayer-Based Tunnel Junction Determined by Impedance Spectroscopy,* Journal of the American Chemical Society **136**, 11134 (2014).

[43] I. Ron, L. Sepunaru, S. Itzhakov, T. Belenkova, N. Friedman, I. Pecht, M. Sheves, and D. Cahen, *Proteins as Electronic Materials: Electron Transport through Solid-State Protein Monolayer Junctions,* Journal of the American Chemical Society **132**, 4131 (2010).

[44] J. H. Golbeck, *Structure and Function of Photosystem I,* Annual Review of Plant Physiology and Plant Molecular Biology **43**, 293 (1992).

[45] L. Luo, S. H. Choi, and C. D. Frisbie, *Probing Hopping Conduction in Conjugated Molecular Wires Connected to Metal Electrodes †,* Chemistry of Materials **23**, 631 (2011).

[46] S. H. Choi and C. D. Frisbie, *Enhanced Hopping Conductivity in Low Band Gap DonorAcceptor Molecular Wires Up to 20 nm in Length,* Journal of the American Chemical Society **132**, 16191 (2010).

[47] W. Li, L. Sepunaru, N. Amdursky, S. R. Cohen, I. Pecht, M. Sheves, and D. Cahen, *Temperature and Force Dependence of Nanoscale Electron Transport via the Cu Protein Azurin,* ACS Nano , 10816 (2012).

[48] L. Sepunaru, N. Friedman, I. Pecht, M. Sheves, and D. Cahen, *Temperature-Dependent Solid-State Electron Transport through Bacteriorhodopsin: Experimental Evidence for Multiple Transport Paths through Proteins,* Journal of the American Chemical Society **134**, 4169 (2012).

[49] T. Rakshit, S. Banerjee, and R. Mukhopadhyay, *Near-Metallic Behavior of Warm Holoferritin Molecules on a Gold(111) Surface,* Langmuir **26**, 16005 (2010).

[50] N. Amdursky, D. Ferber, C. A. Bortolotti, D. A. Dolgikh, R. V. Chertkova, I. Pecht, M. Sheves, and D. Cahen, *Solid-state electron transport via cytochrome c depends on electronic coupling to electrodes and across the protein,* Proceedings of the National Academy of

Sciences **111**, 5556 (2014).

[51] N. Amdursky, I. Pecht, M. Sheves, and D. Cahen, *Doping Human Serum Albumin with Retinoate Markedly Enhances Electron Transport across the Protein,* Journal of the American Chemical Society **134**, 18221 (2012).

[52] N. Amdursky, D. Ferber, I. Pecht, M. Sheves, and D. Cahen, *Redox activity distinguishes solid-state electron transport from solution-based electron transfer in a natural and artificial protein: cytochrome C and hemin-doped human serum albumin,* Physical Chemistry Chemical Physics **15**, 17142 (2013).

[53] E. D. Mentovich, B. Belgorodsky, I. Kalifa, H. Cohen, and S. Richter, *Large-Scale Fabrication of 4-nm-Channel Vertical Protein-Based Ambipolar Transistors,* Nano Letters **9**, 1296 (2009).

[54] Izawa, S., *Acceptors and donors for chloroplast electron transport,* **69**, 413 (1980).

3

Orientation and Incorporation of Photosystem I in Bioelectronic Devices Enabled by Phage Display

The great thing about science is that you can get it wrong
over and over again because what you're after
–call it truth or understanding– waits patiently for you.
Ultimately, you'll find the answer because it doesn't change.

DUDLEY HERSCHBACH

Parts of this chapter were developed in collaboration with colleagues from Polymer Chemistry and Bioengineering and will be published on Adv. Sci., 2017 (10.1002/advs.201600393). Parts related to phage display, single molecule measurements and PSI isolation were carried out by P. Gordiichuk, D. Pesce, A. Marcozzi, M. Loznik and E. Gloukhikh.

3

Abstract

As discussed in the previous chapter, Photosystem I (PSI) is a protein complex that is particularly interesting because of its high internal efficiency. The idea behind this research is to be able to create bio-photovoltaic devices in which the active components are grown rather than synthesized. In order to fabricate successful devices comprising PSI, the orientation of the complexes that form the monolayer is of critical importance since it provides a directional bias of the electron-transfer process, especially in the case of PSI which possesses an electron transport chain (ETC). Up until now, the ability to assemble PSI monolayers with a high percentage of oriented complexes had remained a challenge.

The previous chapter describes a technique with which PSI can be oriented on an ultra-flat Au surface with a maximum success rate of 70% by using the orienting molecule 2ME. This chapter presents a collaboration with Prof. Andreas Herrmann and co-workers to apply a phage-display (PD) technique to engineer short binding-peptides that afford near-perfect control over the orientation. By using this technique, the percentage of oriented complexes increased to almost 100%.

We characterized the orientation in junctions using soft, conformal top-contacts comprising eutectic gallium-indium (EGaIn) and using single-complex conducting atomic force microscopy (AFM).

3.1. *Introduction*

Phage display (PD) is a very powerful method for the selection of peptides that bind a wide variety of molecules and substrates. Phages are viruses for which the host is a bacterial cell. These viruses can be used as vectors to infect standard recombinant DNA hosts. In 1985, G. Smith described a technique where foreign DNA fragments could be introduced into a phage gene to create a fusion. This fusion protein in turn, displayed the foreign amino acids in an accessible form [1]. These phages can then be screened against other sequences, peptides or proteins in order to determine wanted interactions. A mixture of phage clones constitutes what is called a phage-display "library"; in such, each clone carries a different foreign DNA insert and therefore displays a different amino acid sequence or protein domain on its surface [2]. Over the years, the PD technique has evolved and expanded to the point where it is now also used to find binders against inorganic materials [3–7]. This step makes it possible to fabricate multicomponent devices such as state-of-the-art lithium-ion batteries [8] and dye-sensitized solar cells (DSSC) [9]. Yet, thus far, PD had not been performed against photoactive proteins such as Photosystem I (PSI).

Photosystem I is a large complex isolated from *Thermosynechococcus elongatus*, a thermophilic unicellular cyanobacterium. The idea is that by using molecular proteins obtained from nature, absorption and efficiency limitations can be overcome. Additionally, this complex presents special characteristics such as an internal energy yield of approximately 58%, a photovoltage of 1 V and a quantum efficiency close to 100% [10]. Fig. 3.1 shows the crystal structure of PSI; light reactions take place here as the photons harvested by the chlorophyll when light is shone are transferred to the reaction center (RC) P700. From the RC, the electron is transferred via the primary electron acceptors A_0, A_1, F_X, F_A and F_B to the external ferredoxin charge carrier. The high efficiency of this process bids the idea of incorporating PSI into electrical devices. Nonetheless, in order to have optimal performance, most, if not all complexes, should have a homogeneous orientation on a substrate to allow optimal electron transfer. However, when working with PSI, orienting the complexes proves to be a challenge as the complexes tend to self-assemble with random orientations due to their structural complexity as well as its relative large size (diameter of ~ 20 nm). Orienting the RC on a surface had been, so far, attempted by surface modification (where functional groups interact electrostatically with different parts of the complexes), by direct covalent attachment (via mutation) or through a molecular self-assembled monolayer (SAM) [11–13]. Orienting the entire complex, on the other hand, had not been so widely proven. To solve this problem, colleagues from Polymer Chemistry

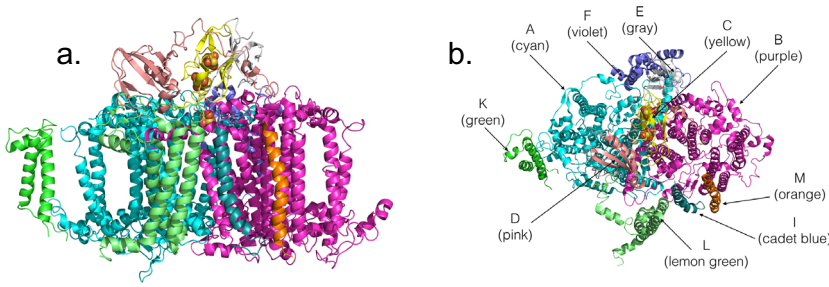

Figure 3.1. Crystal structure of PSI from **a.** side and **b.** top view. Different subunits are color-coded: protein amino acids structures in green, the three iron-sulphur (Fe_4S_4) clusters in yellow and orange.

and Bioengineering developed a technique which makes use of Phage Display to selectively bind and orient PSI to an ITO (Indium Tin Oxide) substrate. The phage display protocol consisted of selecting small peptide binders against PSI trimers. From this selection procedure, they identified three linear 12-mer peptides with high affinity against the stromal side of PSI. These peptides could bias the orientation of PSI such that the F_B cluster faces the substrate.

We determined the orientation by conducting atomic force microscopy (CP-AFM) on single complexes and using eutectic gallium-indium (EGaIn) on the macro scale; the orientation of PSI with respect to the surface of a bottom electrode gives rise to direction-dependent asymmetry in tunnelling currents.

3.2. *Results and Discussions*

3.2.1. Phage Display Against Photosystem I

Oriented immobilization was ensured by first employing an antibody against PsaC, the protein in the stromal side that harbors and coordinates the F_A and F_B clusters –the final unit of the electron transport chain (ETC) where electron ejection takes place. When this antibody is immobilized, it forces the stromal side of PSI to orient towards the surface of the electrode, preventing the binding of phages on that side. Three different well surfaces were prepared to identify peptide binding: the first one contained PSI without any preferential orientation; the second was coated with a monolayer of BSA (Bovine Serum Albumin), a protein often used as standard; and the third was decorated with PSI trimers oriented with the help of an anti-PsaC antibody (which can orient PSI, but decouples it from the surface

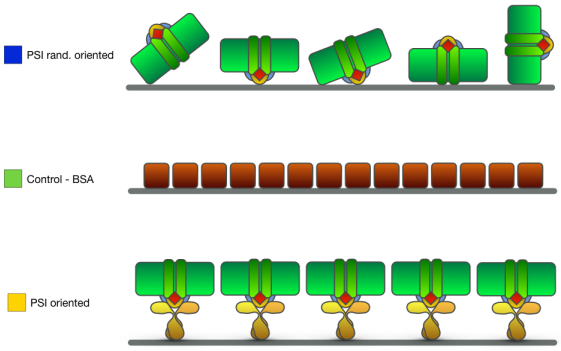

Figure 3.2. Schematic representation of the different well surfaces used to identify peptides binding the lumen side of PSI. Top: PSI is covalently linked without any preferential orientation. Middle: BSA coated (used as control). Bottom: PSI is linked to the well via antibodies. The specific interaction between the antibody and PsaC ensures that PSI exposes only its lumen side.

electronically) with the lumen side facing away from the surface and therefore exclusively accessible for binding (Fig. 3.2).

Binding studies were then performed on all three surfaces with a modified phage-ELISA binding assay. Each surface was incubated in a solution of single clones of bacteriophage M13 conjugated to horseradish peroxidase (HRP, an amplifying enzyme). After washing, a fluorogenic substrate was added and the relative amount of bound phages was determined by measuring the intensity in real time. The outcome of this binding assay is shown in Fig. 3.3. Here, a clear difference in the fluoresence intensity can be seen between the randomly oriented PSI, those bound to antibodies and the control (the ones coated with BSA). By analyzing the results, the peptide sequences that could discriminate between oriented and random complexes became apparent. We observe that sequences 11 (RDQNHYMYSARV), 12 (IQAGKTEHLAPD) and 88 (LATTSHMFMAKG), have high affinity against the surface with PSI randomly oriented, but they display low affinity against the covered substrate and the complexes oriented with only the lumen side of PSI available. Thus, they selectively bind on the stromal side (the same side as the anti-PsaC antibody). A scrambled peptide, 61 (ALFHYNTHGSLH) was also found to have high affinity.

3.2.2. Determination of Orientation of PSI by Conducting AFM

All CP-AFM measurements were conducted by colleague, Pavlo Gordiichuk.
After identifying the peptide sequences that correctly orient the photosynthetic

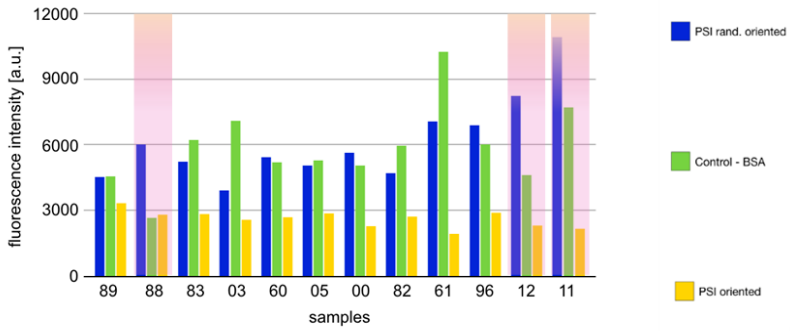

Figure 3.3. Fluorescence signal from ELISA essay. All tested sequences, PSI randomly oriented (blue), no PSI (green), oriented PSI (yellow). Sequences 11, 12, 88 and 61 exhibit higher affinity for PSI at lumen.

complexes, the ability of these peptides to orient PSI on a conducting substrate was characterized by CP-AFM; the peptide sequences were modified at the C-terminus with a phosphorylated serine residue allowing binding to an indium tin oxide (ITO) surface [14]. Two different kind of devices were prepared to compare the percent orientation and electrical properties achieved with the peptides and the short linkers as orienting layers for PSI. On one case, the photosynthetic complexes were incubated with the modified peptides and subsequently drop casted onto the ITO substrates. On the second case, the ITO surfaces were functionalized with dihydroxyacetone phosphate (DHAP), which forms SAMs capable of controlling the orientation and self-assembly of PSI [15]. CP-AFM studies were performed on all PSI-oriented devices. As in the previous chapter, it is possible to know the orientation of the PSI complexes on the metallic substrate by observing the distinct *I-V* curves that result from biasing a single (or a few) complex(es). Each orientation (F_B/PsaC up, down or sideways) induces a certain asymmetry or rectification; when the F_B/PsaC side is pointing towards the substrate (that is, the bottom electrode), a higher electrical current is measured at negative bias compared to the electrical current at positive bias, this gives rise to asymmetric *I-V* curves. Likewise, the opposite orientation, which is accessible with director SAMs of thiolates, gives rise to the opposite asymmetry [16]. In that same paper it was observed that when PSI is laying with the axis of the ETC parallel to the surface (sideways) or if it is thermally denatured, current rectification is absent (that is, the *I-V* data are symmetric). Guided by these observations, we analyzed

Orienting Molecule	Up (%)	Sideways (%)	Down (%)
DHAP	7	13	80
LAT	10	13	77
RDQ	1	15	84
ALF	5	9	86
IQA	1	1	98

Table 3.1. Percentage of average orientation of PSI (electrons going up, down or sideways) when oriented with different molecules (peptides with highest orientation percentage and short molecule, DHAP).

different devices with all four different peptide/PSI and an additional substrate bearing DHAP/PSI.

P. Gordiichuk used Pt/Ir probes for CP-AFM studies on contact mode on a sample at zero voltage to record the topography of the PSI layers. From these data, he identified individual PSI trimers on the ITO surface as an approximately round, bright spots. He then set the CP-AFM to *I-V* ramping to record the electrical characteristics of individual PSI trimers, examining at least 100 trimers for each of the three peptide linkers. The resulting *I-V* curves are shown in Fig. 3.4 and adduce the same orientation-dependent electrical behavior as previously observed on Au. The expected, downward configuration of PSI (electrons traveling towards bottom electrode) is preferred for all four peptides, however, as is shown in Table 3.1, only peptide IQA orients PSI exclusively in this configuration. The SAMs of PSI formed on the other three peptides also contained trimers in the upward configuration. The origin of this rectification was recently elucidated and is most likely due to the permanent dipole of the PSI protein scaffold and not the co-factors of the ETC [16].

3.2.3. Macroscopic Characterization of PSI Monolayers with Peptide Directing Layers

After quantifying the orientation of PSI complexes one-by-one via CP-AFM, we investigated the macroscopic electrical properties of oriented SAMs of PSI using EGaIn as a top electrode.

Eutectic Gallium-Indium (EGAIn) is an electrically conductive fluid metal composed of 75.5% Ga and 24.5% In by weight. It has been extensively used to measure SAMs of small molecules as well as the large protein complex, PSI (see Chapter 2 and [16]). Due to its non-newtonian properties and non-toxicity, it is possible to use to make conical tips to contact molecular SAMs without damaging them.

A solution containing PSI in buffer was added to centrifuge vials, each containing

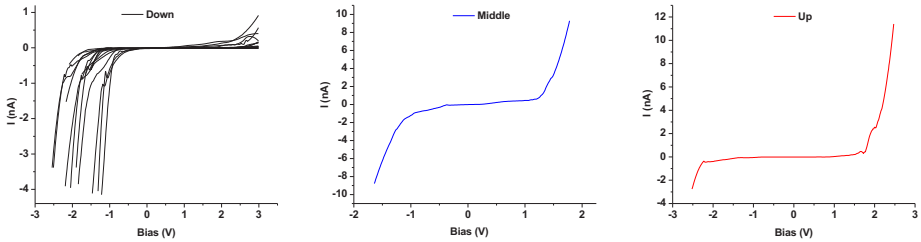

Figure 3.4. *I-V* curves from CP-AFM on PSI oriented with IQA. Fifteen characteristic *I-V* plots are shown for PSI oriented with the F_B cluster towards the substrate (left), PSI oriented parallel to the surface (middle) and PSI oriented with the F_B cluster towards the top electrode.

a different peptide solution (from IQA, RDQ, LAT or ALF). The mixture was shaken for 1 h at room temperature and then drop-casted onto clean ITO substrates for 2 h. The substrates were then rinsed with de-ionized water and allowed to dry at room temperature. For comparison studies, different ITO surfaces were functionalized with a SAM of DHAP as described elsewhere [17] and control devices were prepared by incubating the substrates in only PSI, only peptides and peptides with deactivated PSI (boiled at 99 °C for 1.5 h). I prepared a conical EGaIn tip (ca. 25 m in diameter) by following previously established protocol [18] to contact the different self-assembled monolayers. I lowered it until the point of contact and measured *J-V* curves by biasing from -1 V to +1 V under dark conditions so PSI was not photo-activated. From the results I was able to calculate the asymmetry parameter or rectification ratio (R), defined as R=(J at -1 V)/(J at +1 V) according to the wiring of CP-AFM (which is backwards from EGaIn).

Fig. 3.5 shows the difference (Δ) in log|R| at 1 V of a monolayer of only modified peptides *vs.* the peptides with PSI complexes. Differences in log|R| are an indication of the effect of the PSI/peptide versus possible asymmetry induced by the peptides, which are themselves highly oriented (otherwise they would not be able to orient PSI). RDQ and LAT presented a low value of log|R| which we ascribe to a low coverage of PSI complexes. We hypothesize that due to the non-covalent nature of peptide-PSI interactions and the strong affinity of the peptides for ITO, the peptide-PSI couple dissociated and the surface is left with and passivated mainly by free peptides. This would lead to a low value of Δlog|R| as the difference in rectification would be close to zero. The absolute value of Δlog|R| calculate for all peptides is 0.097 for RDQ, 0.1 for LAT, 0.551 for ALF and 0.737 for IQA (Fig. 3.5). An increasing trend can be observed which may be due to a better coupling of

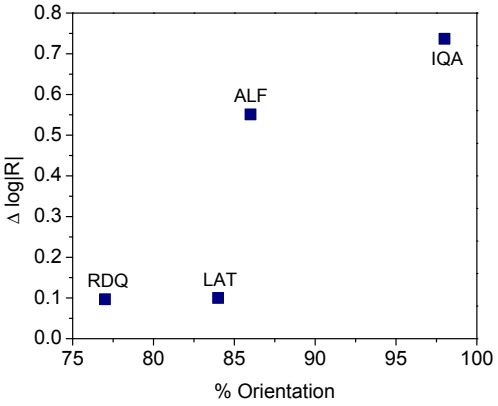

Figure 3.5. Difference or $\Delta\log|R|$ between $\log|R|$ values between peptide monolayers with and without PSI. Values are established from histograms resulting from measuring multiple *J-V* curves with EGaIn. The rectification ratio (R) is defined as R=(J at -1 V)/(J at +1 V).

PSI to the peptides or better affinity of the peptides to the substrate and therefore denser coverage of PSI. The differences of values of $\log|R|$ for devices with oriented PSI with different peptides can be seen by the histograms in Fig. 3.6. Histograms and *J-V* traces of all bare traces were also collected. All measurements were done by biasing from -1 V to +1 V and all histograms were recorded at 1 V.

The transport properties of bare ITO are quite sensitive to adsorbates that lack structure [19] and as such it can be difficult to characterize monolayers of short, small and/or randomly oriented molecules. We believe that this is the reason why SAMs of only peptides, only PSI and boiled PSI yielded unstable junctions: randomly-oriented PSI on bare-ITO, for example, exhibited a broad distribution of R-values while devices comprising only peptides and boiled PSI yielded mostly short-circuit (ohmic) characteristics, indicating that what was measured is not as robust as intact PSI complexes. By contrast, of all of the substrates tested, PSI oriented with IQA peptide was the most stable and reproducible. In addition to experiments on the PD peptides, we measured SAMs of PSI with the short directing linker DHAP. These devices exhibited a value of $\log|R|$=1.22, which is close to those of PSI oriented with peptides, generally, but still lower than PSI oriented with IQA peptide Fig. 3.7. Thus, from these results we hypothesize that the degree of asymmetry is a reflection of the overall degree of the orientation of PSI.

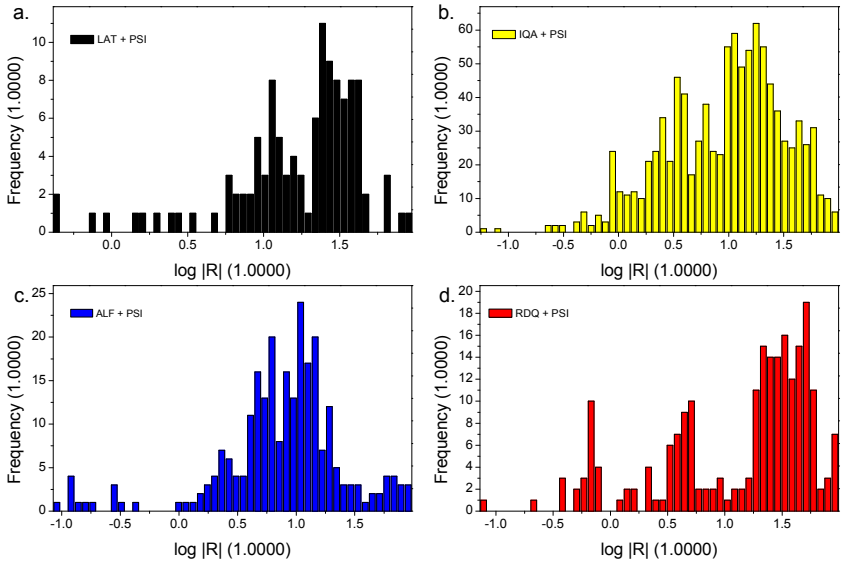

Figure 3.6. Histograms of log|R| for devices with oriented PSI with different peptides. **a.** LAT and PSI. **b.** IQA and PSI. **c.** ALF and PSI. **d.** RDQ and PSI.

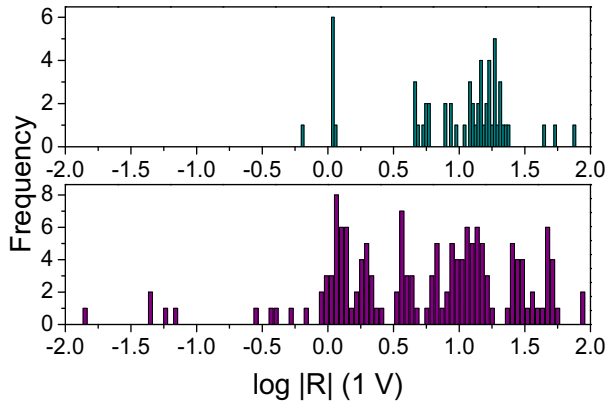

Figure 3.7. Histograms of log|R| top panel: PSI oriented on ITO via the short molecule, DHAP. Bottom panel: PSI drop-casted on ITO. PSI is randomly oriented and thus a clear peak for log|R| cannot be observed.

3.3. *Conclusions*

Using EGaIn as top electrode proved once more to be a useful method for interrogating SAMs of biological molecules. In collaboration with Prof. Herrmann and co-workers we were able to make devices with 100% oriented PSI complexes. PD was used to identify binders against the photosynthetic complex and screened them in order to select the sequences best able to bind PSI on the stromal side (Fe complex towards a semiconductor surface). The PSI monolayer was characterized with both single and large area electrical measurements by making use of CP-AFM and EGaIn tips, they were also incorporated into bulk heterojunction (BHJ) solar cells but this part has been omitted from this chapter. In all three cases, the collective action of the dipoles intrinsic to the complexes (dark) or the electron-transport chain (illumination) affected charge-transport systematically as a function of the direction/degree of orientation. The comparison between single, large area and measurements under illumination, provided a rigorous characterization for devices with optimized orientation. Future work will be directed towards exploiting these peptides for integrating PSI in other bio-solar and biofuel cells and to functionalize PSI in a mild, non-covalent fashion, which requires only the addition of functionalized peptides and their binding to PSI without any chemical coupling reagent. Being able to achieve such results is of major importance as it allows studies that can lead to exploitation of their charge separation capabilities in order to be applied to bio-inspired photovoltaics or other types of bio-electrical devices.

3.A. *Experimental*

3.A.1. Materials and methods

Photosystem I from *T. elongatus* was purified as a trimer and attached to an epoxide-modified surface, which has a sufficiently high affinity for amino groups to cause PSI to orient randomly. Next, a commercial library of filamentous bacteriophage M13 expressing 12 amino acid long random-peptide sequences in fusion with their p3 protein (NEB E8110S) was panned against the immobilized PSI trimer targets. Although the protocol of the vendor was followed, after three rounds of panning and amplification, no selection was achieved. Instead, wild type phages were recovered after the final amplification step. Aiming for a reduction of the number of cycles that could favor the selection of wild type phages, the group of Prof. Herrmann developed a new phage display method that leverages horse radish peroxidase (HRP) conjugated to the viral particles. Usually, during several rounds of PD selection, phages are exposed to the target and can

be eluted after washing without knowing the exact level of phages bound to the immobilized target. In contrast to the classic phage display protocol where the determination of amount of bounded phages to the target before the elution step it is not possible, here we are able to determine said percentage; the modified protocol allowed determining the amount of phages left after each wash enables us to decide whether to continue with the washes or proceed with the elution. In our protocol, prior to panning, M13 phages were covalently functionalized with HRP, which allowed monitoring in real time the level of phages bound to the surface by turnover of a fluorogenic substrate. After the washing, only the PSI-bound phages were retained in the well so it was possible to calculate the amount of phages bound by measuring the fluorescent signal produced by the HRP. The substrate becomes fluorescent only after being digested by the HRP, generating a blue fluorescent product upon reaction with peroxidase. In this way, only the few phages strongly interacting with PSI were eluted, enabling the generation of aptamers (peptide molecules that bind to a specific target molecule) against PSI in a single round of selection. Afterwards, the eluted phages were used to infect *E. coli* to amplify single-phage clones. The single clones were sequenced and their binding affinity towards PSI tested.

3.A.2. Data acquisition - EGaIn tips

Room-temperature measurements are performed in a home-built setup that is described in detail elsewhere [20]. A junction is first formed by slowly bringing the EGaIn tip into contact with the protein monolayer with the help of a manual micro-controller. The source-meter is set at a 1 V fixed bias and once the current is stable, an *I-V* sweep is performed from -1 V to +1 V; 5-10 traces are recorded. The camera is fixed on the EGaIn tip and the diameter of the junction is measured on-screen. Exceeding the current threshold value of 105 μA produces Ohmic *I-V* curves and means that the junction has shorted and data is not recorded. Noisy, hysteretic currents lower than 5 nA indicate “no-contact” behavior. To have representative data points, this procedure is repeated until the data from at least five working junctions per substrate is recorded across several substrates. The aggregate data-sets comprise data acquired on different days, across different devices, and from different batches of PSI and peptides. Although the actual contact area is smaller than what we can optically see [21], this discrepancy is systematic and therefore not corrected for except when otherwise noted.

3.A.3. Data Processing and Analysis

The software used for the gathering and analysis of the data comprise homemade LabView scripts for acquiring raw data and Python scripts that employ SciPy for data analysis. All data come from Gaussian fits made by the software which

automatically prunes no-contact traces and shorts by line-shape and magnitude, which interfere with calculations of the asymmetry ratio; *e.g.*, if a junction shorts mid-trace, the apparent value of R will be on the order of 10^5.
We analyzed the statistical significance of the asymmetry (R) in accordance with previous studies on PSI [16] by comparing the histograms of log R of junctions with and without PSI.

References

[1] G. Smith, *Filamentous fusion phage: novel expression vectors that display cloned antigens on the virion surface,* Science **228**, 1315 (1985).

[2] G. P. Smith and V. A. Petrenko, *Phage Display,* Chemical Reviews **97**, 391 (1997).

[3] Y. Cui, S. N. Kim, S. E. Jones, L. L. Wissler, R. R. Naik, and M. C. McAlpine, *Chemical Functionalization of Graphene Enabled by Phage Displayed Peptides,* Nano Letters **10**, 4559 (2010).

[4] S. Wang, E. S. Humphreys, S.-Y. Chung, D. F. Delduco, S. R. Lustig, H. Wang, K. N. Parker, N. W. Rizzo, S. Subramoney, Y.-M. Chiang, and A. Jagota, *Peptides with selective affinity for carbon nanotubes,* Nature Materials **2**, 196 (2003).

[5] R. R. Naik, S. J. Stringer, G. Agarwal, S. E. Jones, and M. O. Stone, *Biomimetic synthesis and patterning of silver nanoparticles,* Nature Materials **1**, 169 (2002).

[6] S. R. Whaley, D. S. English, E. L. Hu, P. F. Barbara, and A. M. Belcher, *Selection of peptides with semiconductor binding specificity for directed nanocrystal assembly,* Nature **405**, 665 (2000).

[7] S. W. Lee, C. B. Mao, C. E. Flynn, and A. M. Belcher, *Ordering of Quantum Dots Using Genetically Engineered Viruses,* Science **296**, 892 (2002).

[8] Y. J. Lee, H. Yi, W.-J. Kim, K. Kang, D. S. Yun, M. S. Strano, G. Ceder, and A. M. Belcher, *Fabricating Genetically Engineered High-Power Lithium Ion Batteries Using Multiple Virus Genes,* Science (2009), 10.1126/science.1171541.

[9] X. Dang, H. Yi, M.-H. Ham, J. Qi, D. S. Yun, R. Ladewski, M. S. Strano, P. T. Hammond, and A. M. Belcher, *Virus-templated self-assembled single-walled carbon nanotubes for highly efficient electron collection in photovoltaic devices,* Nature Nanotechnology **6**, 377 (2011).

[10] K. Brettel, *Electron transfer in photosystem I,* Biochimica et Biophysica Acta (BBA) - Bioenergetics **1507**, 100 (2001).

[11] I. L. James W. Lee, *Platinization: A novel technique to anchor photosystem I reaction centres onto a metal surface at biological temperature and pH,* Biosensors and Bioelectronics **11**, 375 (1996).

[12] T. Mikayama, K. Iida, Y. Suemori, T. Dewa, T. Miyashita, M. Nango, A. T. Gardiner, and R. J. Cogdell, *The Electronic Behavior of a Photosynthetic Reaction Center Monitored by Conductive Atomic Force Microscopy,* Journal of Nanoscience and Nanotechnology **9**, 97 (2009).

[13] L. Frolov, Y. Rosenwaks, C. Carmeli, and I. Carmeli, *Fabrication of a Photoelectronic Device by Direct Chemical Binding of the Photosynthetic Reaction Center Protein to Metal Surfaces,* Advanced Materials **17**, 2434 (2005).

[14] R. Hofer, M. Textor, and N. D. Spencer, *Alkyl Phosphate Monolayers, Self-Assembled from Aqueous Solution onto Metal Oxide Surfaces,* Langmuir **17**, 4014 (2001).

[15] P. I. Gordiichuk, G.-J. A. H. Wetzelaer, D. Rimmerman, A. Gruszka, J. W. de Vries, M. Saller, D. A. Gautier, S. Catarci, D. Pesce, S. Richter, P. W. M. Blom, and A. Herrmann, *Solid-State Biophotovoltaic Cells Containing Photosystem I,* Adv. Mater. **26**, 4863 (2014).

[16] O. E. Castañeda Ocampo, P. Gordiichuk, S. Catarci, D. A. Gautier, A. Herrmann, and R. C. Chiechi, *Mechanism of Orientation-Dependent Asymmetric Charge Transport in Tunneling Junctions Comprising Photosystem I,* Journal of the American Chemical Society **137**, 8419 (2015).

[17] E. A. Gizzie, J. Scott Niezgoda, M. T. Robinson, A. G. Harris, G. Kane Jennings, S. J. Rosenthal, and D. E. Cliffel, *Photosystem*

I-polyaniline/TiO $_2$ solid-state solar cells: simple devices for biohybrid solar energy conversion, Energy Environ. Sci. **8**, 3572 (2015).

[18] R. Chiechi, E. Weiss, M. Dickey, and G. Whitesides, *Eutectic Gallium–Indium (EGaIn): A Moldable Liquid Metal for Electrical Characterization of Self-Assembled Monolayers,* Angewandte Chemie International Edition **47**, 142 (2008).

[19] G. D. Kong, M. Kim, and H. J. Yoon, *EGaIn Microelectrode for Electrical Characterization of ITO-Based van der Waals Interface and Airborne Molecular Contamination of ITO Surface,* Journal of the Electrochemical Society **162**, H703 (2015).

[20] D. Fracasso, H. Valkenier, J. C. Hummelen, G. C. Solomon, and R. C. Chiechi, *Evidence for Quantum Interference in SAMs of Arylethynylene Thiolates in Tunneling Junctions with Eutectic Ga–In (EGaIn) Top-Contacts,* J. Am. Chem. Soc. **133**, 9556 (2011).

[21] F. C. Simeone, H. J. Yoon, M. M. Thuo, J. R. Barber, B. Smith, and G. M. Whitesides, *Defining the Value of Injection Current and Effective Electrical Contact Area for EGaIn-Based Molecular Tunneling Junctions,* Journal of the American Chemical Society **135**, 18131 (2013).

4

Mechanical and Fluidic Properties of Solid and Soft-Devices

Every great advance in science has issued
from a new audacity of imagination.

JOHN DEWEY

Maikel van Putten helped establish the photolithographic protocol used in this chapter. Xinkai Qiu filled the reticulated long microchannels that were tested. The mechanical properties of filled microchannels were studied in the laboratory of Prof. Michael Dickey from the Chemical Engineering Department at North Carolina State University, Raleigh, U.S.A.

4

Abstract

In this chapter we co-fabricate soft, flexible microfluidic devices of different geometries and dimensions by making use of previously developed techniques. The microchannels that constitute our devices are separated by posts (Laplace barriers) instead of continuous walls to allow cross-communication between channels. We make use of the liquid metal, eutectic gallium indium because of its special rheological properties. Here, we investigate the mechanical properties of these devices and test their electrical properties when filled to study how robust and versatile they can be.

4.1. *Introduction*

Metallic components are essential for most electrical devices including electrical microfluidic devices. Current techniques for successfully incorporating metals into such small and intricate 3D devices range from injecting metals with low melting point (microsolidics) [1, 2] to patterning and meticulously aligning metallic films on one or several of the channel surfaces [3–7]. Although these techniques have been widely used, they all pose limitations such as the need for expensive equipment, difficult aligning, long processing times, poor quality or faulty sealing. Other techniques used during the fabrication of electronic components involve etching, metal deposition and other cooling or heating steps incompatible with many of materials used to make the microchannels themselves. Compared to all of these drawbacks, injecting a liquid metal into a microchannel is truly as easy as it can get. However, the ability to inject liquid metals into microchannels is nothing new. Mercury, for example, had been used to make a tunable organic transistor in 2003 [8] and a microelectrode for heavy metal ion detection [9] and Eutectic Gallium-Indium (EGaIn) to make a frequency shifting antenna [10]. The rheological behavior of EGaIn and Mercury as injected into microchannels was studied by Whitesides and co-workers in 2008 [11]. A disadvantage found while working with Hg (besides its toxicity) was that it tended to minimize its surface energy, making it difficult to form and maintain different geometries.

Being able to readily fill microchannels at room temperature and without the need of specialized equipment opens up the possibilities for the fabrication of flexible electronics, sensors and many other types of devices. Our microchannels were made using the simple technique "co-fabrication". Whitesides reported this strategy for fabricating multicomponent microsystems in a single step. This type of fabrication consists in generating a master with a set pattern and subsequently pouring and curing a polymer (in this case, polydimethylsiloxane, PDMS) yielding a replica. This kind of fabrication is flexible (compatible with different materials) and cost and time-effective [1]. Michael Dickey and co-workers further developed this idea to create inherently aligned microfluidic electrodes [12]. They used channels that were separated by 50 µm tall PDMS posts for electrohydrodynamic mixing by high electric fields. During the injection, EGaIn forms a stabilizing oxide skin that prevents it from flowing between the posts acting as a Laplace barrier [13] (a Laplace barrier is a geometric construction of arrayed posts or ridges that impart Laplace pressure to confine a fluid [13]). Increasing the critical pressure inside the channels would cause an instability allowing the liquid to flow to the adjacent channel through the posts [11].

We sought to demonstrate the mechanical resilience of such channels to make flexible devices. We take advantage of the possibility of extending their length and changing their geometries while still maintaining the liquid components separate. By creating longer and reticulated channels, the surface and contact area is increased providing at the same time more space for chemical reactions to take place. This can be advantageous for potential applications.

4.2. *Co-Fabrication*

Special microfluidic channels of different lengths and geometries were fabricated in a single step of micromolding. By choosing different geometries, we wanted to test whether EGaIn would stay within the microchannels at different angles and widths and what the limitations were. We used a CAD software called Clewin for the design of the masks for photolithography. We designed different patterns to fit in a 1 cm x 1 cm chip by playing with the length, the angles, dimensions and spacing. We designed two different sets of the simple, "short" geometries: one with straight channels, the other one "L-shaped" at a 90 ° angle. In both we varied the number of channels (two and three) as well as the spacing between the posts. We also designed "long", reticulated geometries where we played with the number and size of channels (two, three and five) and the shapes. The channels in the short, two-channel geometries were 475 µm wide and in the three-channel, the two outer were 375 µm and the inner 150 µm wide. The spacing between the 50 µm posts in these geometries was 25 and 50 µm, the total length from inlet to outlet was 12 mm. The "L-shaped" channels had the same dimensions but their total length was 14 mm (see Fig. 4.1). In the reticulated structures (Fig. 4.2), two channel structures were 50 µm wide with 50 µm posts giving a total width of 150 µm, the three channel structures were 120 µm wide in the outer channels and 160 µm in the middle one, whereas in the five channels, all were 160 µm wide with all posts and spacing of 50 µm.

Maikel van Putten, a Top-master student under my supervision, and I developed a protocol to make 50 µm deep channels following some of the guidelines provided by MicroChem. We used MicroChem high contrast, epoxy based, SU-8 photoresist to make the masters. The substrate was a Si/SiO_2 wafer which was cleaned by rinsing with acetone, dried with N_2, then isopropanol, dried again and finally with DI water and dried. Rinsing steps were repeated as necessary. The wafer was then dehydrated on a hot plate at 200 °C for 5 min. The spin coating program was based on a protocol developed by our colleagues in pharmacy and followed a two-step program first ramping 100 rpm/s at 500 rpm in 13 s and then

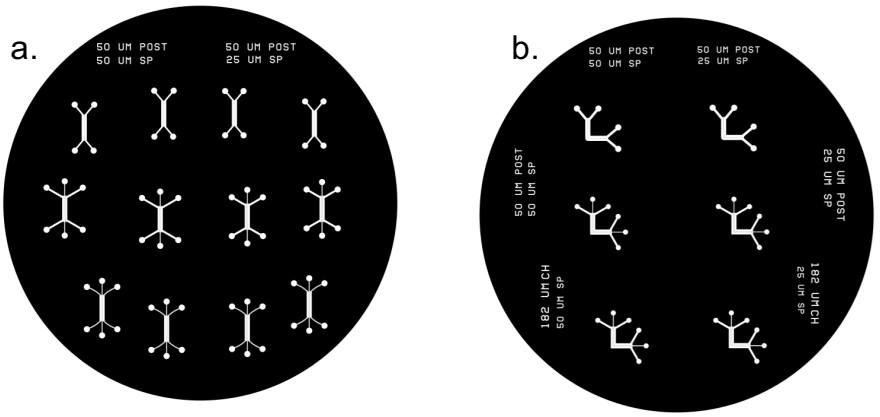

Figure 4.1. Transparency masks designed for the making of rigid masters with "short channels". **a.** "Straight" geometries. The two-channel geometries are 475 µm wide and in the three-channel, the two outer were 375 µm and the inner 150 µm wide. The spacing between the 50 µm posts in these geometries is 25 and 50 µm (as indicated in the mask), the total length from inlet to outlet is 12 mm. **b.** The "L-shaped" channels had the same dimensions but their total length is 14 mm.

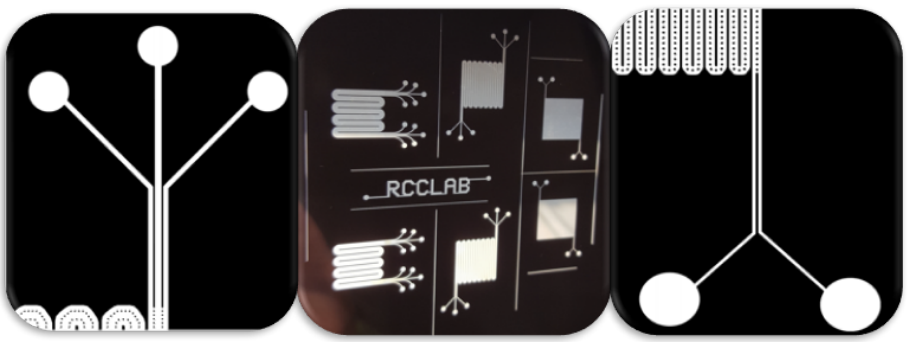

Figure 4.2. Transparency masks designed for the making of rigid masters with "long channels". The two channel structures are 50 µm wide with 50 µm posts giving a total width of 150 µm, the three channel structures are 120 µm wide in the outer channels and 160 µm in the middle one, whereas in the five channels, all are 160 µm wide with all posts and spacing of 50 µm.

ramping at 300 rpm/s until 2000 rpm in 45 s. Approximately 1 mL of photoresist was added per inch of substrate diameter. After the resist was applied, the wafer was soft baked to evaporate the solvent and densify the film. The soft bake was optimized until coming up with a ramp from room temperature to 95 °C in 35 min in order to avoid cracks. In this step the previously designed mask is placed on top of the spun coated wafer (with printed face down) while on the mask-aligner. Exposure time was optimized for our UV light source in the Nanolab keeping the dosage between 185 - 250 mJ/cm^2 for 34 s and using the hard contact option in the mask-aligner. During UV exposure, the transparent parts of the mask start cross-linking. Excessive dose (*i.e.* higher time or intensity) resulted in over exposure of the top portion of the film, giving negative sidewall profiles or T-topping. Under-exposure, on the other hand, leads to adhesion failure, severely negative sidewalls and cracking. Cross-linking is continued during the post exposure bake (PEB) which selectively cross-links the exposed portions of the film so they are rendered insoluble to liquid developers. PEB proved to be the most care-demanding step of the process. Optimum structures were obtained through careful adjustments of heating and cooling ramps. All other patterns resulted on a highly stressed film with excessive cracking. The formulation we devised was increasing from room temperature to 95 °C in 75 min but then cooling in a controlled manner. Our program was set to cool down to 20 °C in a period of 6 h. MicroChem SU-8 Developer (mr-Dev 600) was used for developing the films after complete cooling. The wafer was placed on a holder completely immersed into the developer. The solution was stirred underneath the substrate for 7 min and then the beaker was sonicated for 3 min. The substrate was then rinsed with isopropyl alcohol (IPA) until no white spots were left on the now visible structures. If a white film was still visible (indication that the substrate had been under developed) it was immersed back in the developing solution and rinsed with IPA. Once clean, it was dried with a gentle N_2 stream. The same procedure was followed for all successful masters with all types of geometries.

To make the devices, we prepared a PDMS mix using the Sylgard 184 silicone elastomer kit. The elastomer and curing agent were mixed at a 10 to 1 (10:1) part ratio and then poured onto the masters, degassed and then baked at 60 °C for at least 2 h. Only the needed parts of the replica were removed from the mold by cutting around them with a razor blade (see Fig. 4.3). The inlet and outlets were opened using biopsy punches and consequently the whole PDMS structure was placed (along with a flat PDMS or glass substrate) under oxygen plasma for 30 s. The device was immediately assembled and sealed by applying a gentle force with the fingers.

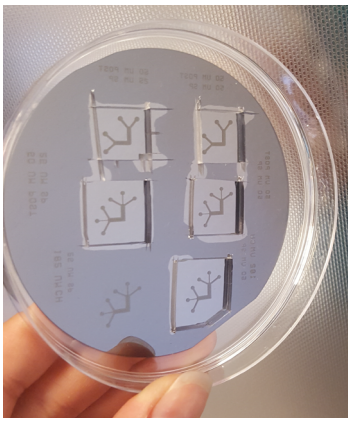

Figure 4.3. Rigid master on Si/SiO_2 wafer with cured PDMS. Chips are cut-out with a razor blade as needed.

Filling the channels

We cut and flattened pieces of a syringe needle and then inserted them into the inlet and outlet of the channels. We connected the inlet to a syringe containing EGaIn via PBTE (polytetrafluoroethylen) tubing (the non-stick properties of PBTE allow the transport of liquids with minimal fluid resistance). The injection of the EGaIn was done in a controlled manner by making use of a syringe pump. We made sure there were no leakages between the needle and the tubing and pumped at a rate of 3 mL/h. The short channels were immediately filled and did not leak between posts. For the long channels, however, injecting water in the channels prior to EGaIn was necessary. As shown by Rashed Khan [14], water creates a slip layer between EGaIn and PDMS which allows it to flow smoothly without sticking to the channel walls. EGaIn was injected subsequently, pushing the water away (in this EGaIn/contact water, the composition of the oxide changes, decreasing its modulus and making it less passivating). To prevent EGaIn from leaking to other channels due to the overpressure created by reticulated geometries, the syringe pump can be stopped as soon as EGaIn starts entering the channels. Letting the pressures stabilize in the channel before continuing injection, sometimes by gently tapping the PDMS, yields more homogeneous and stable electrodes. We also sealed the inlets of the other channels while injecting on a neighboring hole so that the liquid metal would not choose the path of least resistance and flow towards adjacents, open spaces. Injecting the metal required overcoming the interfacial forces, which scale inversely with the diameter of the microchannels [11].

4.3. *Mechanical Properties of Microfluidic Channels*

The mechanical properties of different geometries were tested at the laboratory of Prof. Michael Dickey at the Chemical Engineering department of North Carolina State University in Raleigh. The aim of these tests was to observe the behavior of the liquid electrode while stretching the PDMS devices. This involved determining whether EGaIn stayed inside the channel(s) or leaked through the posts and whether it remained continuous. The mechanical properties of the PDMS microchannels were also observed and their tensile strength was recorded.

The long channels that were tested were made by Xinkai Qiu. The first device to be tested was not long enough for sufficient adhesion and the pressure applied by the grips was so high that it caused the two pieces of PDMS to come apart. The problem was fixed by recasting fresh PDMS around the existing devices and curing as one piece. The PDMS structure for the short channels had an extra 2 to 3 cm of only polymer in order for the clamps to be able to have a firm grip without damaging the integrity of the filled microchannels. The filling was done by following the procedure previously described but fixing the tubing on the inlet and outlet bypassing the need of a blunt needle, the holes were made using a bigger punch to accommodate them. In order to prove that the EGaIn was still continuous in the channels as the devices were stretched, copper wires were inserted into the inlet and outlet of one of the filled channels and connected to a potentiostat. The first few devices were tested by connecting the leads to a potentiostat Reference 600 from Gamry Instruments and biasing at a constant voltage while reading the current output. The measurements proved challenging since it was difficult to keep the Cu wires fixed at the inlet and outlet and this lead to a variation in the reading of the output current. In order to fix this, the tubing used for the injection of the EGaIn was left in and cut about 2 cm above the device with continuous EGaIn from start to end. Cu wires were then inserted into the tubing and pushed all the way in while the other end was fastened to a source meter. The optimized devices were biased at 0.1 V and 0.5 V and their resistance recorded by a Keithley 2400 while the mechanical properties were measured using an Instron 5943 with a 1 kN load cell. Two hydraulic grips held the devices and stretched them at a constant rate of 3 mm/min (see Fig. 4.4). During the tensile strength tests, the gauge length between the two grips was measured by the software Bluehill 3.

We can describe the resistance of the liquid metal inside the devices using Pouillet's law 4.1.

$$R = \frac{\rho \cdot l}{A} \tag{4.1}$$

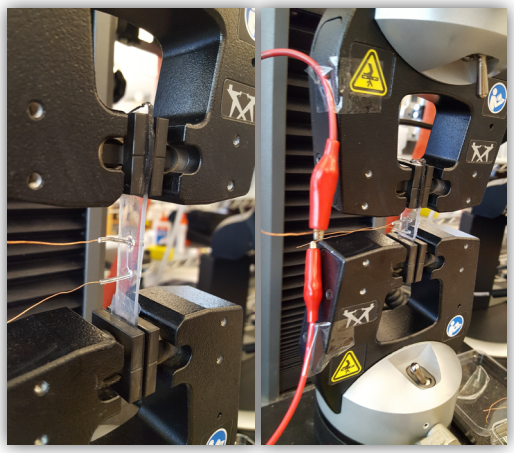

Figure 4.4. PDMS channels and tubbing filled with EGaIn. Cu wires serve as electrical contract between the devices and the source meter. Fastened at ca. 20 PSI on an Instron 5943.

where R is resistance of the conductor, ρ is the resistivity of the conductor, l is the length of conductor, and A is the cross-sectional area of conductor. According to Pouillet's law, the electrical resistance of the EGaIn inside the microchannel should increase as a function of elongation since the length (l) of the whole device increases while the cross-sectional area decreases. Fig. 4.5 shows the effect of percentage strain on the measured resistance and it shows that, as expected, it increases. The plot to the right shows the behavior of current over time as the elongation takes place and follows Ohm's law, that is, it shows that resistance and current are inversely proportional. Fig. 4.6 shows an elastic deformation in our devices, that is, reversible deformation. Most of the devices reached the point of fracture before reaching plastic deformation. From the slope of the curve we can calculate Young's modulus which was 1.25 MPa for this particular device.

The loss of conductivity (continuity) coincided with the physical rupture of the PDMS device or the accidental detachment of a Cu lead, in all other cases we observed no leakage or loss. The devices that were not tested to fracture point were brought to their initial non-stress point. An example of such case is provided in Fig. 4.7. This particular device was about 4mm thick and was stretched to close to 70% from its original value. The elongation was decreased mechanically but stepwise instead of continuously (as is apparent in the figure) and at a set rate.

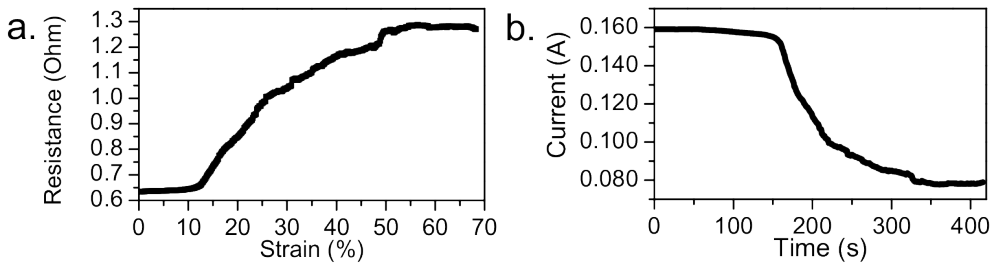

Figure 4.5. a. Percentage strain on the measured resistance *vs.* resistance (ohms). Resistance decreases as a function of device elongation. **b.** Current over time as the elongation takes place. Resistance and current are inversely proportional.

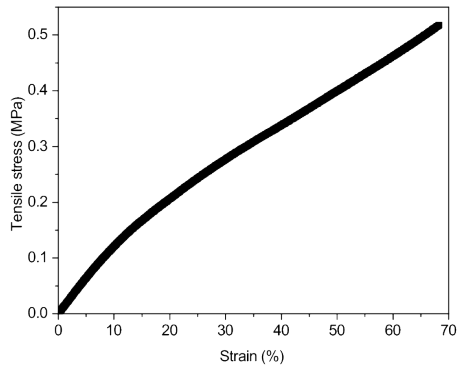

Figure 4.6. Percentage strain *vs.* tensile stress. The curve shows an elastic deformation. Young's modulus can be calculated from the slope (1.25 MPa for this particular device).

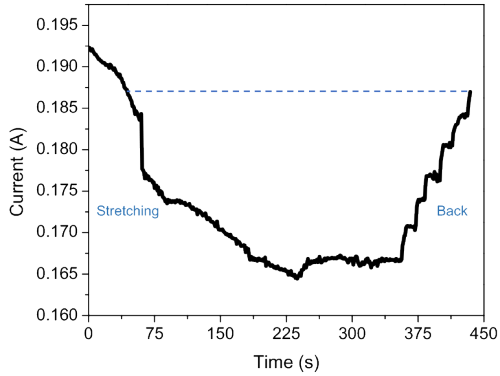

Figure 4.7. Current measured over time as the device was elongated to 70% of its initial value and then cycled back. Dashed line for comparison of both "initial" values. We hypothesize this offset might be due to the rapid decrease of elongation, not giving enough time for the PDMS and EGaIn to regain their starting shape.

We believe this explains why the final value was lower than the initial one –not enough time for the PDMS and EGaIn to regain their starting shape– however, still close. In all cases EGaIn remained in the channel and the surface tension was maintained even under stress. Examples of before and after pictures can be seen in Fig. 4.8.

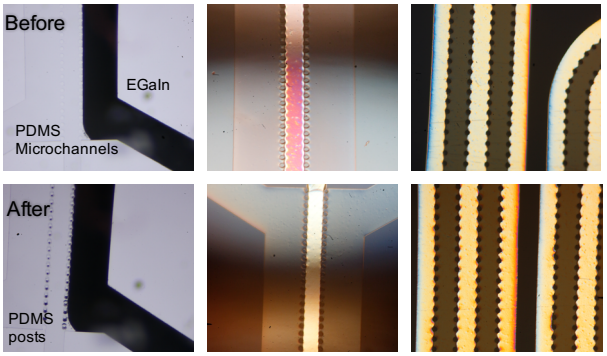

Figure 4.8. Top panel: Filled channels before stretching. Bottom panel: Same devices after stretching. EGaIn is seen as black, pink or gold depending on the light shone and the type of microscope used to image it. Because of its rheological properties, EGaIn stayed within the channels separated only by the PDMS posts (50 μm apart).

4.4. *The Fluidics of EGaIn in Junctions*

The stability of EGaIn in the channels was influenced by the effect of Laplace barriers (*i.e.* the PDMS posts). By making use of these barriers we could block the metal and guide it to only desired areas [10, 12]. The distance needed between posts in order for a fluid to remain confined, depended on the type of fluid (Netwonian *vs.* non-newtonian) and the critical pressure gradient created inside the microchannel. The closer the posts, the higher the critical pressure that can be applied. The relationship of pressure, fluids and dimensions is clear in the case of these Laplace barriers. The question now is, what is the behavior of EGaIn when separated by nanometer-sized complexes and suspended on top by a syringe and the oxide skin?

Chapter 2 elucidated the relationship between surface coverage and current density. This relationship leads us to wonder whether we would be able to predict at what distance between complexes EGaIn would go through and wet the substrate, *i.e.*, short. Taking advantage of having a monolayer composed by Photosystem I (PSI), a complex big enough that can be easily seen by AFM, we were able to count the number of complexes bound to a known surface area. For the

calculations, we made a number of considerations. We considered, for example, a rough surface. For this kind of surface, a wetting liquid would be completely absorbed in between the "pin holes", while a non-wetting liquid would not penetrate resulting in the formation of a composite solid/liquid/air interface. In order to determine a distance where the EGaIn touches the surface, we treated EGaIn like any liquid with a given curvature between pillars (molecules in this case). We can therefore approximate our situation to the Cassie-Wenzel regime transition model where a liquid droplet is suspended on a regular hydrophobic surface consisting of a regular array of circular pillars [15]. The maximum droop of this droplet (δ) would be found in the middle of two diagonally adjacent complexes (see Fig. 4.9). Since the geometry of PSI is "donut-like", we can consider the top of the anchored complex to be flat and circular and we can thus designate a diameter D and height H. The distance between the center of two adjacent molecules is the pitch, P, and the droplet radius is R. We also made the consideration that the local deformation is governed by surface effects rather than gravity. The (geometrically) derived equation becomes then:

$$\delta = \frac{(\sqrt{2}P - D)^2}{8R} \tag{4.2}$$

We performed a series of coverage experiments by changing the dilution of PSI on a buffer and drop-casting onto Au. These experiments helped us to understand the relationship between surface coverage and current density. For this calculation, we took the individual AFM graphs of all different coverages ranging from 1:1 to a 1:130 PSI and studied them. With the information gathered from the AFM images and eq. 4.2, we can solve to calculate a theoretical droop value for each case, but also, by setting the value of δ to the minimum value required for the droplet to touch the surface, that is H or the height of a molecule, we can find the theoretical distance at which our junction would short. Delta (δ) was set equal to the height of a PSI complex according to values reported in literature, that is, 8 nm. The value of D, 22 nm, was taken from literature values for cyanobacterial trimeric PSI [16] and the radius of an average EGaIn tip was set to 6500 nm. By solving for P we found that the minimum distance needed between complexes for EGaIn to wet the substrate is of around 472 nm.

Although from the AFM images we cannot judge which of the areas caused the shorts when gathering the data from each, we calculated the distances (diagonals) between the complexes in the areas where coverage seemed scarce and found a range from about 142 nm to 200 nm. This results are *ca.* two and a half to three

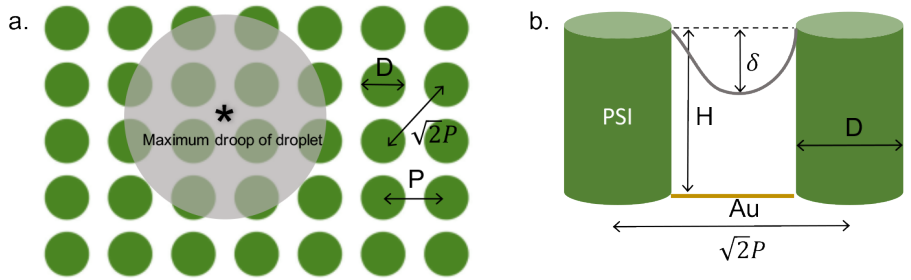

Figure 4.9. a. Cartoon of a suspended EGaIn drop between PSI complexes. We assume uniform and equidistant conformation for calculation simplicity. **b.** Side view of an ideal case of two PSI complexes (cylindrical for simplicity) on a Au surface. The maximum droop of EGaIn is found in the middle of diagonal complexes. δ is the droop of the EGaIn drop and R is its radius. D, H, P, are the diameter or the complexes, their height and the distance in between them (pitch).

times lower than the calculated value. It is, however, necessary to point out that our previous data was taken from electrical measurements with an applied bias up to 1 V. We hypothesize that electrostatic interactions between the electrodes might have caused the junctions to short at smaller distances that what would have been expected.

4.5. *Conclusions*

We proved that our devices are flexible and that EGaIn inside microchannels is extremely stable even under stress. The presence of the oxide skin of EGaIn does not only ensure its mechanical stability in co-fabricated channels (separated only by 50 μm posts), but also allows large-area measurements of monolayers of protein complexes with low coverage, avoiding pinholes and defects.

The ability to fabricate devices in a single photolithographic step, along with the ease of injecting a metal into PDMS microchannels, opens up a wide range of possible applications. Having aligned, reticulated metallic fluids that span the whole length and width of the channel, can provide uniform electric fields, stable junctions and multiple spots for reactions throughout the device. The injection of liquid metal into microchannels offers a simple method of integrating electrodes into microfluidic devices. One possible application for the geometries discussed in this chapter is tested in Chapter 5.

References

[1] A. C. Siegel, S. S. Shevkoplyas, D. B. Weibel, D. A. Bruzewicz, A. W. Martinez, and G. M. Whitesides, *Cofabrication of Electromagnets and Microfluidic Systems in Poly(dimethylsiloxane),* Angewandte Chemie International Edition **45**, 6877 (2006).

[2] A. Siegel, D. Bruzewicz, D. Weibel, and G. Whitesides, *Microsolidics: Fabrication of Three-Dimensional Metallic Microstructures in Poly(dimethylsiloxane),* Advanced Materials **19**, 727 (2007).

[3] R. Jackman, S. Brittain, and G. Whitesides, *Fabrication of three-dimensional microstructures by electrochemically welding structures formed by microcontact printing on planar and curved substrates,* Journal of Microelectromechanical Systems **7**, 261 (1998).

[4] W. Wang, M. R. Holl, and D. T. Schwartz, *Rapid Prototyping of Masks for Through-Mask Electrodeposition of Thick Metallic Components,* Journal of The Electrochemical Society **148**, C363 (2001).

[5] R. J. Jackman, *Design and Fabrication of Topologically Complex, Three-Dimensional Microstructures,* Science **280**, 2089 (1998).

[6] J. Yan, Y. Du, J. Liu, W. Cao, X. Sun, W. Zhou, X. Yang, and E. Wang, *Fabrication of Integrated Microelectrodes for Electrochemical Detection on Electrophoresis Microchip by Electroless Deposition and Micromolding in Capillary Technique,* Analytical Chemistry **75**, 5406 (2003).

[7] D. A. LaVan, P. M. George, and R. Langer, *Simple, Three-Dimensional Microfabrication of Electrodeposited Structures,* Angewandte Chemie International Edition **42**, 1262 (2003).

[8] G. Maltezos, R. Nortrup, S. Jeon, J. Zaumseil, and J. A. Rogers, *Tunable organic transistors that use microfluidic source and drain electrodes,* Applied Physics Letters **83**, 2067 (2003).

[9] X.-s. Zhu, C. Gao, J.-W. Choi, P. L. Bishop, and C. H. Ahn, *On-chip generated mercury microelectrode for heavy metal ion detection,* Lab on a Chip **5**, 212 (2005).

[10] M. Rashed Khan, G. J. Hayes, J.-H. So, G. Lazzi, and M. D. Dickey, *A frequency shifting liquid metal antenna with pressure responsiveness,* Applied Physics Letters **99**, 013501 (2011).

[11] M. D. Dickey, R. C. Chiechi, R. J. Larsen, E. A. Weiss, D. A. Weitz, and G. M. Whitesides, *Eutectic Gallium-Indium (EGaIn): A Liquid Metal Alloy for the Formation of Stable Structures in Microchannels at Room Temperature,* Adv. Funct. Mater. **18**, 1097 (2008).

[12] J.-H. So and M. D. Dickey, *Inherently aligned microfluidic electrodes composed of liquid metal,* Lab on a Chip **11**, 905 (2011).

[13] E. Kreit, M. Dhindsa, S. Yang, M. Hagedon, K. Zhou, I. Papautsky, and J. Heikenfeld, *Laplace Barriers for Electrowetting Thresholding and Virtual Fluid Confinement,* Langmuir **26**, 18550 (2010).

[14] M. R. Khan, C. Trlica, J.-H. So, M. Valeri, and M. D. Dickey, *Influence of Water on the Interfacial Behavior of Gallium Liquid Metal Alloys,* ACS Applied Materials & Interfaces **6**, 22467 (2014).

[15] B. Bhushan, Y. C. Jung, and K. Koch, *Micro-, nano- and hierarchical structures for superhydrophobicity, self-cleaning and low adhesion,* Philosophical Transactions of the Royal Society A: Mathematical, Physical and Engineering Sciences **367**, 1631 (2009).

[16] J. Barber, *The Photosystems: structure, function, and molecular biology* (Elsevier ; Sole distributors for the USA and Canada, Elsevier Science Pub. Co., Amsterdam; New York; New York, NY, USA, 1992) oCLC: 690849375.

5

Soft-Devices Comprising PSI

The most exciting phrase to hear in science,
the one that heralds new discoveries,
is not "Eureka!" but "that's funny..."

ISAAC ASIMOV

Xinkai Qiu carried out the synthesis of crystals and the evaporation of the high-surface Au electrodes. Henry de Vries and Maikel van Putten were involved in the preparation and the measurements of the proof-of-concept devices. Mark Loznik provided the Photosystem I and redox couple.

5

Abstract

The idea developed within this chapter consists in finding the optimal way to contact and use Photosystem I (PSI) and its high internal efficiency to make an "ideal, self-fabricating" photovoltaic device. Our non-conventional techniques do not rely on traditional methods like photolithography, vapor deposition, etching, etc., and therefore are compatible with materials that are more appropriate for extracting charges from PSI. This chapter describes the fabrication of microfluidic devices whose channels are defined by an array of closely spaced posts. By taking advantage of the unique rheology of EGaIn, the liquid metal can be injected and remain confined within the channels allowing the movement of electrons from one electrode to the other if chemical reactions occur between the posts. Here we demonstrate a proof-of-concept device which follows the concept of a dye-sensitized solar cell (DSC) where electrons are cycled through counter electrodes via electrolyte/redox-couple, creating a "self-fabricating" photovoltaic device.

5.1. *Introduction*

Increasing energy demand has led to an increase in diversified research into clean, renewable and low-cost technologies for energy production. Solar power is viewed as one of the most promising alternatives for replacing fossil-based energy sources (it is clean and with self-sustaining potential), in fact, the International Energy Agency projected that by 2050, solar would be the largest source of electricity [1]. There is vast research going on in the developing field of solar cells, but it is not limited to silicon/inorganic and organic, it also includes bio and bio-hybrid. Comparing traditional photovoltaics to bio-hybrid solar cells is not straightforward, especially when the term "efficiency" is so widely used as a measurement of impact and yet its definition is not unified (different assumptions and conditions are made in each case). An article from Science [2] tries to explain this "considerable confusion" by providing consistent definitions and studying the factors that affect said "efficiencies". When talking about "conversion efficiency", or the efficiency of harvesting the entire solar spectrum, the percentage calculated is higher for traditional PV technology than bio/bio-hybrid solar cells (around 40% and 1%, respectively), however, the total integrated cost of the systems must also be considered. Therefore, argues Blankenship, "the technology with the highest efficiency may not necessarily be the best choice to implement in a given situation". The biggest advantage of the bio-photovoltaic cells we propose is that by making use of Photosystem I (PSI), we already have an active ingredient with a 100% internal quantum efficiency with the potential of having almost no power lost through the conversion from chemical to electrical power.

Our target devices are based on the idea of a dye-sensitized solar cell (DSC) [3]. In a DSC, light is absorbed by a "sensitizer", which injects electrons into the adjacent semiconductor. Charges are separated at this interface driven by light reactions that induce electron injection from the dye into the semiconductor. The dye is then regenerated by a redox couple which is, in turn, regenerated by the electrons at the counter electrode (cathode). In our devices, PSI would work as the dye which would be bound to an anode material. Just like in DSCs, a redox couple would regenerate the PSI and EGaIn would act as the cathode. The electrolyte/redox-couple and EGaIn would be in contact, creating a "self-fabricating" photovoltaic device. In the case of a DSC, electrons are injected into the solid electrode and holes into the redox couple. In the case of our PSI device, the flow of electrons takes place in the opposite direction. This direction, however, can be changed as desired by simply re-orienting the PSI complexes by making use of different orienting molecules, as explained in Chapter 2. Being able to

control the orientation and therefore the direction of current flow is yet another advantage provided by PSI that would not be possible with other molecules.

The previous chapters described a fast and facile method for creating solid-state electronic devices comprising PSI. These solid-state devices, however, have many technical limitations when it comes to finding "real-world" applications. An ideal, versatile device for multiple applications, for example, would be flexible, light weight, mechanically resilient, soft, and transparent –among others [4], characteristics that solid devices do not have. A way to bridge these characteristics would be to make use of PDMS (polydimethylsiloxane) microfluidic channels which are inherently transparent and flexible as well as soft, light and easy to make. In order for a microfluidic device to work well with our bio-based idea, the electrodes would have to be in direct contact with the biological complexes inside the channel for the electron exchange to take place but separated from each other to avoid shorts. This poses both, a manufacturing and a material challenge for the fabrication of these bio-devices. Both of these challenges can be overcome by making use of a previously published strategy [5]. This strategy consists in fabricating microfluidic devices via photolithography and co-fabrication [6] in which the channels are separated by small PDMS posts. In this paper, Dickey and co-workers demonstrated that EGaIn can be injected, flows readily into such geometries and stays in the channel thanks to its unique rheological properties and the Laplace barrier created by the posts [7].

By making joint use of these techniques, we can address the matter of safely contacting the biological complexes and providing a space where redox reactions can take place. The advantage of these geometries is that we can simply inject EGaIn as one of the electrodes, PSI as the active element, the electrolyte and redox couple, and have a second electrode in one of the adjacent channels. This chapter describes our proof-of-concept "self-fabricating" photovoltaic device. A schematic of the final concept can be appreciated in Fig. 5.1.

5.2. *Proof-of-Concept Devices*

Whitesides and co-workers reported a strategy for fabricating multicomponent microsystems in a single step; they called this technique co-fabrication [6]. This type of fabrication consists in generating a master with a set pattern and subsequently pouring and curing a polymer (in this case PDMS) yielding a replica (further details given in previous chapter). Researchers from NCSU further developed this idea to create inherently aligned microfluidic electrodes [5].

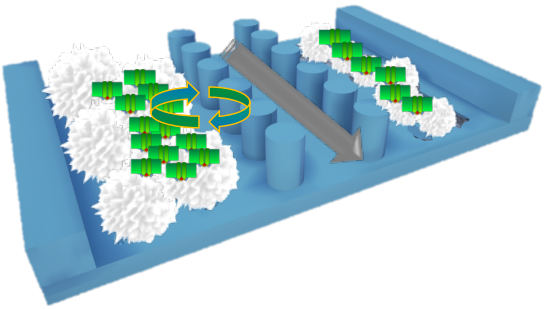

Figure 5.1. Schematic of ideal, "self-fabricating" photovoltaic device. It imitates the concept of a DSC where electrons are cycled through counter electrodes via electrolyte/redox-couple. White crystals indicate a nest-like, 3D structure of a conductive material where Photosystem I (green) can be anchored. EGaIn is injected in the middle channel and chemical reactions take place through the posts via a redox couple (indicated by arrows).

Based on both techniques, we developed our own protocols to construct our own geometries by co-fabrication. The protocols and characteristics of our microfluidic devices are described in detail in Chapter 4. For our proof-of-concept devices, we used the simplest geometries, that is, short two and three channels devices both straight and L-shaped. The two-channel geometries were 475 µm wide each and in the three-channel, the two outer were 375 µm and the inner 150 µm wide. The spacing between the 50 µm tall posts was 25 and 50 µm, the total length from inlet to outlet was 12 mm. The "L"-shaped channels had the same dimensions but their total length was 14 mm.

In order to construct our devices, we injected the liquid metal into the "electrode channel". Once in the channels, EGaIn forms an oxide skin which allows the metal to stabilize and maintain its shape and confinement [8]. The injected EGaIn electrodes are stable and can generate electric fields in both non-aqueous and aqueous systems under DC and AC electric fields [5].

5.2.1. Template-Stripped and Shadow Evaporated Gold

Research concerning PSI solid-state devices in Chapters 2 and 3 provided an insight on the behavior of PSI complexes oriented on Au substrates. We decided, therefore, to fabricate our proof-of-concept devices by making use of Au as the second electrode (anode) and orienting PSI on it. For the fabrication, we fluorinated a Si/SiO_2 wafer for ca. 30 minutes by placing it on a degassing chamber along with a vial containing two droplets of a fluorinating agent. This helps to ensure a correct lift-off of the Au patterns during cleavage. We then evaporated

150 nm of Au on it through masks with established patterns. We cleaned 2 x 2 cm glass pieces by sonicating and rinsing with soap/acetone/ethanol or by immersing in piranha acid with a final ethanol rinse. Afterwards, we placed a drop of Nordson optical adhesive on top of the Au structures and placed the glass pieces on top. Subsequently, we treated with UV light for 5 min. at 50% power to cure the adhesive and cleave the glass with the transferred Au structure.

Immobilizing PSI on flat devices

This part of the research was started by Maikel van Putten and continued by Henry de Vries, both Top-master students under my supervision. Since PDMS can form microcracks after cured, we evaporated the thin film of Au onto glass as second electrode. We plasma cleaned the PDMS short channels plus the glass with the evaporated electrodes for about 30 s. We then proceeded to seal by bringing together both pieces and gently pressing with the fingers. We injected EGaIn in one of the two channels at 0.5 mL/h and then injected the orienting SAM (self-assembled monolayer) or "linker" (MPS or 2ME 1mM as in Chapter 2) at a rate of 0.5 mL/h until the channel was filled. Since immobilization of the linker molecules takes two hours, we kept a constant flow during said time to prevent evaporation (< 0.1 mL/h) while covering the outlet. We rinsed after the immobilization time by increasing the rate to inject the same linker at 0.5 mL/h for about 1 min. We then injected the PSI at 0.5 mL/h and left for 2 h, although we would have liked to keep constant flow during the immobilization, we were limited by the amount of PSI that was available to us. We finished by rinsing with deionized (DI) water . A second way to immobilize the linking SAM is by drop-casting onto the Au electrode before sealing the device. The immersion time is 2 h followed by a rinse with DI-water for H_2O for MPS and EtOH for 2ME and a gentle blow-dry before applying channels. EGaIn and the redox couple (mixture of methyl viologen, dichlorophenolindophenol, and sodium ascorbate prepared by Mark Loznik) were subsequently injected into the right channels. An example of this "flat electrode" devices can be seen in Fig. 5.2.

Immobilization on high-surface devices

In order to increase the area of the anode for the PSI complexes to attach to, we designed high-surface area Au electrodes. The nanoporous Au lines were based on a technique described in literature [9]. Following this technique, we evaporated 100-150 nm of Au at 1 Å/s by electron-beam (e-beam) evaporation onto a rotating platform containing a substrate and a nanoporous anodized aluminum oxide (AAO) membrane oriented at a 45° incident angle. Once the evaporation was finished, we applied the resulting strip unto a cut-out PDMS piece by gently tapping to increase adhesion. We etched the membrane by drop-casting 1M NaOH

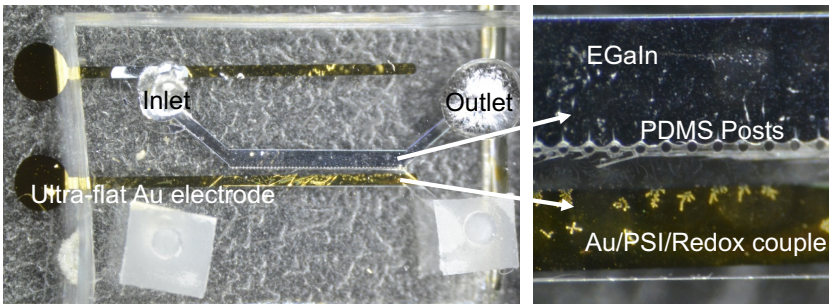

Figure 5.2. Proof-of-concept device with EGaIn and template-stripped Au as electrodes. A monolayer of PSI was oriented on the Au via a monolayer of a short thiolated linker. The microchannel with the PSI also contains the redox couple (methyl viologen, dichlorophenolindophenol, and sodium ascorbate).

on the Au and leaving for 1 h. After this, we rinsed with DI-H_2O and removed the surplus NaOH by absorbing it with tissue. The rinsing was repeated three times. We then proceeded to form a monolayer of the orienting molecules, MPS or 2ME (see Chapter 2 for more details) by drop-casting and incubating for 2 h. We rinsed with corresponding solvents (H_2O or ethanol, respectively) followed by rinsing with DI-H_2O and drying by removing surplus liquid with tissue and finally by blowing with N2. The length of the shadow evaporated Au lines was shorter than the length of the PDMS channels used to make the devices. This difference poses a physical limitation for performing the electrical measurements on the final device. Therefore, we made the devices using the L-shaped channels and leaving a part of the SE electrode uncovered in order to be electrically contacted. We applied Ag-paste on the SE-Au electrode and finished the device by adding the PSI, EGaIn and redox couple as previously described (see Fig. 5.3).

5.2.2. Electrical Measurements

We used a tri-connector in our home-built measuring setup along with a Keithley 6430. The wiring was done as follows: red clamp to gold back electrode, green on the EGaIn, "active" electrode and black for the ground. We warmed up the Keithley for ca. 1 h and in parallel set up an ice bath to be placed underneath the measuring stage to prevent over-heating. We further set up a continuous redox flow through the device to prevent evaporation of the solvents. We used an in-house Labview software to measure current. We set the NPLC (number of power line cycles) in the source meter to 10 to decrease the noise and measured at 0 V bias. We let it stabilize for ca. 10 min while adjusting the injection speed until the output was stable. Multiple devices were measured with the light on and

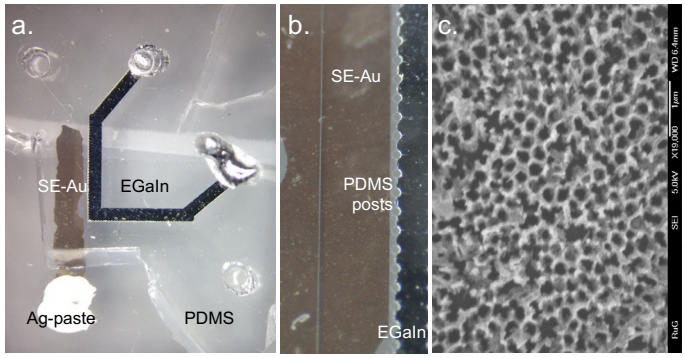

Figure 5.3. a. Proof of concept device with EGaIn and nanoporous Au as electrodes. **b.** Electrodes separated by PDMS posts (Laplace barriers). Orienting layer and PSI are grown on the shadow evaporated (SE) Au and the channel is filled with the redox couple (methyl viologen, dichlorophenolindophenol, and sodium ascorbate). **c.** SEM image of SE Au. Gold was evaporated through a nanoporous anodized aluminum oxide (AAO) membrane oriented at a 45 °.

off. For illuminated measurements we used a laser pointer. We diffused the laser beam making use of negative glasses or scotch tape, the latter resulting in lower intensity. Different wavelengths were tested (650 nm, 532 nm and 405 nm) with 650 nm (red) resulting in the highest current output, followed by 405 nm (purple) and the lowest at 532 nm (green). This last result is consistent with expectation since the chloroplasts in PSI do not absorb (or absorb very little) around the "green gap", that is, wavelengths around 510-600 nm. All measurements were done on a heat sink and inside a vibration-free Faraday cage.

5.2.3. Nest-like Structures

Fabricating the anode from template-stripped gold lines [10] is a good start for a proof-of-concept device, nonetheless, the final devices would require an electrode that takes full advantage of the dimensions of the microchannels and that can work well with stretchable and flexible devices. With the field of "Lab on a chip" growing, many new techniques have emerged to fabricate structures inside microfluidic channels [11–17]. However, most of these techniques require expensive, sophisticated processes that have many technical limitations such as making structures under 100 nm. Chemical fabrication has emerged as a simple method to form 3D structures in microchannels. However, most techniques include off-site modification followed by integration processes that can damage the microfluidic channels. Therefore, in order to bypass elaborated processes, we followed an *in-situ* approach based on work done by Wang a co-workers [18].

There, researchers created 3D networks of semi-conducting crystals on the inner wall of glass capillaries. Their 3D networks consisted of micro and nanoporous structures with large surface areas that could be easily modified by adding and attaching new elements.

Crystal networks synthesis

We followed the protocol of the above-mentioned article for synthesizing the nest-like crystal networks inside PDMS microchannels with the exception of modifications to the setup. All chemicals and reagents used during these steps were purchased from Sigma-Aldrich and used without further purification. Solutions of zinc acetate (0.01 M) and NaOH (0.04 M) were prepared in ethanol and injected into the microchannels. Since the adjacent channels already contained EGaIn, the solutions stayed in the channels and due to capillarity and Laplace barriers, did not go through the posts. We used a Fusion 200 Touch infusion syringe pump from KR Analytical to keep a constant rate from both syringes. We connected them using a home-made "Y"-junction. The "Y"-junction was attached to the microchannel by previously plugging the outlet needle perpendicularly into the inlet of the channel. The PDMS microchannel was then filled at a set rate of 0.05 mL/h. Once the microchannel was completely filled, the device was placed in a conventional oven at 60 °C for 4 h. In order to insure adhesion of the crystals to the microchannel walls, the device was thermally annealed at 150 °C.

Subsequently, Zn(OH)F nest-like networks were prepared by injecting a fresh aqueous solution of zinc nitrate (0.05 M) and ammonium fluoride (0.05 M) at 90 °C over 1 h at a rate of 0.5 mL/h. After the reaction was complete, the microchannel was rinsed with DI-water at a pump rate of 0.5 mL/h for 5 min and dried at 60 °C. Zn(OH)F@ZnS nest-like networks were further prepared by exposing the already formed networks to thioacetamide (TAA) by pumping an aqueous 0.2 M solution at a rate of 0.1 mL/h at 90 °C for 3 h. Once the networks were formed, the microchannel was washed with DI-water and dried at 60 °C.

In the original paper, Wang *et al.* decorate the 3D structures with Ag nanoparticles (np) resulting in Ag-Zn(OH)F@ ZnS. They used sodium thioglycolate (ST) to react with Ag np adsorbed on the surface of the network structure through -SH groups forming Ag-S bonds [19, 20]. We followed a similar procedure by running a solution of 20 nm-Au np through the network since PSI can be easily oriented and characterized on Au. One short-term goal of the project is to confirm the presence of Au np (see Fig. 5.4). Once this is solved, we will proceed to immobilize PSI onto them with a similar protocol as described by Terasaki *et al.* [21]. We expect the capture and detection of PSI will be successful since it was already demonstrated with BSA (bovine serum albumina).

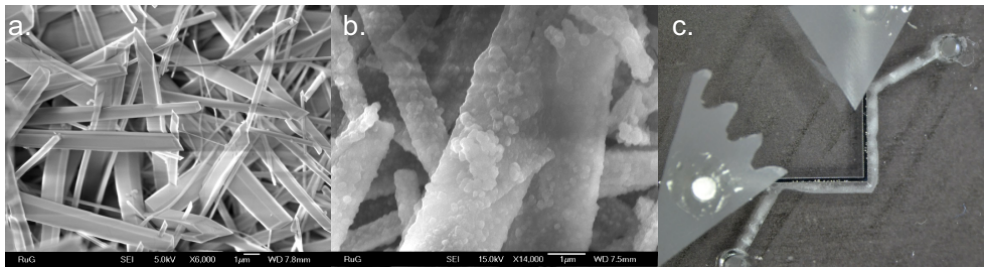

Figure 5.4. a. Scanning electron microscope (SEM) images of Zn(OH)F nest-like network. **b.** Zn(OH)F@ZnS nest-like networks with attached 20 nm Au nanoparticles. **c.** Photograph of microfluidic device with crystals inside the outer microchannel and EGaIn in the inner one. Triangular grey shapes are tape pieces covering the inlet and the outlet of the EGaIn channel.

5.3. *Results and Conclusions*

All measurements were performed on devices with Au electrodes. Measurements on devices containing 3D nest-like structures are still to be performed.
We started by performing control experiments on different test devices: full devices, devices with linkers but without PSI, devices with a thiolated linker ($C_{16}H_{34}$) and without PSI, usual device but with water instead of redox couple. The results (seen in Fig. 5.5) show a stronger photoresponse when PSI is present (difference of at least 4 nm depending on the case), however, photoresponses are also visible in the cases without PSI. We think this observation, along with a clear drift in current is due to solvent evaporation and a lack of proper illumination.

In order to correct for those factors, we established a continuous redox flow and diffused the light beam from the laser. The results from this optimized experiment can be seen in Fig. 5.6. Here, we see a decrease in drift and a noticeable photoresponse (about 5 nm) only in the cases where PSI was present. Next, we proceeded to fabricate high-surface Au electrodes. We used the same conditions as in the previous experiment but without a continuous redox flow. The result is shown in Fig. 5.7 where a photoresponse of about 25 nA is observed. This result is about an order of magnitude higher than the photoresponse observed from the flat electrodes. We believe this proves that higher PSI density leads to an increase in photocurrent. However, to the moment, no other controls have been done on this type of devices.

After further study of our results and considering the nature of our current redox couple which, incidentally, is the same used to study PSI activity by oxygen consumption (MV as electron acceptor, ascorbate as electron donor and DCPIP

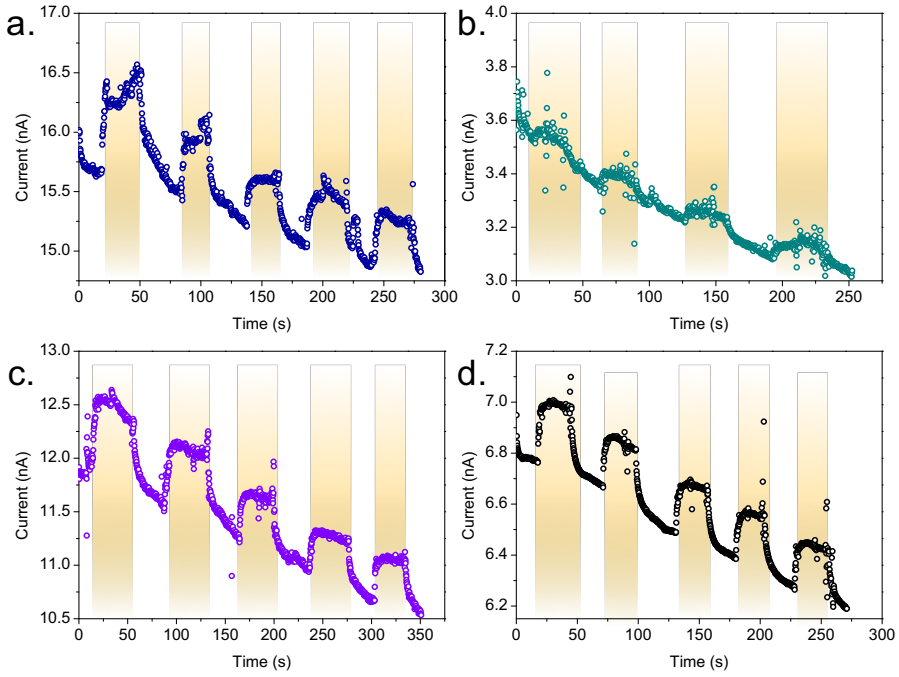

Figure 5.5. Current vs. time curves for full and control devices. Devices were illuminated by a laser with a wavelength of 650 nm. Photocurrent is evidence by golden stripes. **a.** Full device containing PSI, redox couple and linker. **b.** Full device containing with water instead of redox couple. **c.** Device with linkers but without PSI. **d.** Device with a thiolated linker ($C_{16}H_{34}$) and without PSI.

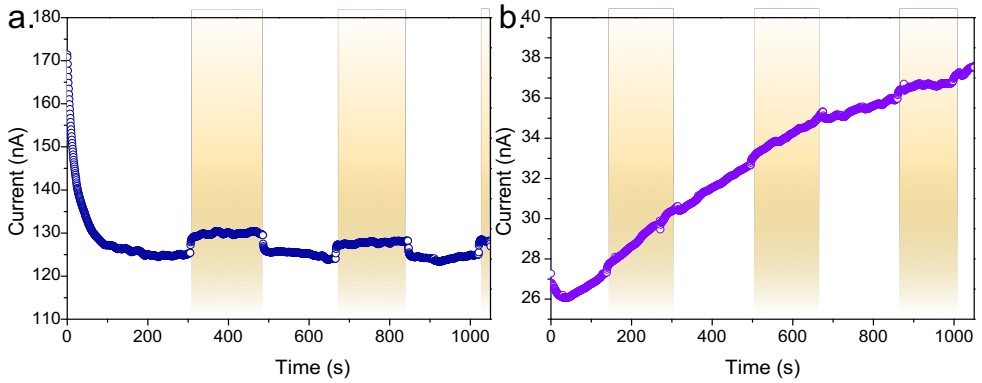

Figure 5.6. Current vs. time curves for full and control optimized devices. Continuous redox flow and a diffused the light source were added to the setup. Devices were illuminated by a laser with a wavelength of 650 nm. Photocurrent is evidence by golden stripes. **a.** complete device containing PSI, redox couple and linker. **b.** control device without PSI.

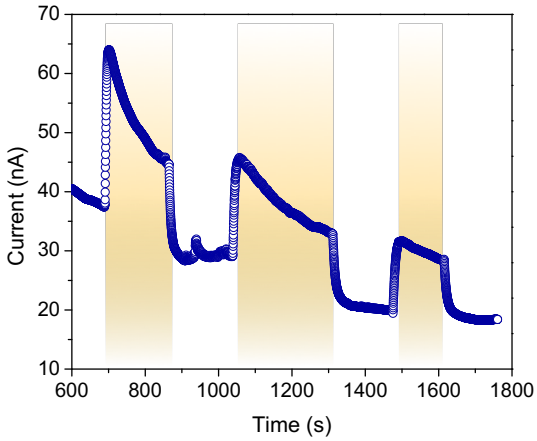

Figure 5.7. Complete optimized device containing PSI, redox couple and linker on high-surface, nanoporous Au.

as "Hill oxidant"), we hypothesize that what is occurring is an oxygen consumption reaction instead of a straightforward redox reaction cycling electrons. We believe this can explain the drift in current and the low values. By optimizing the anode material and the redox couple we hope to improve the performance of our "backwards" DSC circuit.

Our test devices are still far from being a finished project, but we have thus far demonstrated that bio-electrical devices can be made by making use of simple fabrication steps. We also demonstrated the ability to fabricate stable, semiconducting nest-like networks inside PDMS microchannels which had only been successful in glass capillaries. Further optimization needs to be done on design, and standardizing the measurements. Control experiments need to be performed on devices with high-surface Au electrodes and their mechanical properties on PDMS need to be tested. We hypothesize that the best results will come from the devices with nest-like structures as anode since they can expand the whole width of the channel. These networks provide a very high surface area for the attachment of PSI and can be easily modifiable by anchoring metallic or other types of nanoparticles.

References

[1] *Technology Roadmap: Solar Photovoltaic Energy,* (2014).

[2] R. E. Blankenship, D. M. Tiede, J. Barber, G. W. Brudvig, G. Fleming, M. Ghirardi, M. R. Gunner, W. Junge, D. M. Kramer, A. Melis, T. A. Moore, C. C. Moser, D. G. Nocera, A. J. Nozik, D. R. Ort, W. W. Parson, R. C. Prince, and R. T. Sayre, *Comparing Photosynthetic and Photovoltaic Efficiencies and Recognizing the Potential for Improvement,* Science **332**, 805 (2011).

[3] M. Grätzel, *Dye-sensitized solar cells,* Journal of Photochemistry and Photobiology C: Photochemistry Reviews **4**, 145 (2003).

[4] R. F. Service, *MATERIALS SCIENCE: Inorganic Electronics Begin to Flex Their Muscle,* Science **312**, 1593 (2006).

[5] J.-H. So and M. D. Dickey, *Inherently aligned microfluidic electrodes composed of liquid metal,* Lab on a Chip **11**, 905 (2011).

[6] A. C. Siegel, S. S. Shevkoplyas, D. B. Weibel, D. A. Bruzewicz, A. W. Martinez, and G. M. Whitesides, *Cofabrication of Electromagnets and Microfluidic Systems in Poly(dimethylsiloxane),* Angewandte Chemie International Edition **45**, 6877 (2006).

[7] E. Kreit, M. Dhindsa, S. Yang, M. Hagedon, K. Zhou, I. Papautsky, and J. Heikenfeld, *Laplace Barriers for Electrowetting Thresholding and Virtual Fluid Confinement,* Langmuir **26**, 18550 (2010).

[8] M. D. Dickey, R. C. Chiechi, R. J. Larsen, E. A. Weiss, D. A. Weitz, and G. M. Whitesides, *Eutectic Gallium-Indium (EGaIn): A Liquid Metal Alloy for the Formation of Stable Structures in Microchannels at Room Temperature,* Adv. Funct. Mater. **18**, 1097 (2008).

[9] M. D. Dickey, E. A. Weiss, E. J. Smythe, R. C. Chiechi, F. Capasso, and G. M. Whitesides, *Fabrication of Arrays of Metal and Metal Oxide Nanotubes by Shadow Evaporation,* ACS Nano **2**, 800 (2008).

[10] M. Hegner, P. Wagner, and G. Semenza, *Ultralarge atomically flat template-stripped Au surfaces for scanning probe microscopy,* Surface Science **291**, 39 (1993).

[11] A. D. Stroock, *Chaotic Mixer for Microchannels,* Science **295**, 647 (2002).

[12] S. M. Kim, S. H. Lee, and K. Y. Suh, *Cell research with physically modified microfluidic channels: A review,* Lab on a Chip **8**, 1015 (2008).

[13] S. Zheng, E. Ross, M. A. Legg, and M. J. Wirth, *High-Speed Electroseparations Inside Silica Colloidal Crystals,* Journal of the American Chemical Society **128**, 9016 (2006).

[14] P. Li, Y. Gao, and D. Pappas, *Negative Enrichment of Target Cells by Microfluidic Affinity Chromatography,* Analytical Chemistry **83**, 7863 (2011).

[15] S. Cheng and Z. Wu, *Microfluidic electronics,* Lab on a Chip **12**, 2782 (2012).

[16] J. Yan, Y. Du, J. Liu, W. Cao, X. Sun, W. Zhou, X. Yang, and E. Wang, *Fabrication of Integrated Microelectrodes for Electrochemical Detection on Electrophoresis Microchip by Electroless Deposition and Micromolding in Capillary Technique,* Analytical Chemistry **75**, 5406 (2003).

[17] M. C. Liu and Y.-C. Tai, *A 3-D microfluidic combinatorial cell array,* Biomedical Microdevices **13**, 191 (2011).

[18] G. Wang, G. Shi, H. Wang, Q. Zhang, and Y. Li, *In Situ Functionalization of Stable 3d Nest-Like Networks in Confined Channels for Microfluidic Enrichment and Detection,* Advanced Functional Materials **24**, 1017 (2014).

[19] S. W. Joo, S. W. Han, and K. Kim, *Multilayer Formation of 1,2-Ethanedithiol on Gold: Surface-Enhanced Raman Scattering and Ellipsometry Study,* Langmuir **16**, 5391 (2000).

[20] G. N. R. Tripathi and M. Clements, *Adsorption of 2-Mercaptopyrimidine on Silver Nanoparticles in Water,* The Journal of Physical Chemistry B **107**, 11125 (2003).

[21] N. Terasaki, N. Yamamoto, T. Hiraga, I. Sato, Y. Inoue, and S. Yamada, *Fabrication of novel photosystem I–gold nanoparticle hybrids and their photocurrent enhancement,* Thin Solid Films **499**, 153 (2006).

6

Conclusions and Future Work

Imagination is more important than knowledge.
Knowledge is limited. Imagination encircles the world.

ALBERT EINSTEIN

6

Abstract

This chapter presents the general conclusions of this thesis and recommendations on optimization for future work.

6.1. *Conclusions*

Natural photosynthesis is a great source of inspiration for scientists looking to fabricate photovoltaics and light harvesting and conversion systems. In this thesis, however, we sought to stay away from biomimetics and instead used the natural photosynthetic complexes to integrate them into electrical devices. This thesis describes the fabrication of solid-state and microfluidic devices comprising the photosynthetic complex, photosystem I (PSI). Here, I demonstrate the successful incorporation of these photo-active molecules into electronic devices without losing their activity.

Fundamentally, in collaboration with colleagues from Polymer Chemistry and Bioengineering, we were able to successfully orient a monolayer of PSI by making use of director molecules to modify the surface chemistry of the substrate (up to 70%). We established a clear relationship between the average orientation of PSI and the asymmetry (rectification) in solid-state devices. We also established that the dominant mechanism of charge-transport through the monolayer of PSI on Au is likely tunneling. We determined this through variable-temperature measurements and a lack of thermally activated transport. We also found that the observed rectification is the result of the internal electric field that arises from the collective action of dipoles (and multipoles) within the complex. In doing this, we validated EGaIn (Eutectic Gallium Indium) tips as a technique to electrically interrogate arrays of macromolecules. Subsequently, we developed a technique to orient 99% of the complexes on ITO (Indium Tin Oxide) via phage-display. Using EGaIn as top electrode proved once more to be a useful method for electrical measurements.

One of the purposes of the research project was to demonstrate that the concepts studied and developed with solid-state devices could be translated into soft, flexible, transparent devices. The final proof-of-concept devices, made of PDMS and containing PSI as the active material were successfully fabricated and yielded a photocurrent of 25 nA, a significant cipher for our devices. We also demonstrated the ability of synthesizing semi-conducting ZnS-Coated Zn(OH)F (Zn(OH)F@ZnS) nest-like networks inside PDMS microchannels to be potentially used as an electrode in our devices. Lastly, the flexibility of the PDMS (polydimethylsiloxane) devices was studied by stretching under a controlled environment. The devices were stretchable up to 50-60% of their original length and were able of regaining their original form after stretching. EGaIn inside the channels remained confined and did not leak into adjacent channels thanks to Laplace barriers and the unique rheology of EGaIn and its oxide skin.

6.2. *Future Work*

Much of the time allotted to this doctoral research was spent on the characterization and optimization of PSI solid-state devices on different substrates (Au, Ag, ITO, graphene), under different conditions (concentration, annealing, immersion times, *etc.*) and developing new techniques to increase the percentage of PSI orientation. This laid the ground work for further research and clarified key elements such as the best way to orient PSI complexes, their electrical properties and the mechanism of charge-transport in junctions.

Focusing on solid-state devices, however, meant less time developing and optimizing the microfluidic bio-photovoltaic cells. Future work will involve, therefore, improving the proof-of-concept biophotovoltaic device. This optimization will need to take into account standardizing the elements within the cell and improving the redox couple to correctly complete the electrical cycle. Control experiments need to be performed on devices with high-surface Au electrodes to set a baseline for results. The mechanical properties of nanoporous-Au and nest-like structures on PDMS microchannels need to be tested to determine their compatibility with flexible devices. Although ZnS-Coated Zn(OH)F (Zn(OH)F@ZnS) nest-like networks were successfully synthesized and confined within PDMS microchannels, the determination of the presence of metallic nanoparticles (NPs) is still inconclusive. An energy-dispersive X-ray (EDX) spectrum can be taken to determine the presence of these nanoparticles. Transmission electron microscope (TEM) or a high-resolution transmission electron microscope (HRTEM) measurements can be performed to investigate the network structures. They can reveal their composition and give an insight into their structural features. In a TEM image, the metallic NPs would appear as dark dots.

I expect that the best results in our bio-photovoltaic devices will come from systems containing nest-like electrode as anode since they can expand the whole width of the channel. Higher surface area means more spots for the PSI to attach to and therefore provides more sites for reactions to take place.

The methods here described can also serve as a platform for innovative developments in current processes. The ease of co-fabrication and incorporation of metallic components into devices opens up a wide range of possible applications. Having aligned, reticulated, metallic fluids that span the whole length and width of a channel, can provide uniform electric fields, stable junctions and multiple spots for reactions making this a highly versatile option.

6.3. *Closing*

Beyond this work, researchers will need to engage in actively working towards providing better technologies to counter the current energy and climate crisis. To quote Albert Einstein, "we cannot solve our problems with the same thinking we used when we created them". The best possible solution against the aches of the earth, is to reduce our dependence on non-renewable resources and to improve overall conservation efforts.

This doctoral thesis should contribute towards furthering the integration of biological materials into electronics. The techniques here described provide a basis for well-grounded research and a new approach on bio-photovoltaics. I can only hope that they may be of benefit in the research towards cost-effective, greener, cleaner energy sources.

Summary

The goal of this doctoral project was to set the groundwork for the fabrication of an unusual, microfluidic bio-photovoltaic device that is bio-compatible and uses the protein complex, photosystem I, as active material in the light reactions. Photosystem I (PSI) is a complex system composed of more than 110 co-factors where multiple reactions take place. This complex is the single most important unit in the process of photosynthesis in plants and certain bacteria. Although PSI has been widely studied, misconceptions regarding its behavior and properties outside its natural environment are still common.

The first half of the project is elucidated in the first chapters of this thesis where I discuss the transport properties of oriented, self-assembled monolayers (SAMs) of PSI. These protein complexes comprise an electron transport chain (ETC) that moves charges in a given direction. The complexes can be oriented in such a way that the pathway of electrons is directed towards the substrate, away from it or is sideways. Individual complexes in a monolayer can be oriented on Au surfaces by making use of short molecules or "director SAMs". Monolayers of said molecules, 2-mercaptoethanol (2ME) and sodium 3-mercapto-1-propanesulfonate (MPS), can bind to specific sites of the PSI complexes orienting them in turn. By using eutectic gallium indium (EGaIn) as a probe, we were able to observe an asymmetry in *I-V* curves of monolayers of preferentially oriented PSI, which manifests as an asymmetry in tunneling charge-transport. By changing the conditions and varying the temperature while measuring, we found out that there is no observable dependence of current on temperature and thus, the most likely the mechanism of charge-transport would be *tunneling* (the only mechanism where there are no thermally activated processes).

Orienting PSI on ultra-flat Au electrodes had a maximum success rate of 70% by using the orienting molecule, 2ME. In this thesis, I also present Phage-Display (PD), a technique developed by collaborators in which short binding-peptides act as orienting agents affording near-perfect control over the orientation of PSI. By using this technique, the percentage of oriented complexes on indium tin oxide (ITO) increased to almost 100%.

The second half of the project involved the fabrication of soft, transparent and flexible devices. In this work, I present a detailed description of the fabri-

cation of the microfluidic channels and geometries used for this purpose. Co-fabrication is a strategy for fabricating multicomponent microsystems in a single step. This type of fabrication consists in generating a rigid master with an already designed pattern and subsequently pouring and curing a polymer (in this case, polydimethylsiloxane, PDMS), therefore yielding a replica. The PDMS replica can then be sealed with a piece of flat PDMS, creating the enclosed microfluidic channels with the wanted pattern. Metallic components are essential for most electrical devices including electrical microfluidic devices. Current techniques for successfully incorporating metals into such small and intricate geometries require long and difficult processes that lead to low throughput and high prices. By using a liquid metal such as EGaIn, we can circumvent these challenges by simply injecting the electrode into the channels.

The PDMS devices were tested mechanically (stretched, bent and rolled) presenting rupture only after an elongation of 60% of the original. Adjacent channels were separated by PDMS posts that span the height of the channel. We observed that thanks to Laplace barriers and the rheology of EGaIn, the entire filled device can be bent and stretched without presenting leaks to neighboring channels.

The proof-of-concept device fabricated on said microchannels follows the concept of a dye-sensitized solar cell (DSSC). In a DSSC a porous layer is covered with a molecular dye to absorb sunlight. An anode and a cathode are placed on opposite sides separated by a liquid electrolyte. Upon absorption of light the dye transfers an excited electron to the anode material. The electrons flow through an external circuit to reach the cathode, and the electrons are re-introduced into the cell. A redox couple in the electrolye regenerates the electrons in the dye by transfering charge from the cathode. In our devices, PSI works as the dye and is bound to the anode material. Just like in DSSCs, a redox couple regenerates the electrons and EGaIn acts as the cathode. The electrons are cycled through the spacing between the posts and can go from one electrode to the other via the electrolyte and redox-couple.

In the initial proof-of-concept devices PSI was immobilized on ultra-flat Au. The devices were later optimized by introducing nanoporous Au to increase the surface area to accommodate the biological complexes. The results show a photoresponse of over 20 nA. This result is about an order of magnitude higher than the photoresponse observed from the flat electrodes. We believe this proves that higher PSI density leads to an increase in photocurrent. Developments were also made on high-surface area electrodes that can be created inside PDMS microchannels by developing a protocol to make conducting nest-like structures.

The work in this thesis sheds light on the mechanism of PSI on solid-state devices, demonstrates the possibility of incorporating biological complexes in solid and soft devices and shows a successful way of fabricating transparent and flexible devices responsive to light. The ideas hereby discussed should serve as groundwork for more efficient, green, bio-compatible, electronic devices.

Samenvatting

Het doel van dit doctoraatsproject was om de basis te leggen voor de vervaardiging van een ongewoon, microfluïdisch, bio-fotovoltaïsch apparaat dat biocompatibel is en gebruik maakt van een eiwitcomplex, fotosysteem I (Photosystem I, PSI), als actief materiaal voor de reacties met licht. Fotosysteem I is een complex systeem bestaande uit meer dan 110 co-factoren waarop meerdere reacties plaatsvinden. Dit complex is de belangrijkste eenheid in fotosynthese in planten en sommige bacteriën. Hoewel PSI op grote schaal onderzocht is, zijn er nog steeds misvattingen over zijn gedrag en eigenschappen buiten zijn natuurlijke omgeving.

De eerste helft van het project is in de eerste hoofdstukken van dit proefschrift toegelicht. Hierin bespreek ik de transport eigenschappen van georiënteerde, zelf-geassembleerde monolagen van PSI. De eiwitcomplexen bevatten een elektronentransportketen die lading in een bepaalde richting verplaatst. De complexen kunnen georiënteerd worden in verschillende richtingen, zodanig dat de ketens ladingen transporteren naar het substraat, van het substraat af of parallel aan het substraat. Enkele complexen op goudoppervlakken kunnen worden gericht door middel van speciale moleculen. Monolagen van 2-mercaptoethanol (2ME) en natrium-3-mercapto-1-propaansulfonaat (MPS) kunnen aan specifieke plaatsen van de PSI-complexen binden, waardoor deze georiënteerd worden. Met eutectisch gallium indium (EGaIn) als probe, hebben we een asymmetrie in *I-V* curven geobserveerd in monolagen van preferentieel georiënteerd PSI. Het manifesteert zich als een asymmetrie in ladingstransport door *tunneling*. Door het veranderen van de omstandigheden en het variëren van de temperatuur tijdens het meten, kwamen we erachter dat er geen waarneembare afhankelijkheid van de stroom op de temperatuur is, en dus dat het meest waarschijnlijke mechanisme van de ladingstransport *tunneling* zou zijn (het enige mechanisme waar thermische processen geen rol spelen). Het oriënteren van PSI met het molecuul 2ME op een goud substraat had een maximaal succespercentage van 70%. In dit proefschrift, beschrijf ik ook faagdisplay, een techniek ontwikkeld door samenwerkers waarbij korte peptiden werken als oriënterend bindmiddel. Hiermee bieden zij bijna perfecte controle over de oriëntatie van PSI. Door gebruik van deze techniek steeg het percentage van georieerde complexen op indium tin oxide (ITO) tot bijna 100 procent.

De tweede helft van het project betrof de fabricage van zachte, transparante en flexibele apparaten. In dit proefschrift geef ik een gedetailleerde beschrijving van de vervaardiging van de microkanalen en geometrieën voor dit doel. Co-fabricage is een strategie voor het vervaardigen van microsystemen met meerdere componenten in een enkele stap. Dit soort fabricage bestaat uit het genereren van een stijve mal met een vooraf ontworpen patroon en vervolgens van het gieten en uitharden van een polymeer (in dit geval, polydimethylsiloxaan, PDMS) in de mal. Na het verwijderen van de mal houden we het PDMS over met daarin de gewenste structuren. De PDMS replica kan dan afgesloten worden met een vlak stuk PDMS. Dit creëert de ingesloten microfluïdische kanalen met het gewenste patroon. Metallische componenten zijn essentieel voor de meeste elektrische apparaten, dit geldt ook voor elektrische microfluïdische apparaten. De huidige technieken voor het succesvol opnemen van metalen in zulke kleine en ingewikkelde geometrieën vereisen lange en moeilijke processen die tot lage productiesnelheden en hoge prijzen leiden. Door het gebruik van een vloeibaar metaal zoals EGaIn, kunnen we deze uitdagingen omzeilen door eenvoudigweg de elektrode in de kanalen te injecteren.

De PDMS apparaten zijn mechanisch getest (rekken, buigen en rollen) en laten pas breuken zien bij een verlenging van meer dan 60% van de originele lengte. Naastgelegen kanalen zijn gescheiden van elkaar door een rij PDMS pilaren met dezelfde hoogte als de kanalen. We hebben geobserveerd dat dankzij Laplace barrières en de reologie van EGaIn, het gehele apparaat kan worden gebogen en uitgerekt zonder dat materiaal naar een naastgelegen kanaal lekt. De proof-of-concept apparaten van deze microkanalen zijn gebaseerd op het concept van een kleurstof-gesensibiliseerde zonnecel (dye sensitized solar cell, DSSC). In een DSSC, produceert de kleurstof (door absorptie van licht) aangeslagen elektronen die worden afgestaan aan de elektrode, deze elektronen worden geregenereerd vanaf de tegen-elektrode door middel van een redoxkoppel in een elektrolyt. In onze apparaten werkt PSI als de kleurstof en is gebonden aan het anode materiaal. Net als in een DSSC regenereert een redoxkoppel de elektronen, terwijl EGaIn fungeert als kathode. De elektronen stromen tussen de PDMS pilaren en kunnen zich van de ene- naar de andere elektrode verplaatsen via het elektrolyt en redox-koppel. In de eerste proof-of-concept-apparaten werd PSI geïmmobiliseerd op ultra-plat goud. Het ontwerp werd later geoptimaliseerd door het introduceren van nanoporeus goud om het oppervlak te verhogen waar de biologische complexen aan kunnen binden. Het apparaat toont een fotoresponse van meer dan 20 nA. Dit resultaat is ongeveer een orde van grootte hoger dan de fotoresponse waargenomen met de vlakke elektrode. Wij geloven dat dit aantoont dat hogere

dichtheid van PSI leidt tot een toename van de fotostroom. We hebben ook andere hoog-oppervlakkige elektroden onderzocht. Deze kunnen in PDMS microkanalen worden gevormd door het volgen van een protocol om geleidende nest-achtige structuren te maken.

Het werk in dit proefschrift werpt licht op het mechanisme van PSI in vaste stof apparaten en toont de mogelijkheid aan van het opnemen van biologische complexen op vaste en zachte apparaten. Tevens toont het een succesvolle manier om transparante en flexibele apparaten die reageren op licht te vervaardigen. De ideeën die hierin besproken worden kunnen dienen als basis voor efficiëntere, groene, biocompatibele, elektronische apparaten.

Acknowledgments

I would like to express my gratitude to Professors Sabeth Verpoorte, Michael Dickey and Casper van der Wal for taking the time to read and improve this dissertation.
A special Thank you, as well, to those who helped me by proofreading portions of this work.

It is hard to believe that more than four years have already passed by. Especially after having worked with the most amazing team anyone could ever hope for. I will always stand by the idea that doing a PhD should count as a specialization in project management. Yet, after the many scientific and technical lessons, I believe that what I will remember the most will be the people and the memories made together.

I would like to start by thanking my supervisor, Ryan Chiechi for having given me the opportunity of working in his group and taking a chance on someone with a very different educational background. I will never forget everything leading up to and including the day of the interview: the endless road to Groningen due to disruptions on the rails, the university hotel without personnel and in the middle of renovation, and getting in so late that all restaurants and shops were closed. Yet, the day of the interview surprised me with perfect weather, a small but friendly and welcoming research group, and a kind, hopeful and positive future supervisor. That was enough for me to cancel my upcoming interview in Delft and decide to make Groningen my home. In retrospect, it might have been somewhat foolish but it is a decision I never regretted.

I would like to thank, therefore, my amazing co-workers. Starting from Davide, Parisa and Zhiyuan for training me on multiple techniques during the first months. To Thomas for being a great office-mate and helping me to get settled into the Dutch culture. To all the RCC-Lab family: Marco, Andrew, Victor, Xinkai, Yanxi, Gang: thank you for sharing your scientific knowledge but especially for making work such a happy place. To Bouke, once part of RCC-Lab, thanks for the laughs, discussions and help with Dutch homework. To Thijs, who always felt like an RCC-Lab member, thanks for your awesome beard, your help in this work and for helping me with the many Dutch things to regulate and translate. To the extended family from other groups, Jorge and Eric: I hope we keep traveling, dancing and

going to many more concerts together. Thank you all for being more than just co-workers and being part of the special events in my life.

I would also like to thank the Top-Master students under my supervision, Michael van Putten and Henry de Vries for their efforts in making the project work. I enjoyed working with you and learned a lot from your dedication and fresh approaches to challenges. I would also like to thank our close colleagues from CMMD: Mehrnoosh, Jenny, Difei and Dr. Qiu for the helpful discussions. A special thanks to Prof. Kees Hummelen for always asking the tough questions and giving helpful advice.

I would like to thank my second advisor, Prof. Andreas Herrmann and the PCBE group for making my research possible. I would like to give a special thanks to Pavlo Gordiichuk for working alongside me for many years. Thank you for your important contributions and all of your help. I would also like to thank Mark Loznki for his disposition and for providing me with proteins and small molecules to conduct my research. From Pharmaceutical Analysis at UMCG, thanks to Pieter Oomen and Patty Mulder for your help with soft lithography. Also to Patrick van Rijn from BISM for allowing me to collaborate with your group.

I would also like to thank a very special group of people without whom things would not work so well. Renate, your help in the group is invaluable. You have helped me even before I made it to Groningen and until the very last steps, always with a smile. Reinder, I always admired your disposition and genius at coming up with equipment and tools to make our research possible. To the technicians involved with the Nanolab, Johan and Martijn and to Arjen for keeping the clean-room up to standards. Rick, thanks for coming in with such enthusiasm and the help during my last months. To Alfred, thank you for taking care of our lab notebooks.

I would also like to take a chance to thank Prof. Michael Dickey and my temporary colleagues from his group at NCSU. Thank you for allowing me to experiment the world of Chemical Engineering once again and for welcoming me so warmly into your group during the two months of my research. A special thanks to Dishit, Ishan, Collin L. and Duncan for taking the time to train me, for the helpful ideas and discussions and the fun times in the lab.

I must also thank those who have been part of my life outside the university, acquaintances and close friends. Whether we met in Groningen, the U.S., Italy or whether we go way back to childhood and teenage years in Colombia: thank you for being part of my journey. St. Augustine community, without you my life here would not be this complete and happy. Thank you for the interesting discussions ranging from deep, faith-related topics to great food, and the many fun

or meditative times we have spent together. You all have played a very important role in my life.

And last but certainly not least, I would like to thank my small but wonderful family. I would not be who I am without your unconditional love and support. Mom, you have always believed in me. You have sacrificed everything so that Juan and I could have the best possible life. Your strength has pulled me through difficult times and has inspired me to be the best person I can be. Your faith has moved mountains and your love has travelled oceans and continents. There are no words to express my gratitude towards you!

Fefis, hermanito, thanks for putting up with me and the consequences of me choosing a life abroad. Your sacrifices for my wellbeing have never gone unnoticed. You have been a wonderful brother.

Carlitos, my dear husband, how would I have even survived our Master's degree without you? Your love and patience have helped me believe in me again. Thank you for your care and support all these years and for making sure I pursue and reach my dreams.

I love you all with all of my heart!

I believe in a kind and loving God who has blessed me with everything and everyone I am grateful for. To Him I give the biggest Thank You of all. May my life and work be a light in the darkness.

Olga Elena Castañeda Ocampo
Groningen, February 2017

Curriculum Vitæ

Olga Elena Castañeda Ocampo was born on April 18, 1985 in Medellín, Colombia. She received an associate's degree in arts from Edison College (now Florida South-Western State College) in 2004, graduating with Honors and other distinctions.

Olga continued her Bachelor of Science in Chemical Engineering at the University of South Florida where she also worked as an undergraduate research assistant until graduating in 2006. Her projects comprised researching the controlled release of drug delivery to brain tumor sites, engineering constructs of metallic nanoparticles and stimuli-sensitive polymers as well as the engineering of an extended-release trans-dermal skin patch for the treatment of ADHD (attention deficit hyperactivity disorder).

After holding different industry positions in the U.S.A. and Colombia, she moved to Turin, Italy in 2009 to pursue a Master's Degree in Chemical Engineering at the Politecnico di Torino. Her Master's thesis consisted in designing a pilot plant to remove pollutants from a natural gas stream originating from a refinery. In 2012 she joined the University of Groningen to pursue a PhD where she would strive for the fabrication of unconventional, bio-photovoltaic devices out of the protein complex, Photosystem I.